A Theoretical and Experimental Investigation into Fire Induced Flashover of High Voltage Transmission Lines

Aroon Sukhnandan

This thesis was submitted to the University of KwaZulu Natal in fulfillment of the requirements for a Master's degree in Electrical Engineering.

To my parents, Kamraj and Indrani Sukhnandan!

Acknowledgements

I would like to convey a special thank you to my supervisor Dr Derek Hoch for being invaluable in his guidance and direction. I also acknowledge his foresight and knowledge from which I drew much inspiration.

I also acknowledge Marlini for her constant friendship and support as well as fellow postgraduate students for the much needed laughs and distractions.

I wish to thank my family for their love, support and for always being on my side. I also thank my Masters Sri Swami Sivananda and Sri Swami Sahajananda for all the love and kindness.

Declaration

I, Aroon Sukhnandan, declare that the work contained in this thesis is my own and has not been submitted, in part or otherwise, to another university.

Aroon Sukhnandan

1st June 2004

Abstract

This thesis documents a research study of High Voltage transmission line faults induced by fire. Conductor to conductor and conductor to ground flashovers have been experienced by electricity utilities around the world under conditions of veld and sugar cane fires. These types of faults are unpredictable and negatively impact line reliability and quality of supply. This is a crucial problem when the revenue of the industry is sensitive to voltage dips.

Electricity utilities have taken a preventative approach, like clearing vegetation from the line servitude in order to decrease the frequency of line faults. There has also been a drive to collaborate with sugarcane farmers in order to have harvesting fires planned with utilities. Some success has been achieved with these initiatives however there still remains a large number of faults.

The focus of this study is on the mechanism of fire-induced flashover. Previous work has displayed the existence of two theories. The first theory suggests that flashover is due to the reduction in air insulation strength caused by a reduced air density that results from the thermal effect of the fire. The second theory suggests that small particles present in the fire cause electric field distortions that induce flashover. This study is focused on a theory, which indicates that flashover is induced due to an enhanced electric field which is a result of the conductive properties of the flames present in the air gap (the flame conductivity theory). The effects of particles and a reduced air density is said to support this mechanism that is the primary reason for flashover.

This thesis presents a summary of the literature where firstly an understanding of air insulation behavior is displayed. Thereafter specific interest is given to the effect of fire and flames wherein the physics of flames are discussed. This then leads to the description of the flame conductivity theory. Chapter 4 deals with a simulative investigation into the effect a conducting flame has on the electric field distribution. This is looked at with a varying flame conductivity and gap length in mind. The simulations specifically cover the 275 kV and 400 kV line configurations. The simulative investigation results in a mapping of electric field enhancement against conductivity values and gap sizes. Thus a flashover probability is assessed by using the two factor flashover criteria when analyzing the electric field stresses.

The objective of the experimental work in this study is to obtain insight on how the flame geometry and orientation affects flashover and the dependence of flashover on gap size. Tests involving a fire beneath a conductor were carried out for different gap sizes. Experimentation with particles above a flame was also conducted.

It was concluded that flame structure does have an impact on flashover since a flame with sharp edges is more likely to cause flashover. Particles have a reducing effect on air insulation strength. This is mainly due to the fact that the particle reduces the effective air-gap size. No significant effect over and above this is noticed. For gaps spanned by clean Liquid Petroleum Gas (LPG) flames flashover voltage increases as gap-length increases with some degree of non-linearity. Flame resistances and conductivity were approximated from measured currents and voltages.

Nomenclature

2D	Two-Dimensional
3D	Three-Dimensional
AC	Alternating Current
FEM	Finite Element Method
FIF	Fire Induced Flashover
GMR	Geometric Mean Radius
HVDC	High Voltage Direct Current
IEEE	Institute of Electrical and Electronic Engineers
IREQ	Institut de Recherché d'Hydro-Québec
LPG	Liquid Petroleum Gas
RAD	Reduced Air Density
STP	Standard Temperature and Pressure

A^m	represents a metastable ion
B	represents a neutral atom
A	represents a neutral atom or molecule
A^+	represents a positive ion
E_c	corona inception field strength
h	Planck's constant
k	Universal Boltzman's constant
m_e	mass of electron
n	number of kilo moles of gas
p	pressure
R	Universal gas constant
r	conductor radius
T	absolute temperature in degrees Kelvin
T_{cr}(crit)	critical time-to-crest
V	volume
u	average drift velocity
u_e	electron velocity
w	mean energy per molecule of gas
W_i	ionisation energy of the gas

α	Townsend's first ionization coefficient
λ_i	ionic mean free path
τ	distance traveled
δ	relative air density
ζ	stranding factor

List of Figures

Chapter 1

Chapter 2

Chapter 4

Chapter 5

List of Tables

Contents

Appendices

Chapter
1

Introduction

1.1 Historical Context

Eskom has experienced flashover problems as a result of bush and sugar cane fires underneath 275 kV and 400 kV transmission lines. It is known that this type of fault is more serious than other transient faults because the line often re-trips and locks out [1]. In order to reduce the frequency of such faults Eskom has implemented a program with farmers whereby sugar cane crop burning is conducted at convenient times. Due to this close cooperation with farmers, a decision is made either to switch the line out of service or to switch the auto-re-close off.

Work has also been done to provide a system for the early detection of fires in the vicinity of transmission lines [1], [2], [3]. Increased corona activity on the conductors during fires has been reported by Britten et al, who conducted both field and laboratory based experiments [4]. It was found that this increased corona generated increased levels of background radio noise, which is detectable in the carrier system communication channels [2]. Work done by Evert et al in detecting this high frequency noise has resulted in a prototype fire detection device [2].

1.2 The cane fire problem

Sugarcane farming is a major agricultural activity along the costal regions of Kwa-Zulu-Natal since the hot humid conditions along the east coast are conducive to cane farming. The cane growing area stretches for hundreds of kilometers along the coast and up to a hundred kilometers inland. Many thousands of kilometers of transmission lines are therefore affected [1].

Harvesting of the sugar crop involves the burning of excess leaves, some of which is completely dry. The dry leaves that drop from the growing plant collect over many months and are very combustible, hence these fires are intense and huge but burn for a few minutes only. Often the situation arises when these harvesting fires are directly beneath transmission lines. At times the flames are tall enough to engulf the conductors. This is depicted in Figure 1.1 [5]. Sometimes a major part of the air-gap is filled with the flame leaving a small gap between the flame-tip and the conductor. This gap is often filled with smoke and particles, as can be seen in Figure 1.2 [5]. The presence of the flame reportedly causes phase to phase and phase to earth flashovers. These occurrences are called Fire Induced Flashover (FIF). This not only causes damage to transmission line hardware but also causes voltage depressions due to the large fault currents.

The subsequent voltage depressions affect voltage sensitive loads with concomitant loss of production and/or damage to equipment [1]. It is known that this type of fault is more serious than other transient faults because the line often re-trips and locks out [1].

Figure 1.1: Sugar cane fire rising into a transmission line showing conductor engulfment by a conical flame [Courtesy of Eskom TSI]

Figure 1.2: A sugar cane fire showing the flame in the vicinity of the conductor with the rest of the gap filled with smoke and particles [Courtesy of Eskom TSI]

Problems similar to these have also been reported from Mexico, Brazil and Canada [6], [7], [8], [9]. In Brazil there has been a move to keep the line right of way free of dense vegetation, and through educational campaigns involving farmers, have controlled burnings [7].

Hydro-Québec's High Voltage Direct Current (HVDC) power lines cross vast wooded areas on their way from production sites to load centers. Forrest fires often decrease the reliability of the line. At first many disregarded the possibility of FIF. Lanoie and Mercure [8] have accepted that a definite correlation exists between the proximity of fire and the occurrence of faults. This then resulted in an experimental research project being initiated by the Institut de Recherché d'Hydro-Québec (IREQ). The details of this work are contained in [8].

The decline in quality of supply due to voltage dips as a result of FIF is a real problem and deserves much attention. Quality of electricity supply is a top priority issue with Eskom in South Africa and every effort is being expended to improve the present situation [1] [3].

FIF is not only confined to South Africa and Eskom. Research initiatives have been made in Brazil [7], Italy and Argentina [10], Canada [8] and Mexico [9]. Fonseca et al [7] and Lanoie and Mercure [8] have both produced results from field investigations. Most of the other work like [11], [12], [9] and [13] have been confined to lab- scale investigations.

1.3 Previous work

Some still have doubts that a fire can induce line faults since it is not always that a flame under a transmission line causes flashover. The lack of repeatability causes the concern. The probable cause of the lack of repeatability is due to varying physical properties (shape and length of flame, flame conductivity and flame temperature).

There are currently three major theories about the mechanism of flashover (discussed in chapter 3). The first theory postulates that the lack of air insulation strength is caused by the Reduced Air Density (RAD). This theory has truth but a claim that RAD alone is responsible for the breakdown is arguable according to the standards set out by the Institute of Electrical and Electronic Engineers (IEEE) [14]. Results obtained by Allen et al also reinforce this statement [15], [16].

The second theory involves the fact that there are a large number of particles present in the flame and the thick smoke. It is said that these particles induce flashover. Naidoo and Swift [17]

and Sadurski [58] conducted laboratory investigations using parallel tubular conductors and mid-gap particles.

The third is the theory of flame conductivity [5], [18]. This forms the basis of this study. It is postulated that due to the conductivity of the flame, an enhanced electric field is created between the flame tip and conductor. This is due to the voltage being divided between the conductive flame and the air-gap (between flame and conductor), as displayed in figure 4.3. In effect, the flame raises the ground plane and most of the voltage appears across the air-gap.

This study is focused on the physical properties of the flame itself which when changed decides whether flashover is induced or not. The hypothesis that is developed has its basis on the fact that the flame itself is conductive. The flame causes an enhancement in the electric field near the conductors. It is conceivable that a sufficiently strong electric field near the conductors may cause corona inception.

Flashover probabilities cannot be predicted by merely taking the reduced air density and the concentration of particles into account. There are many other factors that are characteristic to the flame that have a significant impact on flashover voltage.

Much work has been done using air insulation at elevated temperatures and pressures by Allen et al [15], [16], [19]. Their findings are used in this research and can be categorized as basic supporting theory. This study uses a simulative and an experimental approach which differs from previous work which were mainly experimental studies. It can be added that this research topic has a practical bearing on the smooth transmission of electrical energy in regions where FIF is experienced.

1.4 The objective of this study

The objective of this study may be described as an investigation to understand the problem of FIF rather than to provide a solution to utilities for the eradication of the flashover problem.

The simulations are aimed at displaying the effect of flame conductivity on the enhancement of the electric field in the air-gap. More insight on the effect of flame height on electric field enhancement was also one of the objectives. The experimental study is aimed at understanding the relationship that flame properties such as geometry and orientation has on fire induced flashover. The effect of mid-gap conducting particles was also investigated.

1.5 Experimental Restrictions

As with any form of experimental work there are restrictions that are dependent on cost and time. In this case, restrictions in experiments were experienced because fire is not easily controlled and seldom allows for consistent repeatable experiments. This problem becomes more significant when experimenting with bigger flames. Most properties of the flame, like temperature for example, cannot be controlled easily as it depends on a host of other flame parameters. The shape of the flame is also relatively difficult to control.

AC voltages available for experimentation also had an upper limit. This placed restrictions on air-gap sizes that could be flashed over. Thus all experimental work was conducted within the constraints due to the restrictions mentioned above.

1.6 Thesis Structure

This thesis has eight chapters in total. The first few chapters discuss the research topic from a background and basic theory standpoint while the other chapters involve a description of the simulative and experimental work. The last few chapters are a discussion and analysis of the results, which culminate in a conclusion and recommendations for further work. A description of each chapter follows.

Chapter 2 details the physics of air gap breakdown. It covers the Townsend and Meek theories, which includes the discussion of Townsend's first and second Ionization constants. Large air gap breakdown is also dealt with and the various factors that affect breakdown strength are described. A detailed view on the properties of the leader mechanism is documented

Chapter 3 is entitled " Air gap breakdown in the presence of fire and flames". It deals with the three major theories that are used to describe the effect of reduced air insulation strength due to the presence of fire beneath transmission lines. These theories are referred to throughout this thesis as the Reduced Air Density (RAD) theory, the particle initiated flashover theory and the flame conductivity theory.

Chapter 4 documents the simulative study carried out using a software tool called FEMLAB®. The aim of the simulation can be summarized as evaluating the electric field stresses that occur in the air-gap between a transmission line and a fire directly beneath it. The investigation is directed at finding a relationship between electric field enhancements and flame properties such as conductivity and height.

Chapter 5 describes the experimental investigation. The apparatus, experimental procedure, experimental setup and objectives are presented. Experiments were carried out using models of different flame geometries, particles and a flame itself. The results that are obtained from the experiments are explained using supporting theory. There is also a comparison with previous published work.

Chapter 6 contains the discussion of the results.

Chapter 7 consists solely of the conclusion to the research study. Significant findings are emphasized once again.

Chapter 8 is a recommendation for further work in this area of research. As with any form of study a lot can be said with hindsight and thus these recommendations could be used as a springboard for further research.

Chapter
2

Air Gap Breakdown

2.1 Introduction

"Ever since Edison developed the use of electric energy as a means to do work, man has looked for ways to isolate the two wires required to convey electricity to the place of usage." [20].

In a power distribution network air insulation is widely used making the stability and smooth operation of the power system dependent upon the performance of the air insulation. A large amount of work has been performed to investigate, from a physical point of view the phenomenon of dielectric discharges in air gaps subject to high voltages.

The purpose of this chapter is to present an understanding of the basics of electric discharges and air breakdown. High voltage discharge in air gaps can be categorized into two broad sections: Small air gap breakdown (streamer mechanism) and large air gap breakdown (leader mechanism). This chapter deals with small air-gaps first and later progresses into large air-gaps. Meek's streamer theory and corona discharges are also described.

Scientists till now have been exploring the two mechanisms in order to understand their operation and to predict their behaviour with the aid of mathematical models. An important motive of most air insulation research is to determine the insulation strength of air so that the design of electrical transmission lines and apparatus can be aided so as to estimate minimum clearances for transmission line applications [21].

The limitations encountered in the prediction of air insulation clearances are directly related to the physical mechanisms of corona effects. Thus the understanding of the behaviour of air predischarges plays a fundamental role in the refinement of models and in the improvement of electrical system design.

2.2 The Kinetic Theory

The fundamental principles of the kinetic theory of gases are pertinent to the study of electrical breakdown and gaseous ionisation. The results of the kinetic theory need to be examined.

2.2.1 Boyle's Law

For a given amount of enclosed gas at a constant temperature, the product of pressure and volume is constant.

$$pV = C = Constant \tag{2.1}$$

also,

$$v/v_0 = T/T_0 \qquad \text{(GayLussac's Law)} \tag{2.2}$$

From these formulae the equation that describes the state of an ideal gas is formed, namely:

$$pV = nRT \tag{2.3}$$

where:

R = universal gas constant equal to 8.314 joules/K mol

n = number of kilo moles of gas

and T = absolute temperature in Kelvin.

An alternate form of this equation is:

$$pV = NkT \tag{2.4}$$

where:

k = universal Boltzman's constant equal to 1.3804×10^{-23} joules/K

Also the mean energy per molecule of gas is determined by:

$$w = 3/2\ kT \tag{2.5}$$

2.2.2 The free path λ of molecules and electrons

The free path is defined as the distance molecules or particles travel between collisions. The free path is a random quantity and its mean value depends upon the concentration of particles or the density of the gas.

2.2.3 Collisions and energy transfer

There are two types of collisions between gas particles:

(1) Elastic or simple mechanical collisions in which the energy exchange is always kinetic

(2) Inelastic – in which some of the kinetic energy of the colliding particles is transferred into potential energy of the struck particle or vice versa.

2.3 Townsend's First Ionisation Coefficient

In air under normal conditions the recombination process counterbalances the creation of free electrons and positive ions and equilibrium exists [22]. If however the external electric field is sufficiently high the state of equilibrium will be upset. Townsend studied the gas current variation with respect to changes in the applied field. The current at first increased proportionally with the applied voltage and then remained nearly constant at a value i_o which corresponded to the background current (saturation current). If the cathode was irradiated with ultraviolet light then the emitted photocurrent was also equal to i_o

When the external voltage was increased further the current increased above the value of i_o at an exponential rate. Townsend ascribed this increase in the current beyond a threshold value to the ionisation of gas due to electron collision. As the field increases, electrons leaving the cathode are accelerated more and more between collisions until they gain enough energy to cause ionisation on collision with gas molecules or atoms.

Townsend introduced the first ionisation constant called α defined as the number of electrons produced by an electron per unit length of path in the direction of the field. If n is equal to the number of electrons at a distance x from the cathode, the increase in electrons dn in additional distance dx is given by:

$$dn = \alpha n \, dx \tag{2.6}$$

Integration over the distance from anode to cathode (d) gives

$$n = n_o e^{\alpha d} \tag{2.7}$$

Where:

n_o = number of primary electrons generated at the cathode

The above equation becomes:

$$I = I_o e^{\alpha d} \tag{2.8}$$

Where:

I_o = current leaving the cathode.

2.3.1. Photoionization

If on collision an electron has energy lower than the ionisation energy of the other colliding body then the collision may excite the gas atoms to higher states. i.e.:

$$A + e + Kinetic\ Energy \rightarrow A^* + e \quad (2.9)$$

$$A^* \rightarrow A + h\nu \quad (2.10)$$

where:

A represents the neutral atom or molecule

A^+ represents the positive ion

$h\nu$ represents the photon energy

The excited atom on recovering from its excited state radiates a quantum of energy or photon ($h\nu$) that in turn may ionise another atom whose ionisation energy is equal to or lower than the photon energy. This process is known as Photoionization and is represented as:

$$A + h\nu \rightarrow A^+ + e \quad (2.11)$$

Photoionization is a secondary ionisation process and may be acting in the Townsend breakdown mechanism and is essential in the streamer breakdown mechanism and in some corona discharges. Photoexcitation is a process whereby an atom or molecule just absorbs a photon and is raised to a higher energy level due to the energy in the photon being not sufficient in order to ionise the atom or molecule.

2.3.2. Ionisation by Interaction of Metastables with Atoms

A metastable state is an excited state that lasts for several seconds. The atoms in this state are referred to as metastables and have a relatively high potential energy and are able to ionise neutral particles. Consider the following case:

$$A^m + B \rightarrow A^+ + B + e \quad (2.12)$$

Where:

A^m represents the metastable

B represents the neutral atom

Other examples of ionisation by interaction of metastables are as follows:

$$A^m + A^m \rightarrow A^+ + A + e + KE \quad (2.13)$$

(usually when the density of metastables are high)

$$A^{m} + 2\,A \rightarrow 2\,A^{*} + A \;\; ; \;\; 2A^{*} \rightarrow A + A + h\nu \qquad (2.14)$$

The photon released in the above reaction may cause ionisation in the cathode rather than the gas molecules due to its low energy value.

2.3.3. Thermal Ionisation

Thermal Ionisation occurs when atoms or molecules gain sufficiently high velocity to cause ionisation on collision with other molecules or atoms. This is the main source of ionisation in flames and high-pressure arcs. Work done by Saha resulted in an equation in order to describe the degree of ionisation θ in terms of gas pressure and absolute temperature:

$$\frac{\theta^2}{1-\theta} = \frac{1(2\pi m_e)^{3/2}}{ph}(kT)^{5/2} e^{-W_i/kT} \qquad (2.15)$$

Where:

p = pressure in torr

W_i = ionisation energy of the gas

k = Boltzman constant

T = absolute temperature

m_e = mass of electron

h = plank constant

2.3.4. Deionization by Recombination

Recombination is a process that occurs wherever there are negative and positive ions present. Upon recombination of these ions a quantum of energy is released. In some cases a third body may be involved and may absorb the excess energy released in the recombination. The reactions are represented as follows:

$$A^{+} + e \rightarrow A + h\nu(\text{radiation}) \qquad (2.16)$$

$$A^{+} + e \rightarrow A^{m} + h\nu \qquad (\text{recombination}) \qquad (2.17)$$

$$A^{+} + C + e \rightarrow A^{*} + C \rightarrow A + C + h\nu \qquad (2.18)$$

$$A^+ + e + e \rightarrow A^* + e \rightarrow A + e + h\nu \quad (2.19)$$

2.3.5. Deionization by Attachment – Negative Ion Formation

Electronegative gases are gases that are lacking one or two electrons in its outer shell and thus have a tendency to readily acquire a free electron to form a stable negative ion. For these negative ions to remain stable for some time, the total energy must be lower than that of an atom in the ground state. The electron affinity is the change in energy that occurs when one electron is added to an atom in the gaseous state. The following are the processes for negative ion formation:

- Radiative attachment: Excess energy upon attachment is released as a quantum.

  $$A + e \Leftrightarrow A^- + h\nu \quad (2.20)$$

  The captured electron can be released by absorption of a photon (photodetachment). Thus the process is reversible.
- Third body collision attachment: Excess energy upon attachment is absorbed by a third body as kinetic energy.
-

  $$e + A + B \rightarrow A^- + (B + W_k) \quad (2.21)$$

  where:

  W_k = change in kinetic energy of body B
- Dissociative attachment: Excess energy is used to separate the molecule into a neutral particle and an atomic negative ion.

  $$e + AB \Leftrightarrow (AB^-)^* \Leftrightarrow A^- + B \quad (2.22)$$

  This process is predominant in molecular gases.
- In the above process the molecular ion is at a higher potential level and upon collision with a different particle this excitation energy may be lost to the colliding particle as potential and/or kinetic energy.

  $$e + AB \Leftrightarrow (AB^-)^* \quad (2.23)$$

  $$(AB^-)^* + A \Leftrightarrow (AB)^- + A + W_k + W_p \quad (2.24)$$

- There are other processes of negative ion formation; one such process involves the splitting of a molecule into negative and positive ions upon impact of an electron without attaching the electron.

The process of electron attachment cumulatively describing the removal of electrons by attachment from ionised gas by any of the above processes may be expressed by a relation analogous to the expression that describes electron multiplication in a gas. The loss of electron current in a distance dx due to attachment is:

$$dI = -\eta I dx \tag{2.25}$$

Where η is the attachment coefficient indicating the number of attachments produced in a path of a single electron travelling a distance 1cm in the direction of the field.

Thus for a gap length d and with electron current I_o starting at the cathode,

$$I = I_o e^{-\eta d} \tag{2.26}$$

The number of electrons produced by collision in distance dx is,

$$dn_i = -n\alpha dx \tag{2.27}$$

At the same time, the number of electrons lost in dx by attachment is

$$dn_a = -n\eta dx \tag{2.28}$$

So then the number of free electrons is

$$dn = dn_i + dn_a = n(\alpha - \eta)dx \tag{2.29}$$

Integration from zero to x with n_o electrons starting from the cathode gives the number of electrons at any point x in the gap as:

$$n = n_o e^{(\alpha - \eta)x} \tag{2.30}$$

The steady state current will have two components.

- Electron flow
- Negative ion flow

The increase in negative ions in distance dx is,

$$dn_{-} = n\eta dx = n_o \eta\, e^{(\alpha - \eta)x}\, dx \tag{2.31}$$

Integration from zero to x gives,

$$n_{-} = \frac{n_o \eta}{\alpha - \eta}\left[e^{(\alpha-\eta)x} - 1\right] \tag{2.32}$$

The total current equals the sum of the two components or

$$\frac{n + n_{-}}{n_o} = \frac{\alpha}{\alpha - \eta} e^{(\alpha-\eta)d} - \frac{\eta}{\alpha - \eta} \tag{2.33}$$

and the current becomes,

$$I = I_o\left[\frac{\alpha}{\alpha - \eta} e^{(\alpha-\eta)d} - \frac{\eta}{\alpha - \eta}\right] \tag{2.34}$$

α - η *is* defined as the *effective* ionisation coefficient.

2.3.6. Mobility and De-ionisation by diffusion

In the presence of an electric field, charged particles in a gas will experience a force causing them to drift with a velocity that varies directly with the field and inversely with the density of the gas through which it moves.

$$k = \frac{u}{E} \qquad (\text{m}^2/\text{v sec}) \tag{2.35}$$

u is the average drift velocity in field direction and E is the electric field strength. In a region of low values of E/p it is possible to derive an expression for mobility of ions in a gas since the drift velocity will be small compared to thermal velocity. An expression for the reduced mobility at 0°C and 760mm Hg is as follows:

$$k_o = k \frac{p}{760} \frac{273}{T} \tag{2.36}$$

By letting τ equal the time between two successive collisions,

$$\tau = \frac{\bar{\lambda}_i}{\bar{c}} \tag{2.37}$$

where λ_i is the ionic mean free path and c is the mean thermal velocity of the ion. The acceleration a is,

$$a = \frac{eE}{m} \tag{2.38}$$

and the distance travelled in time τ is,

$$s = \frac{eE}{2m}\tau^2 \tag{2.39}$$

which makes drift velocity,

$$u = \frac{eE}{2m}\tau = \left(\frac{e\tau}{2m}\right)E = \left(\frac{e\lambda_i}{2mc}\right)E \tag{2.40}$$

and

$$k = \frac{u}{E} = \frac{e\lambda_i}{2mc} \tag{2.41}$$

Taking the statistical distributions of the mean free path into account, the average value of s becomes,

$$\bar{s} = \frac{eE}{mc^{-2}}\lambda_i^{\,2} \tag{2.42}$$

If mean free time,

$$\bar{\tau} = \frac{\lambda_i}{c} \tag{2.43}$$

then

$$\bar{s} = \frac{eE}{m}\bar{\tau}^2 \tag{2.44}$$

and the drift velocity,

$$u = \frac{\bar{s}}{\tau} = \frac{eE}{mc}\lambda_i \tag{2.45}$$

and finally,

$$k = \frac{u}{E} = \frac{e\bar{\lambda}_i}{mc} \tag{2.46}$$

This shows that when the distribution of free paths are taken into account, k doubles. If the initial velocities of the particles are taken into account i.e. the velocities of the particles after collision, then k can be defined as follows:

$$k = \frac{0.815e\bar{\lambda}}{mc}\sqrt{\frac{m+M}{m}} \tag{2.47}$$

For thermal equilibrium,

$$\frac{mc_i^{\,2}}{2} = \frac{mc^2}{2} = \frac{3}{2}kT \tag{2.48}$$

For the special case of an electron:

$$k = 0.815 \frac{e}{m} \frac{\overline{\lambda_e}}{c_1} \tag{2.49}$$

The presence of impurities is found to have a significant effect on the measured mobility. This ion and electron mobility can be used for the determination of conductivity of an ionised gas. The following is a simple case:

Let the concentration of electrons and positive ions be equal, i.e.:

$$[n_+] = [n_e] = [n] \tag{2.50}$$

Therefore the total current density,

$$J = J_i + J_e = n(u_i + u_e)e \tag{2.51}$$

therefore,

$$J = neE(K_e + K_i) \tag{2.52}$$

and,

$$\sigma = \frac{J}{E} = n(K_e + K_i) \tag{2.53}$$

Since $K_e >> K_i$, the conductivity is given by,

$$\sigma = nK_e \tag{2.54}$$

However in the presence of appreciable space charge, $n_e \neq n_i$, the conductivity components must be considered separately.

2.4. Cathode processes – Secondary effects

In a gas discharge electrons are supplied by the cathode for initiation, sustaining and for completion of the discharge. The energy required to remove an electron from the surface of a cathode is called the work function and is specific to that material. The required energy may be supplied in several ways:

2.4.1. Photoelectric emission

If the energy of photons that hit the surface of the material exceeds the work function of the material then electrons may be ejected from the material. Any excess energy may be transferred into kinetic energy of the electron. The following relation applies:

$$mu_e^2/2 = h\nu - h\nu_0 \tag{2.55}$$

where:

m = electron mass

u_e = electron velocity

$h\nu$ = energy of the photon = (plank's constant * photon frequency)

$h\nu_0 = W_a$, the work function of the material

2.4.2. Electron emission by Positive ion and excited atom impact

Due to bombardment by positive ions or metastables, electrons are emitted from the metal surface. To cause a secondary emission of an electron the impinging ion must release two electrons, one of which is utilized to neutralize the ion charge. The minimum energy required for positive ion electron emission is twice the work function, since the ion is neutralized by one electron and the other electron is ejected.

2.4.3. Thermonic Emission

If a metal temperature is increased to some 1500-2500K, the electrons will receive energy from the violent thermal vibrations. Their energy will sometimes be large enough to cross the surface barrier and leave the metal. The emission current is related to the temperature.

2.4.4. Field Emission

In this case the electrons are drawn out of the field by the high electric field at the surface of the metal. An important effect to mention at this point is the tunnel effect where the strong electric field at the surface of the metal modifies the potential barrier at the metals surface to such an extent that electrons in the upper level close to the Fermi level will have a definite probability of passing through the barrier [23].

2.5 Townsend Second Ionisation Coefficient γ

Townsend, during early measurements of current in parallel plate gaps observed that at higher voltages the current increased at a more rapid rate than explained by the first mechanism postulated. Townsend thus postulated a second mechanism. Meek sums it up as follows: "These secondary mechanisms cause the production of additional electrons from the cathode as a result of the impact on the cathode of positive ions, photons and metastable molecules. The various secondary processes may be described quantitatively by a secondary ionisation coefficient γ which is defined as the number of secondary electrons produced at the cathode per ionising collision in the gap." [6].

Consider the following:

Let n_0 = the number of electrons liberated from cathode per second. (e.g.: by uv radiation

from an external source)

Let n_e = the number of electrons reaching the anode each second

Let n_γ= the number of electrons released from the cathode per second by secondary mechanisms related to the production of positive ions in gas.

$$n_e = (n_0 + n_\gamma)\, e^{\alpha d} \tag{2.56}$$

The number of positive ions n_+ produced within the gas per length of path:

$$n_+ = n_e - (n_0 + n_\gamma) \tag{2.57}$$

and so for $n_\gamma = \gamma n_+$

$$n_\gamma = \gamma (n_e - n_0 - n_\gamma) \tag{2.58}$$

therefore:

$$n_\gamma = \gamma (n_e - n_0) / (1 + \gamma) \tag{2.59}$$

and:

$$n_e = n_0\, e^{\alpha d} / [1 - \gamma (e^{\alpha d} - 1)] \tag{2.60}$$

Thus the steady state current may be described as:

$$I = I_0 e^{\alpha d} / [1 - \gamma (e^{\alpha d} - 1)] \tag{2.61}$$

As the voltage applied to the gap is increased the quantity $\gamma e^{\alpha d}$ increases until, when it reaches the value 1, the denominator becomes zero and the current reaches infinity theoretically. In reality the current is limited by the limitations of the circuit.

In the 1960's many studies were conducted by different scientists around the world to examine the variation of the current in uniform field gaps in different gases. Values for α and γ have been determined as functions of electric field and gas pressure. The influences of the electron attachment and detachment processes have been carefully studied. Their results confirm the correctness of the basic ideas of the Townsend theory. Although the Townsend theory gives a consistent account for spark growth and streamer onset in a uniform field it does not give a clear picture of other aspects of spark development. Problem areas:

- Explanation of short formative times of gaps subject to high over voltages.
- Breakdown of a long gap between a positive point and an earthed plane appears to be independent of cathode material.
- Cathode effects can hardly be invoked to explain the growth of lightning discharge between negative cloud and ground.

- The branched and irregular nature of sparks is also difficult to reconcile with the Townsend theory.

2.6 Meek's Streamer Theory

In 1939 Meek put forward a theory known as the streamer theory of spark. This theory has the following ideas:

- Depends primarily on the ionisation processes occurring in the gas.
- Explanation is independent of secondary emissions of electrons from the cathode.

The theory is well presented in [6] where Meek states:

" Consider the application of a voltage gradient of E volts per centimetre across a gap of length d centimetres between parallel plane electrodes in a gas of pressure p millimetres Hg. If the ratio E/p is sufficiently high, an electron leaving the cathode will ionise the gas molecules and the additional electron so created will be accelerated in the applied field and so cause further ionisation. When the original electron has moved a distance x centimetres in the direction of the applied field, the number of additional electrons created is $e^{\alpha x}$. The process is rapidly cumulative and is appropriately named an 'electron avalanche'. In a field of the magnitude required to cause breakdown, the electrons travel at a speed of the order of 2×10^5m/s, while the positive ion from which the electron has been detached has a speed of 2×10^3m/s. The positive ions may therefore be considered as virtually stationary in comparison with the faster moving electrons, and the avalanche develops across the gap as a cloud of electrons behind which is left a positive ion space charge in roughly conical channel..."

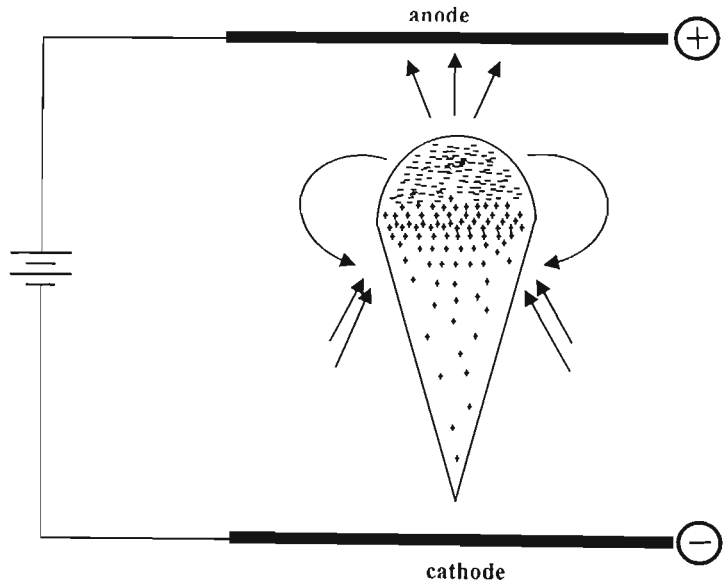

Figure 2.1. Diagram illustrating the distribution of electrons and positive ions in an electron avalanche, redrawn from [6]

Figure 2.1 shows a pictorial view of the streamer. The space charge contained in the head of the avalanche produces a distortion in the electric field. The distorted electric field is the greatest at the head of the avalanche where the ion density is the greatest. A field radial to the direction of the avalanche axis is also produced. When the tip of the avalanche has reached the anode, the electrons are absorbed into it and the slower moving positive ions are left in the cone shaped volume extending from the anode to the cathode. The ion presence does not cause breakdown of the gap. In the gas surrounding the avalanche, photoelectrons are produced by the photons produced from the densely ionised gas forming the avalanche track.

These electrons initiate auxiliary avalanches which, if the space charge field is E_r is of the order of the external field E, will be directed towards the axis of the main avalanche as shown in Figure 2.2.a.

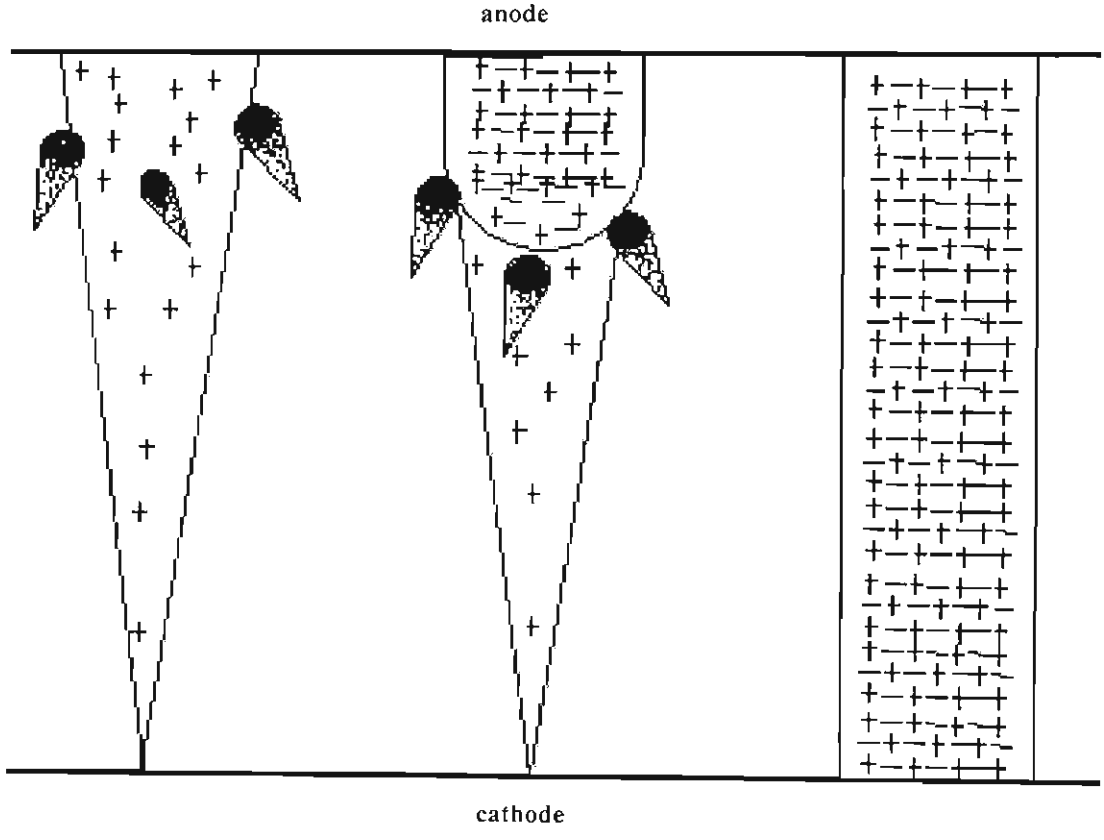

Figure 2.2 Diagram illustrating the transition from an electron avalanche to a streamer and the subsequent growth of the streamer across the gap (left to right a, b, c) - (redrawn from [6])

The greatest occurrence of these avalanches will be where the space charge field supplements the external field. The positive ions left behind by these avalanches effectively lengthen and intensify the space charge of the main avalanche in the direction of the cathode. The process continues as a self-propagating streamer as shown in Figure 2.2.b. The streamer proceeds across

the gap to form a filament of highly ionised gas between the electrodes as shown in Figure 2.2.c. This filament formation constitutes breakdown of the gap. The voltage collapses and the external circuit discharges through the gap.

" If a voltage is applied to the gap in excess of the minimum breakdown value, the space charge field E_r developed by the avalanche attains a value of the order of the external field E before the avalanche reaches the anode. In this case mid gap streamer formation occurs with both cathode-directed and anode directed-streamers developing from the head of the avalanche. The value of the radial field E_r caused by space charge in the electron avalanche can be calculated and is given by:

$$E_r = 5.3 \times 10^{-7} \alpha e^{\alpha x} / [(x/p)^{1/2}] \quad \text{volt/cm} \qquad (2.62)$$

Where x centimetres is the distance travelled by the avalanche, p millimetres Hg is the gas pressure and α is the primary coefficient of ionisation by electrons corresponding to the externally applied field E. The transition from an avalanche to the more rapidly growing positive and negative growing streamers is considered to occur when $Er \cong E$" [6].

Rapid breakdown occurs for higher applied voltages due to the streamer transition taking place in the mid gap region, thus a shorter formative time for the production of spark. The ion multiplication in an avalanche required to cause the avalanche streamer transition is approximately 10^8 [24].

Through investigations scientists have concluded that the minimum breakdown value of gaps up to 10 cm is set by the Townsend mechanism while the streamer mechanism initiates the breakdown if an over voltage is applied. Meek states that it is possible to reconcile the Townsend theory and the streamer theory of spark if one considers that the streamer theory is an elaboration of the Townsend process of ionisation by electrons and secondary ionisation in the gas.

2.7 The Corona Discharge

The word "corona" literally means the disk of light that appears around the sun. However in the field of high voltage it refers to the partial discharges that develop in zones of highly concentrated electric fields. The corona discharge is quite distinct in nature and appearance from the complete breakdown of air gaps between electrodes. The following is a list of observable effects:

- Visible light
- Audible noise
- Electric current
- Energy loss
- Radio interference
- Mechanical vibrations and
- Chemical reactions producing small amounts of O_3 and nitrogen oxides.

The mechanism of corona discharge depends on the polarity of the voltage applied.

2.7.1 Positive Corona

Positive corona starts off due to ionisation by collision at the anode, which then leads to an electron avalanche. Positive ions formed due to the ionisation process form an extension to the anode. Secondary generation of avalanches called onset streamers leads to a glow discharge where numerous onset streamers that are short in length overlap in space and time. The current through the HV electrode is said to be quasi steady.

2.7.2 Negative Corona

Negative corona is sometimes referred to as Trichel pulse corona that has a rapidly and steadily pulsating mode [6]. The photons from initial avalanches get radiated in all directions. Photoelectrons thus start subsidiary avalanches. With an increase in applied voltage, the trichel pulses increase at a repetitive rate up to a critical level at which the negative corona gets into the steady "negative glow" mode.

2.7.3 AC Corona

The basic difference lies in the periodic change in direction of the applied field and its influences on the residual space charges left over from the discharge during preceding half cycles [25]. If the applied voltage has a suitable magnitude, both positive and negative glows and streamer coronas can be observed in each cycle.

2.7.4 The Corona Onset Level

Corona starts at the HV electrode and conductor surface when voltage gradients reach a critical value E_0.

E_0 depends on:

- Voltage polarity
- Pressure

- Temperature
- Conductor Diameter
- Conductor surface irregularities

2.8 Large Air-Gap Breakdown

Investigations carried out by Allibone and Meek (1937-38) using a rotating film camera enabled finer details of the corona and leader stroke growth to be recorded [6]. By adjusting circuit conditions it was found that the speed of development of the spark could be controlled. An increase in the series resistance causes a decrease in the speed of the leader stroke. Leader propagation is an important phase in the discharge breakdown of long gaps. The voltage drop along the leader channel and therefore the flashover voltage is largely governed by the electric properties of the leader channel [26]

A typical discharge between a positive high voltage point and an earthed plane (using a 130cm gap as an example) follows the following observable pattern:

- The discharge is seen to be initiated at the positive point by a leader stroke that grows across the gap to the negative plane.
- When it reaches the plane a return stroke develops along the filamentary ionised track traced out by the leader stroke.
- A branch of the leader stroke from the point electrode is retraced by the main stroke of the discharge. The time interval between the initiation of the leader stroke and the main stroke was observed to be 95μs.
- The initial velocity of the leader stroke was 8×10^3m/s.
- The final velocity of the leader stroke was 2.5×10^4m/s.
- Total time from the initiation of the leader stroke to the occurrence of the main stroke depends on the gap length and circuit conditions and varies appreciably between successive discharges. Typical values for a 100cm gap are: 10μs for 1kΩ series resistor and 16μs for a 1000kΩ resistor.

If the set-up was changed and a point electrode was placed on the negative plane then the mechanism of spark is altered. After the downward growing positive leader travels a part of the way through the gap a negative leader starts growing upwards from the earthed point. The two leaders then grow towards each other and when they meet the main stroke occurs. This main stroke follows the track traced out by the two leader strokes.

When a negative impulse voltage is applied to the point electrode distinct differences are noticed. The discharge is initiated by a negative leader stroke that develops in a series of sharply defined steps from the negative point. Each step extends the path traced out by the previous step. When the process has developed across more than one fifth of the gap length a continuous leader stroke proceeds. While all this is happening a positive leader stroke is initiated at the other electrode and these two leaders grow to meet in the mid gap region. When the two meet, the return stroke occurs. The upward growing positive leader stroke and the downward growing negative leader stroke are branched in the direction of their propagation. A voluminous shower of discharge occurs between them. A frequent occurrence of mid gap streamers which may be several centimetres in length is an interesting feature of negative discharges. Meek states that the height above the plane of the junction point of the two leader strokes, when expressed as a percentage of the gap length, decreases as the gap length increases. If a point electrode is placed on the earthed positive plane the upward growing positive leader stroke is initiated at the point and its progress is enhanced, with the result that the junction point with the downward growing negative leader occurs relatively closer to the high voltage negative point.

Meek has stated the following in [6]: "There is, as yet, no complete quantitative theory of corona and spark breakdown in uniform fields, although various theoretical explanations have been given of some of the observed features and leader-stroke growth."

Quantitative criteria based on the Townsend theory and the streamer theory are of limited value to the high voltage engineer since the results are not sufficiently accurate and can often not be applied at all, because the necessary physical data are not available.

Pedersen in a paper on calculation of corona starting voltages in non-uniform fields points out that Photoionization is important to the formation of the streamer [27]. Pedersen uses an empirical method to calculate a function from which the breakdown voltage is inferred. This was just another effort by another scientist to give some sort of calculation to determine the spark breakdown or corona starting voltages.

2.9 Parameters Affecting the Breakdown Process

2.9.1 Distance and Voltage

With long gaps under divergent conditions, the breakdown develops in three main phases [28], [29]:

- First corona
- Leader propagation
- Final jump

Each of the above stages has statistical fluctuations in their parameters. These fluctuating values are combined together to form the variance in the 50% breakdown voltage and the spread in the time to breakdown for each voltage level. There is also observable discontinuity in the spread of the 50 % breakdown voltage. Baldo and Gallimberti [12], studied the influence of the different phases upon σU_{50}(the variance in the 50% breakdown voltage), T_B(time to breakdown) and σT_B(the variance in the time to breakdown), by varying in a wide range both the gap spacing and the peak value of the applied voltage [30].

It was found that if the crest voltage and hence the field rate of rise *dE/dt* is increased, the minimum and the mean inception time lag together with the dispersion in the distribution decreases. The opposite behaviour was observed for measured inception fields. It was observed that both the minimum and the mean values of the measured inception fields decreases with *dE/dt*. Baldo and Gallimberti found that both quantities had the minimum value of 31.2 kV/cm at *dE/dt* equal to zero [31]. The amount of charge injected into the gap at a specific inception field depends upon the gap length because the streamer path extends into the region where the field distribution is no more the same.

It was found that the mean value of T_L(time from leader inception to final jump) together with its standard deviation σT_L, have a tendency to decrease as the over voltage ratio is increased. The real leader length is proportional to the time of leader propagation. This means that for a fixed applied voltage, the average value of the velocity and the standard deviation of the average velocity are independent of gap length.

Baldo and Gallimberti state that the average current associated with the leader propagation is strongly dependent on both the gap length and the over voltage ratio.

The final jump occurs within 1 or 2 μS after the arrival of the streamers at the plane. Baldo and Gallimberti have also proven just as Gracia and Hutzler did, that the axial length of the leader channel at the transition time to the final jump and hence the height of the final jump depends strongly on the applied voltage [31], [32].

"The corresponding time duration of the final jump T_j is of the order of 20μs and this value together with its dispersion σT_j (about 2μs) is practically independent of both the voltage and the gap length. This depends on the fact that the velocity of the leader grows almost exponentially in time: therefore the total duration of the final jump does not vary appreciably with its length." [31].

2.9.2 Effect of Wave Shape Variation

One of the most important parameters affecting the breakdown process is the effect of wave shape variation due to switching surges of different shapes.

Under this topic one of the main considerations is that the change in the amount of the charge injected into the gap by pre-discharges generated at the high voltage electrode depends upon the time taken by an impulse to reach its crest value. Thus a larger amount of charge is injected for longer times. Since the electric field along the gap is modified by space charges, this process affects the magnitude of spark over voltage.

The effect of impulse time-to-crest on spark over voltage is noticeable when the 50% spark over voltage is plotted as a function of time to crest. "The characteristic, shaped like a 'U' is called the 'U-curve' and is also observed in most other configurations such as rod-plane, rod-rod or conductor-plane for gaps >1m" [33]. The minimum of this curve represents the most extreme case, since it determines the lowest electrical strength for a given air gap arrangement. (See figure 1 in [33]). The coordinates of this minimum are called 'the critical time-to-crest' and 'the critical flashover'.

Thione expressed the critical time-to-crest as:

$$T_{cr}(crit) = (50 - 35\,[k\text{-}1]\,d) \qquad \mu s \tag{2.63}$$

where:

d = gap spacing in meters

T_{cr}(crit) = critical time-to-crest in μs, and

k = the gap factor defined by Paris.

The definition and a description of gap factor is given in Appendix 1.

When the critical time-to-crest is plotted as a function of gap spacing the general trend is that the critical time to crest increases linearly with gap spacing. It has also been found that for gap spacing ≥ 2m the critical time to crest for the rod-rod gap is lower than that of the rod plane arrangement. Since the dielectric characteristic of the rod-rod gap is comparable to that of a conductor-conductor arrangement, the result will indicate that for the conductor-conductor geometry, the critical time to crest can be lower than for that of a reference rod-plane gap.

By experimentation it has been seen that an increase in air humidity shifts the critical time-to-crest towards lower values [33]. The influence on the breakdown voltage of wave tail time can be summarized as follows:
"The 10% and the 50% spark over voltages were found to increase with wave tail reduction when the time to crest is kept more or less constant" [33].

The most crucial geometry used to assess the electrical strength of external insulation is the rod-plane gap stressed with positive switching impulses. Gallet expressed the minimum breakdown strength of any air-gap configuration under critical conditions as:

$$V_{50}(\min) = V_{50}(crit) = \frac{k \times 3400}{1 + \frac{8}{d}} \qquad [\text{kV}] \qquad (2.64)$$

Parris expressed the spark over voltage for the standard switching impulse of 250/2500 μs as [33]:

$$V_{50} = k.500d^{0.6} \qquad [\text{kV}] \qquad (2.65)$$

It has been stated by Boutlendji and Allen in [33] that the value of k depends upon the atmospheric conditions and the minimum of the U-curve and thus the critical value of the spark over voltage becomes a function of both air density and humidity variations.

For small times to crest, close to the critical value there is no extinguishing of the leader propagation. There are also no primary dark periods for electrodes with large curvature radii, however at least one primary dark period exists for electrodes with small curvature radii.

Tests performed on rod plane gaps with impulses having critical time to crest have shown that spark over occur practically on the impulse crest [34]. Waters in [35] has stated: "The minimum spark over voltage arises when the time to breakdown T_B is equal to the time to crest T_{cr}. Under these critical conditions T_B is mainly controlled by the leader velocity. Neither gap length nor geometry has any influence upon this minimum stable velocity."

The whole phenomena of the discharge process present dispersions in each of its stages. The effect of these dispersions is shown by the existence of a probability function. The lowest impulse that could lead to spark over is that for which the most favourable conditions occur, i.e. leader progression along shortest path and minimum continuous leader inception time.

2.9.3 Influence of Air Humidity

The influence of air humidity is important when positive streamers are the determinant pre-discharges during the pre-breakdown process. A humidity coefficient ε is defined using the linear characteristic $V_{50\%}$ versus absolute humidity h as follows:

$$V_h = V_{11}[1 + \frac{\varepsilon}{100}(h - 11)] \tag{2.66}$$

valid for $0.5 \leq d \leq 8m$ and

$5g/m^3 \leq h \leq 20g/m^3$

Where:

V_h = 50% spark over voltage at humidity h

V_{11} = 50% spark over voltage at humidity 11g/m3 (corrected to standard air density δ, numbered to unity, when the pressure and temperature are equal to 1013 mbar and 293 K respectively.

The humidity correction factor is then defined as:

$$K_h = \frac{V_h}{V_{11}} = 1 + \frac{\varepsilon}{100}(h - 11) \tag{2.67}$$

2.9.4 Temperature and density effects

The progress of a streamer in air depends upon the availability of negative ions in the atmosphere to provide successive initiating electrons and also upon the dynamics of negative ion reformation behind the electron head. A review of data on the dependence of negative ion type and relative concentrations show that there are sharp dependencies upon temperature.

Allen and Ghaffar have shown that the principal effect of a variation in temperature is caused by the consequent change of air density [19], [36]. The specific effects of temperature upon ionic species, thermal energy of neutrals, etc are insignificant. They conducted some experiments on the effect of temperature on the propagation field. When the results were adjusted by a factor $(\delta)^{1.5}$, the temperature dependence of the propagation field is insignificant. Relative air density δ is defined as:

$$\delta = (\frac{p}{1013}) \times (\frac{293}{T}) \tag{2.68}$$

Where p is the pressure and T is the temperature in Kelvin.

This phenomenon was constant over the temperature range -14°C to 148°C (259K to 421K)

2.10. Properties of the Leader

2.10.1. Leader Gradient

The electrical gradient within the leader cloud is one of the most important single parameters governing the spark over characteristics in highly non-uniform fields. Field probes have played an important role obtaining measurements of this gradient.

A typical example of the leader gradient as given in [35] is in table 2.1.

Table 2.1 Typical values of leader gradient and length (10m rod/plane gap at $V_{50\%}$ (critical spark over))

Leader Length(m)	2	3	4	5
Gradient MV/m	0.5	0.35	0.25	0.18

This shows that the leader tip potential varies slowly during its development.

2.10.2. Leader Diameter

Measurement of the leader radius by direct photography is difficult due to the limited resolving power of this method. Strioscopy and high-speed image recording have overcome this problem.

Ross found that the thermal boundary of a leader channel could be measured with a precision of ± 0.1 mm. By using this method it was noticed that the diameter of a given section of the channel increased with time, giving a tapered appearance to the leader at any instant. The rate of radial expansion was less than 100m/s in all cases measured [35]. This indicated that the gas pressure within the leader channel remained constant at the ambient value.

With the aid of image converter recording and strioscopy, Gilbert was able to detect the density change within the leader core and also the generation of a sonic wave associated with the leader [37].

2.10.3. Gas Density Reduction

The expansion of the leader channel and the decreasing axial gradient characteristic are clearly related parameters. Waters states that the records of the channel show that the neutral particle density within the channel is a decreasing function of time [35]. This reduced density is the basic explanation of how the leader channel conductivity can be studied.

At atmospheric density, a field of about 3 MV/m is necessary to maintain direct impact ionisation. An expansion of the leader radius by a factor of 3 will reduce the required field to little over 0.3 MV/m. This value approaches the average fields available in long gap flashover.

2.10.4 The Final Jump

Gracia and Hutzler used an image converter camera on different gap length rod plane configurations in order to observe the effect impulse wave shape has on the final jump [32].

From the observed images it can be seen that as the leader develops into the gap, it is preceded by a corona cloud effect. The streamers forming the corona have a length depending on the external field strength. The final jump is said to begin when the streamers reach the negative plane due to the electric field in the unbridged gap being sufficiently high.

A luminous phenomenon starts from the negative electrode following probably the same path of the streamers and climbing up to the leaders head. As soon as the final jump-starts, there is an exponential growth in the leader speed. The return stroke is said to travel at approximately one fifth the velocity of light [32].

It was found that the height of the final jump increased with the crest voltage applied to the gap [32]. When the height of the final jump was plotted against the value of the breakdown voltage, the data fitted well about a straight line having the equation as follows:

$$U_B = 0.44\,S + 0.15 \qquad (2.69)$$

Where:

S = the height of the final jump in meters, and

U_B = the breakdown voltage in Mega volts.

The same dependence was seen for different electrode configurations, different distances and different wave shapes. This would mean that the final jump height is independent of gap geometries and time to crest. Circuit parameters also have no influence on the start of the final jump. Gracia and Hutzler found that for an electrode spacing less than 2.4m direct breakdown occurs, i.e. no leader and no final jump. For gap distances greater than 2.4m, the curve follows a linear law. This means that the condition $D = 10R$, where R is the curvature radius of the hv electrode, usually used to define the transition between direct breakdown and leader breakdown is not observed.

The duration of the final jump was seen to be constant and had a value of between 15 to 25μs. The mean axial velocity during the final jump is a function of the applied voltage. The values of the mean electric fields in the leader, in a first approach, can be estimated to be 1 kV/cm and the mean electric field in the streamers during the final jump can be approximated to be around 4 kV/cm.

2.11 Conclusion

This chapter has taken us from the basic concepts of the kinetic theory of gases through to the concepts of Townsend's coefficients and Meek's streamer theory. This has resulted in a better understanding of the relatively more complicated leader type breakdown of large air gaps. The different mechanisms of ionisation and electron recombination have been presented. The phenomena of corona have also been explained. The latter part of the chapter gave attention to the leader mechanism and its observed properties.

Many scientists and engineers have made great effort to model the leader breakdown mechanism. One such attempt was made by Rizk [38] which tried to address the following issues:

(a) There exists no formula for continuous leader inception voltage, related to gap length and electrode geometry.
(b) Several useful empirical formulae are available for calculation of spark over voltage of a rod plane gap, however each is naturally valid within a certain range of gap spacing and bears little or no physical correlation to our present day knowledge of the discharge mechanism.
(c) Critical radius can only be determined from experimental results or empirical formulae.
(d) There appears to be basic contradiction between a widely used formula for the height of the final jump and the latest spark over data of very large air gaps at that time

By modelling the space charge in the air gap as a cylinder having its axis on the rod-plane axis, Rizk[38] was able to derive a formula for the electric field strength at any position along the air gap. Using this it was possible to derive an expression for the leader inception voltage of the rod-plane configuration. Meek also provided an analytical tool to predict the critical radius of the HV electrode [38].

There has been great effort to model the development of the positive spark in long air gaps [29], [39], [21], [40], [41], [42]. This type of research is still on going especially with the advances

that are made in computing and imaging resources. Our study is not concentrated on the mathematical modelling of the mechanisms but rather on the physical attributes of the fire-induced flashover.

Chapter
3

Air Gap Breakdown in the Presence of Fire and Flames

3.1 Introduction

This Chapter can be divided into three major sections. The particle-initiated flashover theory is explained first. This is followed by the Reduced Air Density (RAD) theory and the latter part develops the theory of the flame conductivity.

The particle-initiated flashover has been researched in the past by Naidoo and Swift who have published results of their work in [17]. Sadurski and Reynders [11], [58] also performed experiments with both flames and particles as described in section 3.4. A summary of the findings of all work in this area prior to 1992 is provided in the Cigre guideline [59].

At the conclusion of this chapter lies the completion of the flame conductivity theory of flashover. All the reasons as to why this hypothesis is to be deemed reasonable is built up in sections 3.5 to 3.7 and is summarized in section 3.8.

3.2 The General Influence of Forest Fires on Line Insulation

In order to determine the extent to which the phase to ground and phase to phase breakdown voltage is affected by the presence of fire, Mercure and Lanoie [8] in 1987 performed tests where spruce trees were burned under transmission lines. These tests were conducted on the following lines:

(a) ±450 kV dc

(b) 735 kV ac

Analysis of voltage and video recordings allow the flame resistance Rf and flame resistivity ρf to be estimated. Results for a 6.7-meter air gap were as follows:

$$50\text{k}\Omega \leq Rf \leq 1000\text{k}\Omega$$

$$70\text{k}\Omega\text{m} \leq \rho f \leq 500\text{k}\Omega\text{m}$$

The current flowing in the flame is concentrated into an arc in less than 5 ms [8]. There was no explanation provided for this. Mercure and Lanoie's preliminary results show that the mean electric field gradient $E < 33\text{kV/m}$.

They also observed the following [8]:

(a) Smoke has no effect on the line insulation. This same effect was observed in [43].

(b) Changes in air insulation were observed only when the tips of the flames began to approach the line.

(c) The flame temperature was approximately 1000°C giving a relative air density ≈ 0.2. According to IEEE standards one could expect a 50% reduction in the efficiency of the air insulation based on temperature effects alone, but test results yield a figure of ≈ 90%. Therefore it can be concluded that a RAD effect alone cannot explain the drastic change in air insulation

(d) It was noted that when the flames were produced by burning spruce trees without the needles, which is known to contain far more dissolved mineral salts than the bark, flashovers were more difficult to record. This implies that the physical characteristics of the fire are important criteria in flashover determination.

3.3 Particle-Initiated Flashover

In order to investigate the effects large particles related to sugar cane fires have on the AC breakdown strength of air insulation, Naidoo and Swift used an experimental method with parallel tubular conductors 500mm apart [9]. The following three parameters were varied and the effects were recorded:

(a) Type of material: No set pattern can be seen when the type of material was changed. Thus no solid conclusion can be drawn.

(b) Length of material: There is an exponential decrease in breakdown strength as particle length increases.

(c) Spacing between particles: There is a greater reduction in breakdown strength if one end of the particle is in contact with the electrode surface. When the total particle length is fixed at 300 mm and the number of particles is varied the following is observed – Smaller individual spacing does not necessarily mean a lower breakdown voltage. The effect of particles in contact with the electrode is greater but not so noticeable when particles are very many. (Noted case =10)

In the above experiments it was noted that the breakdown path was through these particles whose configuration substantially reduced the breakdown voltage and along the surface of those particles whose configuration did not substantially reduced the breakdown voltage. It was found that in an electric stress of 10kV/m the resistance of the sugar cane particles was about 10MΩ/m for those particles that substantially did reduce the breakdown voltage.

3.4 Reduced Air Density Flashover

In the late 80's, a high temperature furnace was used by Sadurski and Reynders [11] to detect the effects of temperature on air insulation. A temperature range of 20°C to 500°C was investigated. The results showed that the effect of thermal ionisation over the entire abovementioned range of temperatures is negligible and that the flashover voltage may be considered as a function of the gap size and air density only.

However at 1100°C the breakdown voltage tends (due to extensive thermal ionisation) to be only about 15% lower than that obtained from the density effect alone.

In order to separate the effect of temperature and the effect of the presence of a flame in small air gaps, the following two cases were investigated. Different electrode configurations were also used.

(a) AC flashover voltage of the gap at 24°C. The results were then adjusted to an air density corresponding to 900°C.
(b) AC flashover of the air gap when spanned by a butane flame.

The results are summarized in Figure 2 in [11]. From the obtained results it is apparent that the flashover voltage of the gap spanned by the flame is independent of the shape of electrodes and is influenced by a parameter other than the temperature. To investigate this parameter, the leakage current was monitored during the test and it was noticed that the high frequency peaks of discharge currents are caused by the discharge to and from the carbon particles released from a soot covered (from the fire) electrode. The effect was less pronounced after cleaning the electrode. It is said that the discharge between particles and the electrodes changes the field distribution in the gap from uniform to non-uniform.

For long air gaps, a series of AC tests were carried out by Sadurski, in order to determine the influence of the flame and the presence of floating particles. The following statements describe their test setup and procedure:

(a) Rod-plane and conductor-plane electrode configurations were used.
(b) A particle injector was used to inject a fixed amount of particles (between 2 and 5 milligrams) into the gap.
(c) First a clean butane flame spanned the air gap and tests were conducted.
(d) With the air gap at room temperature the following floating particles were injected:

(i). Aluminum -size 0.005 to 0.2 mm

(ii). Sawdust –size 0.01 to 0.2 mm

(iii). Fine ash obtained from burned grass.

(e) Lastly the gap was spanned by flame with floating particles obtained from burned grass.

The following are the conclusions that can be drawn:

(a) There was 75% reduction in the breakdown voltage of the air spanned by a clean butane flame.

(b) The presence of floating particles in the air gap at room temperature reduces the flashover voltage by 20 to 30%.

(c) The following was observed for a particle filled flame-spanned gap:

(i). Non –self sustained breakdown

(ii). Flashover was triggered by floating particles

(iii). Corona was extinguished when particles move to non-crucial areas.

(iv). No conditions leading to a stable arc, even when large amounts of particles are introduced into the gap.

(v). The resistance of the gap is high and depends on the amount of particles in the gap.

However one must keep in mind that this applies to small gaps of up to 1m.

3.5 Flames and Combustion Phenomena

"Combustion commences in chemistry with the occurrence of self supporting exothermic reactions" [44]. The conduction of thermal energy, the diffusion of chemical species, and the bulk flow of gasses all follow from the release of chemical energy in the exothermic reaction. Strictly speaking, "the term explosion refers to the violent increase in pressure which must accompany the self acceleration of the reaction" [44].

Basically a flame is described as a combustion wave. A flame is caused by a self-propagating exothermic reaction that is accompanied by a luminous reaction zone. There are two main types of flames, viz. diffusion flames and premixed flames.

3.4.1 Premixed Flames

In a premixed gas flame the reactants gasses are intimately mixed and the burned gas leaving the flame front has a higher velocity, a lower pressure and a lower density than the initial

reactant gas. When the release of chemical energy is taken into account, with the consequent rise in temperature, it is found that the pressure change across the flame is relatively low. This pressure change is typically 1/1000th or less of the total pressure and is therefore usually unimportant [44].

An element of flow can receive heat in two ways i.e. either from the chemical reactions occurring within it or by conduction from the hotter gas ahead. The temperatures of flames for some common fuel gases are listed in Table 3.1, [44].

Table 3.1 Flame Temperatures for some common fuel gases

Reactants	Flame Temperature(°C)
$H_2 + O_2$	2500
$CO + O_2(+ H_2O)$	2925
$CH_4 + O_2$	2780
H_2 + Air	2045
CO + Air($+H_2O$)	2000
CH_4 + Air	1960
C_2H_3 + Air	2250
C_2H_4 + Air	1975
C_2H_6 + Air	1895
C_2H_8 + Air	1925
C_2H_{10} + Air	1895

The adiabatic flame temperature, which is the other fundamental property of the flame, can be calculated from the thermodynamic properties of the reactants for relatively cool flames [44]. The following is the approach:

(i). Calculation of energy released by conversion to products at room temperature

(ii). Thereafter the calculation of the temperature at which these products will have acquired an enthalpy equal to this heat release.

Flame temperatures usually lay in the range 1000 K to 3500 K [44], [10], [45], [47].

3.4.2 Diffusion Flames

Diffusion flames, also known as jet flames differ from premixed flames in that combustion occurs at the interface between the fuel gas and the oxidant gas and the burning process depends more upon the rate of mixing than on the rate of the chemical processes involved. In slow burning diffusion flames (like a candle) the fuel rises slowly and laminar flow occurs. The mixing process occurs solely by molecular diffusion and the properties of the flame will be

determined only by molecular quantities. In industrial burners the fuel is usually introduced in the form of discrete droplets, burning is rapid and the mixing process is associated with the turbulence of the flow.

If a cross section through the diffusion flame were to be taken the following would be observed:

(a) The fuel concentration is a maximum at the flame axis and falls away rapidly towards the flame boundary.

(b) The oxygen concentration starts of as zero at the boundary and slowly increases outwards.

(c) The product concentration is at its peak at the boundary and decreases both towards the axis and away from the boundary.

The position of the boundary is the point at which the fuel oxidant ratio is stoichiometric. As the fuel concentration will decrease with height, the position of the boundary moves towards the axis and converges at the tip where all the fuel is consumed. This basically says that the flame is conical in shape with the flame boundary corresponding to the reaction zone. The flicker observed in diffusion flames is generally due to the eddy effect. [44]

3.6 High Temperature Combustion of Hydrocarbons

In premixed flames, the mechanism of combustion differs markedly from that of low temperature oxidation. This type of flame combustion is often referred to as true ignition. When true ignition occurs, the majority of the enthalpy of the reaction is released rapidly in a narrow reaction zone leading to the production of very high temperatures. These high temperatures produce steep temperature gradients and the transport of heat or of active centers makes the flame self-propagating.

High temperatures generated provide the key to the change in the mechanism. At high temperatures, ion concentration will be high because the Boltzman factor tends to unity and because the increase in entropy always favors dissociation [44]. Typical flames in oxygen at 2000-3000°C may contain 10-50% of the fuel in the form of ions [44]. As a result of the high temperature all reactions will become correspondingly faster. The nature of the dominant active ingredient is also likely to change. Simple ions and atoms replace the degenerate branching species such as peroxides and aldehydes.

3.7 Ionisation in Flames

A study of the hydrogen flame spectra has shown that the band head at 2608 (ultraviolet) corresponds to energy of excitation of the OH ion [45]. The OH radiation is not appreciably

stronger in the reaction zone than in the burned gas downstream. The reaction zones of hydrocarbon flames show a stronger radiation than that of the hydrogen flame. In flames of hydrocarbons and other organic compounds, the free zone of chemical reaction is distinctly marked by chemiluminescent radiation. Prominent among the emitting species are free ions C_2. They apparently owe their origin and excitation to a highly exothermic reaction step in the mechanism of formation of carbon. This is a two-step reaction [45]:

(i). Partial stripping of hydrogen molecules by reactions with free ions such as OH that are present in the reaction zone in substantial concentration.

(ii). Polymerization of several such highly unsaturated carbon skeletons into graphite groups C_6, releasing large amounts of energy and splitting of excess carbon atoms.
E.g.: $8C \rightarrow C_6$ (graphite nucleus) + C_2 (radical)

Other numbers are also possible and there is evidence for the presence of free C and C_3 in hydrocarbon flames. The predominance of C_2 in hydrocarbon flames over other ions is due to the relatively high stability of C_2. The graphite nuclei C_6 disappear quickly when sufficient oxygen is present but forms centers of carbon particles in over rich mixtures. The mechanism of hydrogen stripping and carbon concentration is complex and varied. The dehydrogenated fuel molecules largely break down to acetylene, which then aggregates with further dehydrogenation. It is found that the C_2 concentration increases as the hydrocarbon concentration increases. Ions are found in hydrocarbon flames due to chemi-ionisation reactions [44], [27], [46].

$$CH + O \rightarrow CHO^+ + e \qquad (3.1)$$

Followed immediately by the charge exchange reaction

$$CHO^+ + H_2O \leftrightarrow H_3O^+ + CO \qquad (3.2)$$

H_3O^+ is the dominant ion in both fuel lean and slightly rich hydrocarbon flames. CH_3^+ is the dominant ion in very rich and near-soothing flames formed by:

$$CH + C_2H_2 \rightarrow C_3H_3^* \qquad (3.3)$$

Ions decay by reactions such as:

$$H_3O^+ + e \rightarrow H_2O + H \qquad (3.4)$$

It is suggested that a mechanism for ion formation based on the consideration that the thermonic work function of a comparatively small aggregate of carbon atoms may be expected sensibly to be that of a large carbon particle which has a Thermonic work function of only 3.93 eV. Therefore graphite carbon nuclei that are formed from dehydrogenated hydrocarbon molecules may act as a source for ionisation [27].

Measured concentrations of ions in propane-air flames equals 10^8 to 10^9 ions/cm^3 [27], [48]. Table 3.2 shows the concentration of ions in three different types of flames. Flames containing potassium have a high ion concentration value since potassium has a relatively low ionisation potential. The principal reactants, CH and O, are produced by decomposition and other reactions of the fuel and oxidant. The CO and H species will continue to react and eventually will be incorporated into final products like CO_2 and H_2O. Over the years researchers have come to an agreement that the reaction in 3.1 is the main contributor for ion generation.

Table 3.2 Ion densities in various flames. Data taken from ref [10]

Flame	Typical Ion density (ions/m^3)	
	Observed	Predicted
Hydrocarbon-air	10^{18}	10^{12}
CO or H_2-air	10^{12}	10^{12}
Gas seeded with K or KCL	10^{18}	10^{18}

In most flames H_3O is the most abundant ion, being formed by the charge exchange reaction. There are many secondary ions formed by similar reactions- e.g.: CH_3O^+, $C_3H_3^+$, and $C_2H_3O^+$. A technique of sampling ions with a microprobe and identifying them with a radio-frequency (rf) mean spectrometer revealed ion concentration profiles.

When an electric field is imposed on a flame and the rate of ion generation is measured by measuring the current from charged particles striking the electrodes, it was found that the rate was dependent on composition. A maximum value of $4x10^{23}$ ions /m^{3}sec of the reaction zone was observed in flames with low N_2 concentration and with CH_4/O_2 ratio slightly richer than stoichiometric.

If a flame passes through a strong electric field a number of complicated disturbances take place:

(a) The concentration of ions rises rapidly due to the ionisation of neutral molecules by collisions with the accelerated ions and electrons in the flame.

(b) Since the electrons are much more mobile than the gas, they are drawn to the positive electrode. This leaves the body of the gas positively charged

(c) The migration of the charged gas particles towards the negative electrode causes a Chattock pressure or an electric wind that distorts the flame in various ways.

(d) This effect may be macroscopic, changing the area of the combustion wave. It may also be microscopic affecting the structure of the combustion wave.

(e) Therefore it is understandable that a variety of phenomena may appear depending on the experimental arrangement and conditions.

3.8 The Effect of Electric Field on Flames

When an electric field is applied to a hydrocarbon-air flame, the flame is attracted towards the cathode. This is independent of the nature of flame being premixed or diffusion. The following are the effects that electric fields can have on flames:

(a) Increases the flammability limits of premixed flames

(b) Shortens the flame lengths

(c) Increases stability

(d) Flame temperature variation

(e) Impacts on heat release rates

(f) Changes noise and soothing characteristics

Electrons and ions are produced in small concentrations as by-product of complex chemical kinetics of combustion. Charged particles are also produced in flames seeded with alkali metals and salts.

"The electric field affects the motion of the charged particles, which then interact strongly enough with the surrounding neutral gas molecules to affect the concentration and flow of the neutral species" [10]. During the 18^{th} century many experiments were conducted in Europe that showed that flames were conductors of electricity and could be deflected by electric fields.

3.8.1 Ionic wind

As described before, charged particles that have preferential speed and direction, transfer momentum to the neutral gas in which the charges were submerged. This in time gives rise to a net force on the neutral gas.

Positive ions and electrons are produced in the fast reaction zone of hydrocarbon flames as by-products. Their concentrations are governed by the rate of production, recombination and

diffusion. When an electric field is applied to the flame, positive ions are accelerated preferentially in the direction of the cathode. Each time they undergo a collision they give up a portion of their momentum to the molecules with which they collide. The collision partners of the ions must be neutral species. Because the mean free path is small and the field reaccelerates the ions after each collision, each ion is responsible for causing a large number of neutrals to be displaced towards the cathode. The net result is that the electric field produces a body force or "ionic wind" which is the cause of the observed deflection of a flame toward the cathode.

Electrons have small masses and therefore the momentum transfer is low. Electrons need to travel long distances for momentum transfer to be efficient. Therefore collisions take place after long distance travel, often out of the flame region. In effect momentum transfer is from negative ions rather than electrons.

3.9 Conclusion

Section 3.5 describes the different types of flame structure. However bush, grass and cane fires do not specifically fall under either premixed or diffusion flames. They can be categorized as having some characteristics specific to both divisions. An important consideration that comes out of this section however is that hydrocarbon flame temperatures can be in the range of 1000°C to 3500°C. These severe temperatures will however greatly affect the degree of ionisation as described by Saha in equation 2.15. Thus the conductivity of the flame will increase with this increased ionisation.

It is further explained in section 3.6 that in high temperature combustion of hydrocarbons that the majority of the enthalpy of reaction is released rapidly in a narrow reaction zone leading to the production of very high temperatures and as a result of the high temperature all reactions will become correspondingly faster. Sugar cane fires are noted to be fast burning fires. It is therefore leads one to suspect that the fire itself must have very high temperature flames.

From section 3.7 it is quite clear to see that there are a large number of ions present in the hydrocarbon flame. Table 3.2 also shows that this value would be in the order of 10^{18}. It can be assumed that there are three sources of ions:

(a) Ions present due to the chemi-ionisation process involved in hydrocarbon combustion
(b) Ions that are created due to thermal-ionisation due to the temperature of the flame.
(c) Ions present due to photo-ionisation.

Two of the most important conclusions that can be drawn from section 3.8 is that the presence of the electric field in a flame changes the heat release rate and causes an ionic wind. This allows us to believe more easily that the flame could possibly get very hot at times, and thus becoming very conductive.

All of the above points to the fact that there is a high possibility of there being a very conductive flame present, even for a very short time. This is the basis for the flame conductivity theory. It is believed that the flame channel itself becomes very conductive due to the presence of ions [48] and allows most of the voltage to be dropped across the air-gap between the flame tip and conductor. This causes an enhanced electric field in the air-gap itself. Often the enhanced field is sufficient to engage corona inception and sustenance throughout the gap. Thus flashover is the result.

Chapter
4

A Simulative Study of Fire Induced Flashover on 400 kV and 275 kV Transmission Lines

4.1 Introduction

The purpose of this chapter is to document the simulations performed with the aim of understanding the physical aspects of the FIF. The objective and focus of the simulations are discussed and an outline of the simulative approach is also provided. The simulations were carried out using the Finite Element Method (FEM) hence the fundamental concepts of FEM are also touched on. FIF exists under various physical conditions; this study is focused towards some specific cases. The details and the reasons behind why these cases were of interest are presented. The majority of this chapter deals with the actual results and analysis, which are most important of all.

Finite Element Analysis is a subdivision of simulative research. It is discussed in Section 4.4. Under the heading of limitations however it is a well known fact that in any finite element simulation there is a problem when it comes to variation of the size of objects in the simulation geometry, i.e. it is difficult to work with both very large and very small objects at the same time within the same geometric setup, like a large air-gap (gap-length>1m) and a very small conductor. This was one of the difficulties experienced in this study.

4.2 Objective of Simulation

Due to the nature of the cane fire problem it is relatively difficult to do full scale experiments out in the field. It would be costly and difficult to arrange a cane fire under an energized transmission line. The other factor is that the physical attributes of the fire vary under different environmental conditions. The problem is wide and has a lot of depth.

As always simulations are undertaken in order to give some understanding of the problem without large amounts of effort and money. The objective of the simulations is to analyze the problem from many different angles. The Electric Field (E) is regarded as being very important in any flashover study. The effect of a number of factors influencing the E field strength is required in order to get a greater understanding of the flashover process. These factors are:

(a) Flame conductivity,
(b) Flame height,
(c) Line Voltage and
(d) Conductor sizes.

The effect of each of the abovementioned factors is investigated by conducting simulations of flame, air-gap and conductor geometries under various settings of the respective factors. The fundamental objective of this study is to get some understanding of the relationship between FIF and these factors.

One of the most important objectives is to gain some knowledge of how the flame conductivity changes the probability of flashover. It is believed that the temperature of the flame directly affects the conductivity and hotter flames are more likely to cause flashover [18].

The question arises: How will one know if the abovementioned objective is reached? It is already known from an observer's point of view of how breakdown strength is affected for different conditions in a cane fire. The results of the simulations can be evaluated against these observations. The objective of the simulations will be met if it results in a more reliable understanding of the problem in terms of the different conditions. It is important to the study that the results of the simulation are valid in the real world. As stated before validity comes from comparing observations in the real world scenario with the conclusions that can be drawn from the results.

4.3 Simulative Approach

If one looks at the cane fire flashover problem holistically it comprises three basic things:

(a) A Flame,
(b) An energized conductor, and
(c) An Air-gap in between

Basically the flame alters its properties in terms of shape, size and temperature during a cane fire. The changing flame structure is accompanied by a change in the properties of the air-gap. These two go hand in hand. The most basic form of any simulation can be done on the geometry of a flame beneath the conductor with a variable air-gap between the two.

The most important result is the electric field between the conductor and ground when the flame is in-between. One can evaluate the electric field strength in order to establish if flashover will take place. This is done by the two-factor corona inception and sustenance criteria as explained in section 4.6.

The simulative study was carried out for the cases of worst conditions:

(a) The worst condition of a flame beneath a conductor is when the flame tip is directly below the conductor as this will give the smallest air gap between flame and conductor.

(b) The critical time for the flame to be present is when the voltage on the line is at its sinusoidal peak since this will give the most intense electric field distribution in the air-gap.

4.4 Finite Element Analysis

The cane fire problem becomes very suitable for finite element analysis since it is a complex geometry with regions of different physical properties. To solve the electric field distribution by hand is almost impossible hence a finite element solution is not only very attractive but also crucial.

This study is conducted using a finite element software package called FEMLAB® that harnesses the mathematical computing power of MATLAB® by using it as an engine to do matrix computations. FEMLAB® is an interactive environment for modeling and solving scientific and engineering problems [51], [52]. FEMLAB® has the following attributes, which were advantageous to this study:

(a) Multidimensional – Allows one to simulate one-dimensional, two-dimensional and three-dimensional systems with full integration with MATLAB® and its toolboxes. Hence both two and three-dimensional models were simulated.

(b) Multiphysics – It is able to solve simultaneously a problem of multiple branches of science and engineering.

(c) Post-processing Flexibility – allows one ample freedom to view a solution in different visual modes. This allowed the effective extraction of electric field and voltage values at crucial points within the FIF geometry.

(d) Multiple Solvers – iterative solvers for linear and nonlinear stationary, time dependent, and eigenvalue problems. The stationary solver was used to get good convergence of the result.

(e) Adaptive mesh generation – Allows interactive mesh control. This feature was particularly helpful in increasing the mesh density around the HV conductors where electric field gradients were the highest.

(f) The interactive graphical user interface adapted to modeling in the field of Electromagnetics enhanced the ease of use.

The different steps that are carried out in the simulation of a single geometry are as follows:

(1) Drawing of the geometric model – The model geometry is sketched using the Drawing mode and the drawing toolbox.

(2) Boundary conditions – boundary conditions are set on both internal and external boundaries.

(3) Sub-domain settings – properties of the various sub-domains are set according to the respective material properties e.g. conductivity and material type.

(4) Mesh Generation – division of the geometry using a mesh creates finite elements.

(5) Solver operation – this is the solution step of the process, i.e. where the numerical method is used to solve the problem. Often the most difficult step.

(6) Post Processing – the many variables that have been solved may be viewed graphically in various ways. Data is extracted from the solution and plotted for analysis.

Note: (a) Steps 1 to 6 have to be repeated for every change in geometry, e.g. different flame height.

(b) Steps 3 to 6 have to be repeated for every change in a sub-domain property, e.g. different flame conductivity.

FEMLAB® is different from other FEM packages in that it takes both the resistivity and the permittivity of a medium into account when computing the electric field values of a geometry. Previously computational algorithms have been programmed to either operate on only one of the abovementioned, either resistivity or permittivity. Due to the fact that the cane fire problem has both conductive and insulating media, it is favorable to have a package that considers both resistivity and permittivity.

4.5 Simulated Conditions

As stated before, the problem may be reduced to basically a flame, an energized conductor and an air-gap in-between. Figure 4.1 and 4.2 show the geometric sketch of the simulation setup. As with the solution of most wide problems certain assumptions need to be made in order to narrow down the scope.

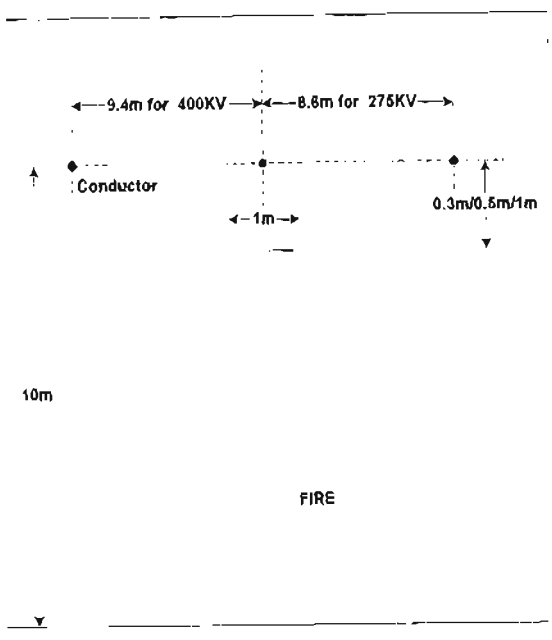

Figure 4.1: Model Geometry showing only one conductor representing the GMR case for a twin bundle

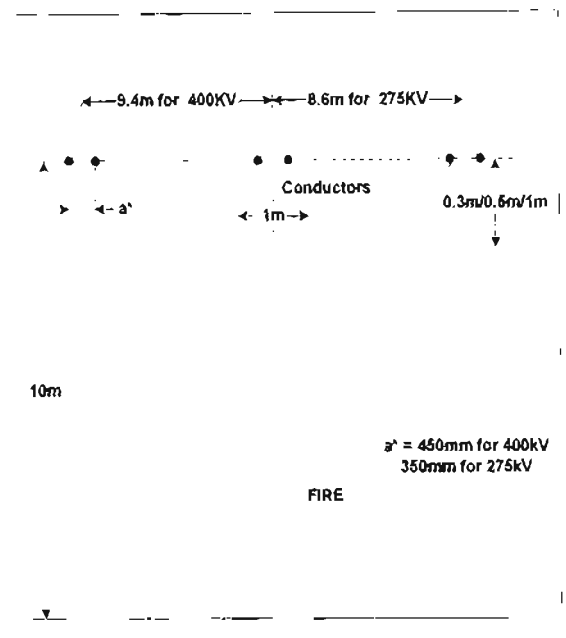

Figure 4.2: Model Geometry showing a twin bundle conductor

4.5.1 Assumptions

The following is a description of the assumptions made:

(1) A conical shaped flame – This shape is assumed due to field observations. The cane fire flames however erratic seems to more often than ever assume a shape that is wide at the bottom and narrow at the top. Thus the simulated flame is conical in shape.

(2) 400kV and 275kV lines - The focus of this study is on these two line configurations since these lines are most affected by cane fire flashovers.

(3) Four air-gap sizes – The investigation is based on four different gap sizes, 0.15m, 0.3m, 0.5m and 1m. These settings allow one to investigate the effect of gap-length on the electric field

(4) Ground clearance of 10m – This parameter is set as the minimum clearance by South African government specification and thus is the worst-case scenario.

(5) Flame base of 10m and width at tip of 1m – set by choice

(6) Flame positioning – The flame is positioned directly below the center conductor. This is the worst-case scenario for the center conductor.

(7) Smooth Conductors – The conductors were assumed to be smooth rather than being stranded. In order to represent stranded conductors the surface of the conductor has to be rough. This causes a problem in the mesh generation stage of the simulation. The software tries to fill the small gaps between strands with finite elements. This causes the number of elements in the mesh to increase phenomenally and the problem becomes too big to handle in terms of memory and computing power. This assumption is compensated for in this investigation as explained in section 4.5.3.

4.5.2 Simulated Cases

The simulative study is focused on the 275kV and the 400kV line configurations. These type of lines form the backbone of the national grid in South Africa. The impact is greater when these lines are tripped due to FIF. The structural drawings for both these lines and suspension towers are shown in Appendix 2. The regulation as to ground clearances warrants that these lines be at least 10 meters above the ground.

Simulations have been conducted in both the two-dimensional and three-dimensional environments. The other varying parameters are the flame properties:

(a) Flame height allows an air-gap between 0.15m to 1m

(b) Flame conductivity can be selected at will

Each simulation was done separately using the Geometric Mean Radius (GMR) of the conductor bundle and the exact conductor bundle itself. The concept of GMR is described in Appendix 3, which also contains the values of the GMR for the conductors represented in the simulation.

4.5.3 Simulation of the conduction problem using a static model

Figure 4.3 shows a simplified electrical model of the flame conductor geometry. The electrical elements are as follows:

(a) R_a is the resistance of the gap between conductor and flame-tip

(b) C_a is the capacitance between conductor and flame-tip

(c) R_f is the resistance of the flame, and

(d) C_f is the capacitance of the flame

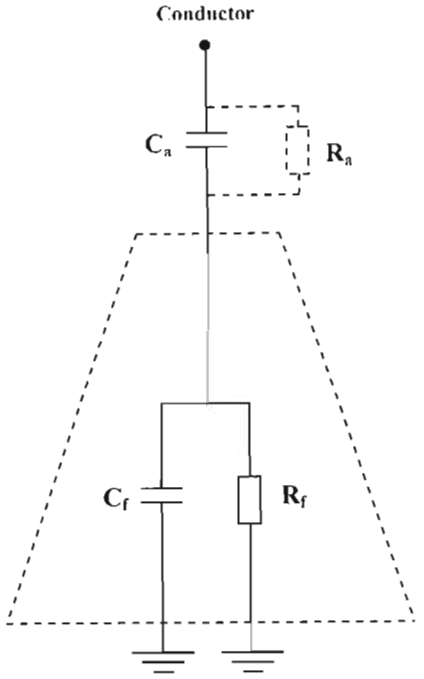

Figure 4.3: Electrical model of the flame-conductor geometry

The flame has impedance due to its capacitance and resistance, which varies with its conductivity. The air-gap also has both resistance and capacitance with the capacitance being the dominant impedance.

FEMLAB® is used in the electrostatic mode to investigate the FIF scenario. However the FIF scenario is a conduction problem with capacitive impedances as described above in the electrical model. In order to force the electrostatic representation of this model towards the conduction model an increased flame conductivity is used in FEMLAB®. The approximate relationship between these simulated conductivity values and the real values can be calculated. This is achieved as follows:

(a) For a particular value of simulated flame conductivity, the voltage at the flame tip is extracted out of the results of the simulation.

(b) Using this flame-tip voltage the required flame conductivity for the electrical model to hold true is calculated.

(c) Finally, this results in a mapping of conductivities between the simulations and the electrical model.

Figure 4.4 shows a graphical mapping of the flame conductivities between the simulations and the simplified electrical model. This result is extracted as an average value mapping of both the 275kV and 400kV cases. There is however some degree of non-linearity in this mapping as can be seen in Figure 4.4. This non-linearity can be attributed to the fact that the electrical model is a simplification of the real life geometry. Nonetheless, a good relationship between values is obtained. The range of values obtained for the electrical model is typical for a hydrocarbon fire [53].

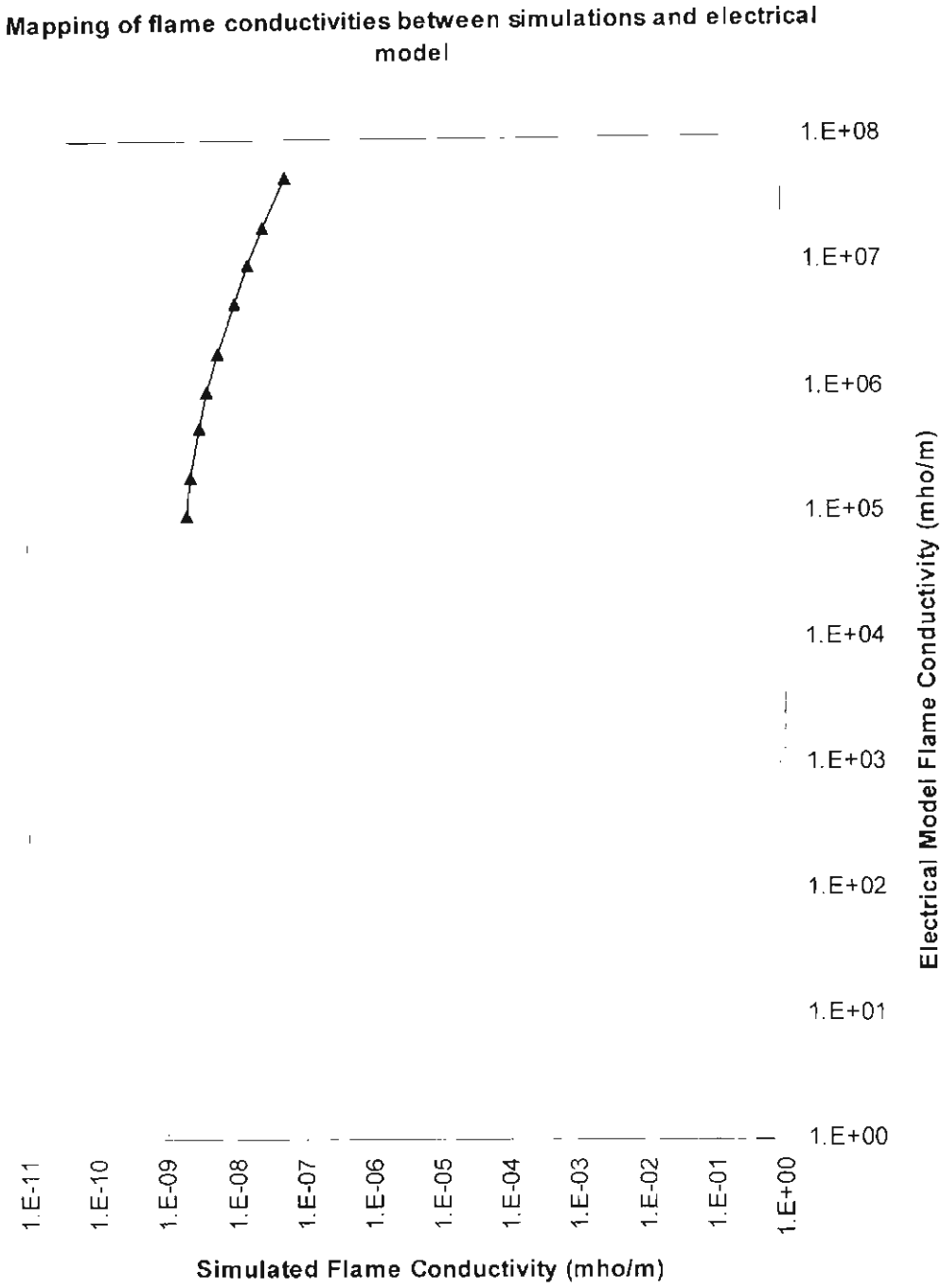

Figure 4.4: Graphical mapping of the simulation and electrical model flame conductivities

4.5.3 Limitations

The investigation suffered a major geometric limitation, which involved stranded conductors. Since the geometry has both very large objects like the flame and very small objects like the conductor the mesh generator is already challenged. Finite element analysis problems are increased exponentially in size by having very small objects. The method requires many elements on the boundary of small objects. This places much strain on the mesh generator and also on the memory capacity.

Stranded conductors are generally made up of an inner steel core consisting of individual strands and an aluminum outer core also made up of strands. The inner core improves mechanical strength while the outer strands are designed more for conduction taking the impact of weight into account. If a conductor of this type had to be used in the simulations it would be represented as a cylinder with a bubble like surface. A cross-section of this is shown in Figure 4.5. These bumps on the conductor surface create small valleys and troughs. The finite element method needs a lot of very small elements to fill these, thus the complexity of the problem increases drastically. This often results in a malfunction in the mesh generator or a solver error due to resource limitations.

This study handled the problem as follows:

(a) All conductors simulated were smooth conductors.

(b) An electric field investigation using a smooth conductor and the corresponding stranded conductor were carried out. Results were then compared and a conclusion was reached as to how the electric field changed.

(c) A correction factor for using smooth conductors was established. This is discussed in section 4.5.3.1.

(d) Results were analyzed using this factor to correct results.

4.5.3.1 The stranding factor

Due to the problem as mentioned above an electric field investigation of stranded and smooth conductors was carried out. The following process was adhered to:

(a) A basic geometry of a conductor above an earth plane was set up. The cross-sections of the stranded and smooth conductors are shown in Figure 4.5.

(b) This is done for the smooth conductors that were used in the simulations and for their stranded equivalents. Both the Zebra and the Dinosaur conductor cases were investigated.

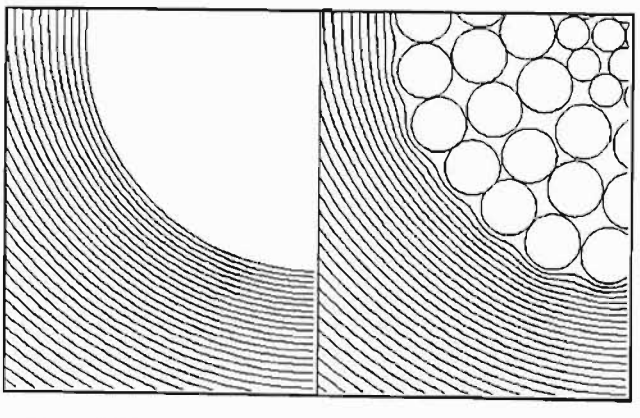

Figure 4.5: A comparison of the equipotential line plots of a stranded and a smooth conductor

The results showed the there is a local enhancement of the electric field for the stranded type conductor by a factor called the stranding factor (ζ) [41]. This factor is often referred to as a surface roughness factor, which is quoted as being the inverse of ζ. The investigation in FEMLAB® gives ζ the values displayed in Table 4.1 for the two different conductors.

Table 4.1: Stranding Factor values for Dinosaur and Zebra conductors

Conductor Type	Dinosaur	Zebra
Stranding Factor (ζ)	1.475	1.406

4.6 Results

4.6.1 General

The results can be divided into two parts due to a geometric classification. They are the two and three-dimensional subdivisions. The mesh generators and the solvers work differently in FEMLAB® for two-dimensional and three-dimensional scenarios. The two-dimensional results are presented first and thereafter follow the three-dimensional component.

Sections 4.6.1(a) to (d) illustrates examples of result outputs from FEMLAB® and describes how the pertinent data was extracted from these. The actual results that are extracted from these colour maps and cross-sectional line plots are presented and discussed in sections 4.6.3.

As explained in section 4.4, the last step of the FEM analysis is post processing. The solution of each of the cases investigated were processed in the following way:

4.6.1(a) Voltage Plot

A voltage colour map of the geometry is the default FEMLAB® result that is displayed once the iterative solver has converged to a solution. Figure 4.6 shows a typical output of this type. This is the result of a 400 kV twin conductor configuration with a 0.3m air-gap. The voltage plot of this type is important for analysis since it displays the fact that the boundary conditions are met.

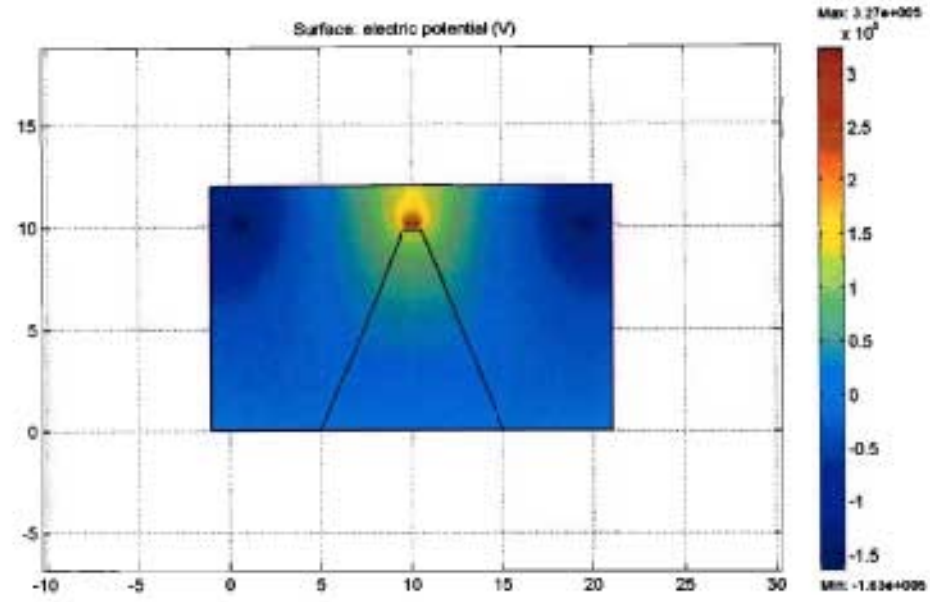

Figure 4.6: Voltage Colour-map of 400kV configuration having a twin conductor bundle

4.6.1(b) Electric Field Plot

This colour graph is important since it provides an overall picture of the regions of high electric stresses. Field enhancement at the conductors was an expected result. Figure 4.7 is a representation of the electric field colour map corresponding to the voltage colour map of Figure 4.6.

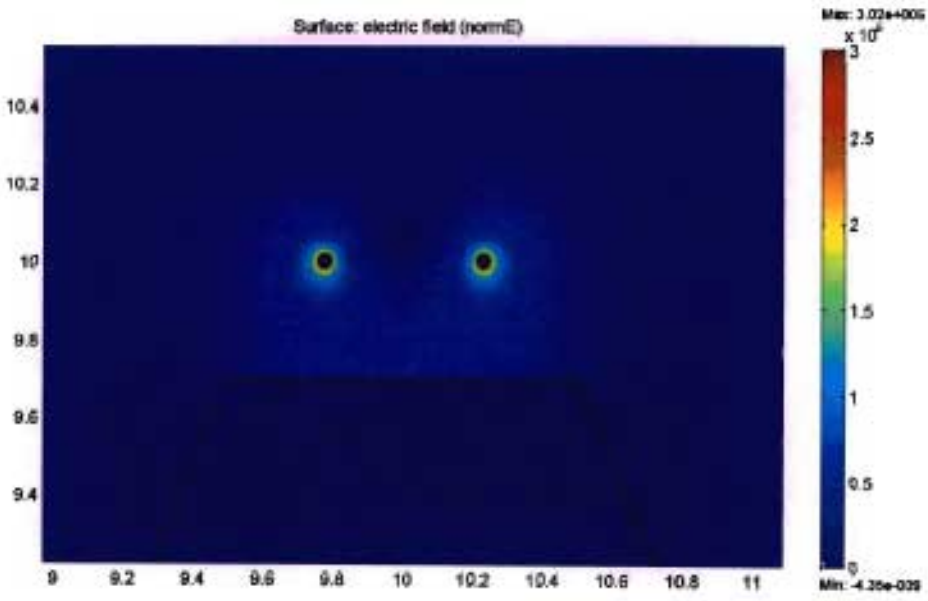

Figure 4.7:Electric Field Colour-map corresponding to voltage plot in figure 4.6

4.6.1(c) Line Plot of Voltage in the Air-gap

The profile of the potential drop across the air-gap is of importance. This plot basically is the value of the electric potential along a vertical line 2m in length that is drawn from the conductor through the flame tip. Figure 4.8 is an example of the voltage profile for a 400 kV system voltage and a flame creating a 0.3m air-gap

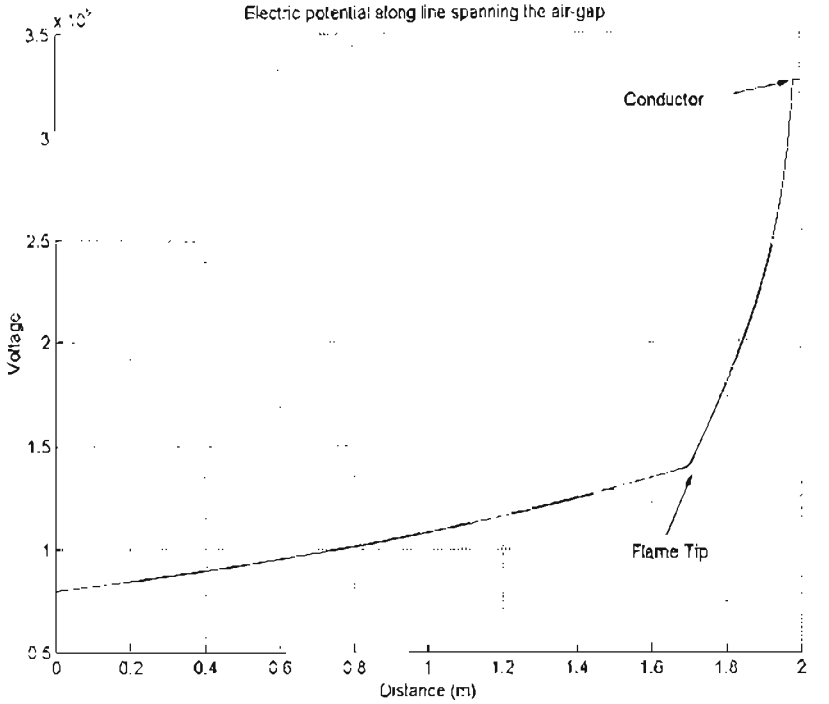

Figure 4.8: Electric potential long a vertical line passing through air-flame boundary and stopping at the conductor.

There is an abrupt point on this curve that corresponds to the flame-air boundary. It is noted that the gradient on the left side (flame side) of this boundary is less steep than that on the right (air-gap side). In Figure 4.8, approximately 43% of the line to ground voltage is dropped across the 9.7 m high flame and the rest is dropped across a 0.3m air-gap.

4.6.1(d) Line Plot of Electric Field in the Air-gap

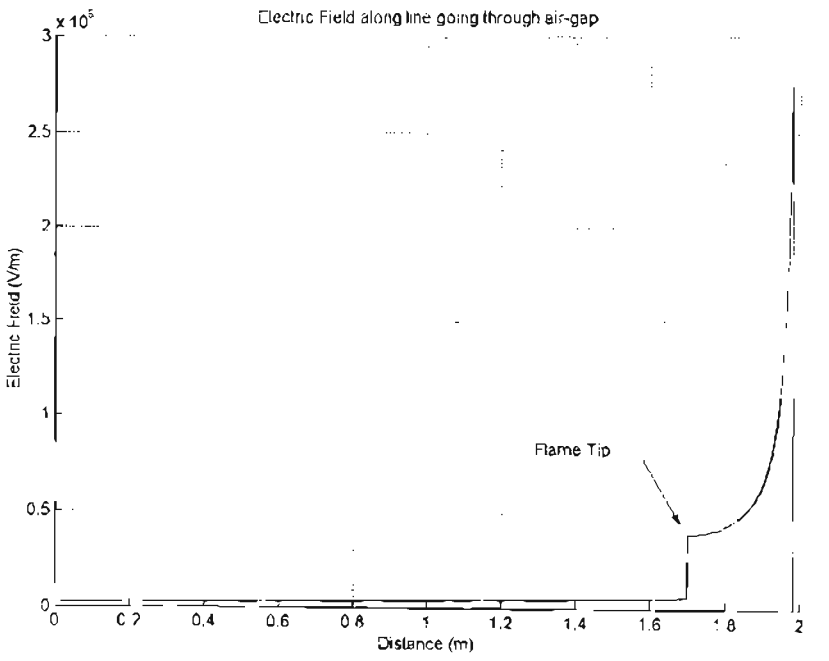

Figure 4.9: Electric Field along line through air gap

As explained above in 4.6.1(c), this is a plot of the electric field along a vertical line through the flame. The information represented in this graph is regarded as being very important since flashover is determined using this. Figure 4.9 is the electric field representation that corresponds to the scenario in Figure 4.8.

In Figure 4.9 there is a sharp rise in the electric field strength at the flame-air-gap boundary. To the left of this boundary (the flame region), the electric field is fairly low and has a relatively small positive average slope. In the air-gap, the electric field rises exponentially and falls instantaneously to zero at the conductor surface. The electric field strength at the conductor surface E_{peak} and at the flame tip E_{ft} are of significant importance as explained in section 4.6.2.

4.6.2 Flashover Determination

The result of most interest however is the plot of electric field along a line that spans from the conductor surface to the flame tip. This shows the value of the electric field at the conductor surface and at the tip of the flame, the importance of which will be seen in the subsections to follow. The method for evaluation of whether flashover will take place is commonly referred to as the two factor flashover criteria. It is based on the following two principles:

1. Corona Inception – The corona inception threshold field needs to be exceeded at the conductor.
2. Streamer Sustenance – The field along the entire path of the discharge must be greater than the minimum streamer gradient, else corona will be extinguished in the mid-gap region.

4.6.2(a) Corona Inception

The corona inception electric field (E_c) at the conductor is calculated from Peek's law [54]:

$$E_c = \delta\left(31.53 + \frac{9.63}{\sqrt{\delta r}}\right) \qquad (4.1)$$

Where E_c is the corona inception field strength in kV/cm,
δ is the relative air density defined by equation (2.68) as D (δ=D), and
r is the conductor radius in centimeters.

For corona inception to be possible, E_{peak} must be greater than or equal to E_c [54]. Appendix 4 has a listing of the E_c values for the different conductor configurations used in the simulations.

4.6.2(b) Streamer Sustenance

According to many researchers, corona sustenance through a medium will take place if the electric field along the path that the corona travels is above a certain value called the minimum streamer gradient, (E_{min}) [40], [36], [15] and [16]. According to Rizk, E_{min} under standard temperature and pressure conditions is assumed to be 4.5 kV/cm [40], [55]. However due to the temperature of the air above the flame being ~393°K [5] E_{min} will decrease. Allen and Ghaffar [36] have shown that in this temperature range, E_{min} has to be corrected by a factor of ($\delta^{1.5}$). Thus E_{min} at 393°K is reduced to 2.7 kV/cm [41].

Due to the criteria used for predicting the occurrence of flashover the electric field throughout the air-gap is an important result especially along the line joining the conductor and flame-tip. The crucial point is E_{peak} itself due to the corona inception criteria. Since the electric field is always decreasing away from the conductor, the value of E_{ft} will determine whether streamers will bridge the whole gap. This is the crucial factor for flashover after corona inception takes place [41]. For the reasons discussed above the results will be presented by only showing a plot of E_{peak} and E_{ft}.

4.6.3 Two-Dimensional Results

4.6.3(a) 275 kV – Geometric Mean Radius

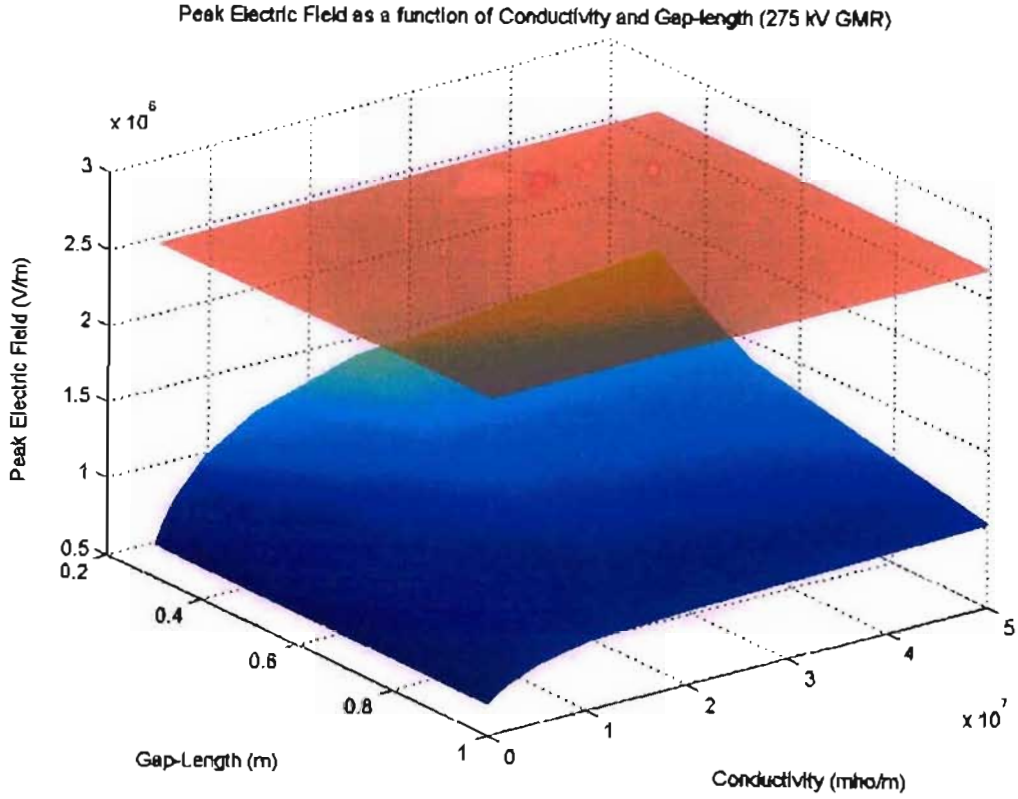

Figure 4.10: Peak Electric field strength (E_{peak}) at conductor surface as a function of conductivity: 275 kV (GMR). The corona threshold field is shown as a red semi-transparent horizontal plane.

Figure 4.10 is a graphical representation of E_{peak} as a function of flame conductivity and gap-length. There is a visible trend of an increase in E_{peak} as conductivity increases and gap-length decreases. There is however some degree of saturation present with respect to conductivity. This surface plot never exceeds the corona inception threshold E_c (shown as a red semi-transparent horizontal plane). Thus it can be concluded that corona inception will not take place for the simulated conditions. However it can be said with confidence that if gap-length were to decrease further, corona inception will be highly probable.

E_{fl} as a function of conductivity and gap-length is shown in Figure 4.11. The corona sustenance threshold is shown as a red semi-transparent horizontal plane. The plane intersects the surface plot separating it into regions distinguished by the corona sustenance criteria. Important to note is that this is of little impact since corona inception is absent. However with a surface irregularity on the conductor, corona inception could take place as a result of the enhanced electric field. Thus under normal conditions for the 275kV GMR case, flashover is unlikely within the simulated conditions.

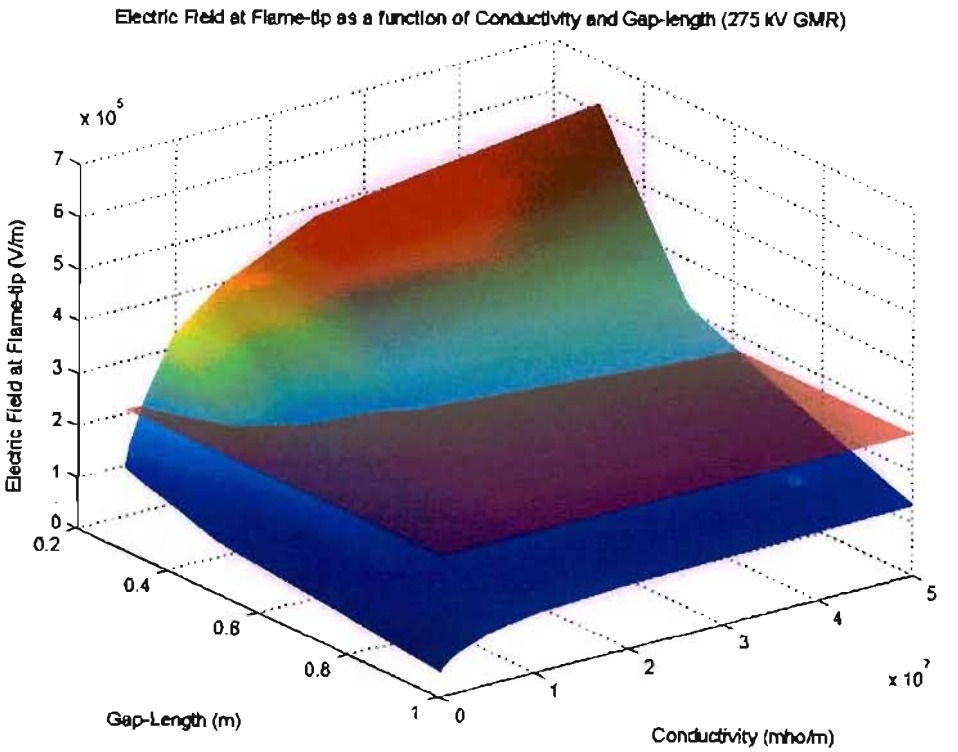

Figure 4.11: Electric field strength at flame tip (E_{fl}) as a function of conductivity: 275kV (GMR). The corona sustenance threshold is shown a red semi-transparent horizontal plane.

4.6.3(b) 275 kV – Twin Bundle Conductor

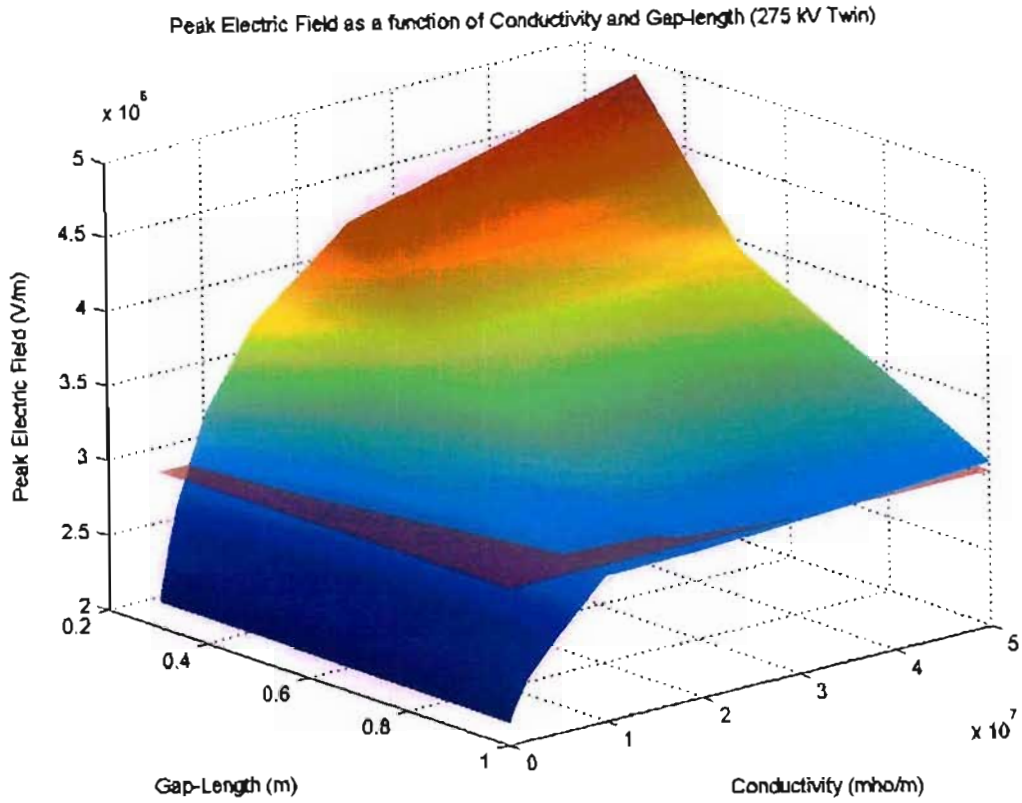

Figure 4.12: Peak Electric field strength at conductor surface as a function of conductivity: 275kV (Twin Bundle conductors). The corona inception threshold field is shown as a red semi-transparent horizontal plane.

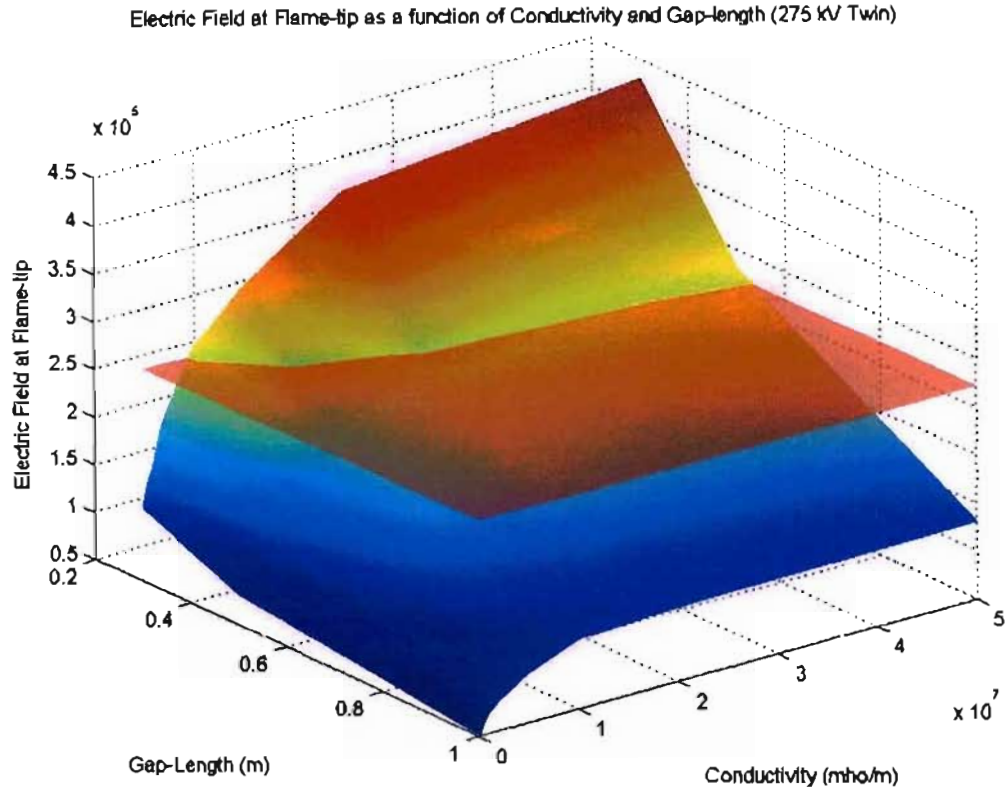

Figure 4.13: Electric field strength at flame tip as a function of conductivity: 275 kV (Twin Bundle conductors). The corona sustenance threshold is shown as a red semi-transparent horizontal plane.

Figure 4.12 illustrates the results obtained for the 275 kV Twin conductor configuration. It is seen that the corona inception threshold cuts the curve relatively low. The difference between Figure 4.12 and Figure 4.10 amplifies the variation in results obtained in FEMLAB® between the GMR and twin cases. It was noted that E_{peak} for the Twin case is always approximately two times greater than that of the GMR case.

Figure 4.13 shows the intersection of the corona sustenance threshold and E_{fl}. An appreciable part of the curve penetrates the sustenance threshold. Therefore for the 275 kV twin conductor case, flashover is highly probable within the simulated parameters.

The exact intersections of E_{peak} and E_{fl} with the corona threshold and sustenance fields are presented and discussed in section 4.6.5 under the results summary.

4.6.3(c) 400 kV – Geometric Mean Radius

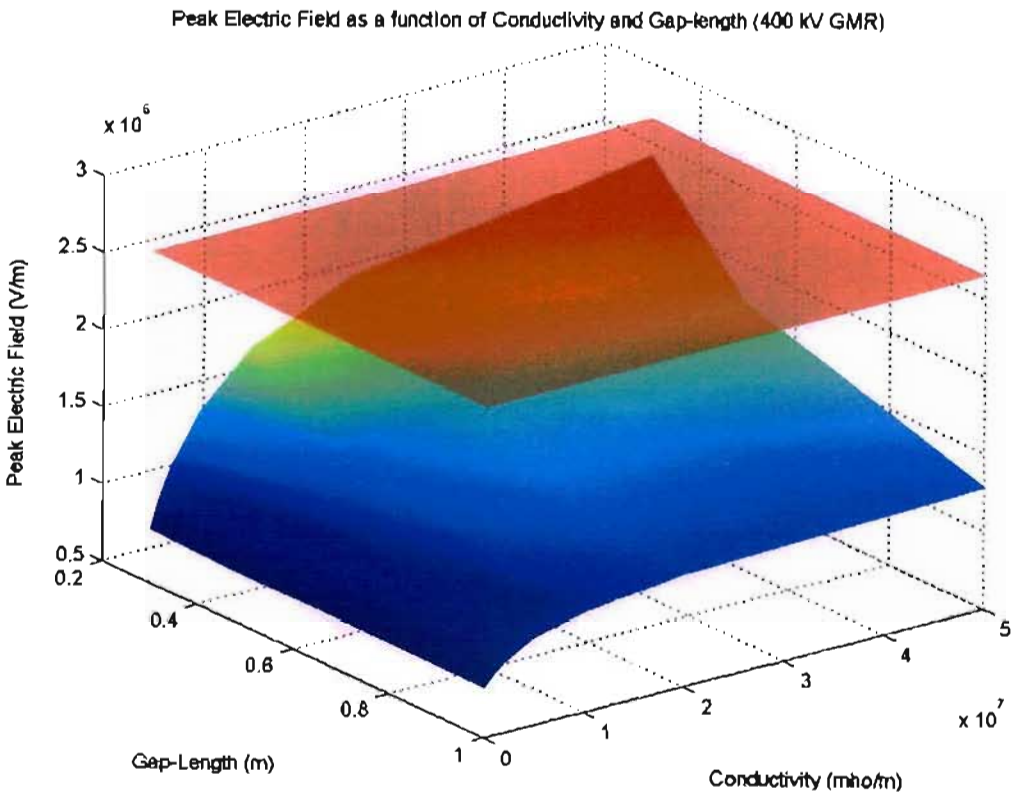

Figure 4.14: Peak Electric field strength at conductor surface as a function of conductivity: 400kV (GMR). The corona inception threshold field is shown as a red semi-transparent horizontal plane.

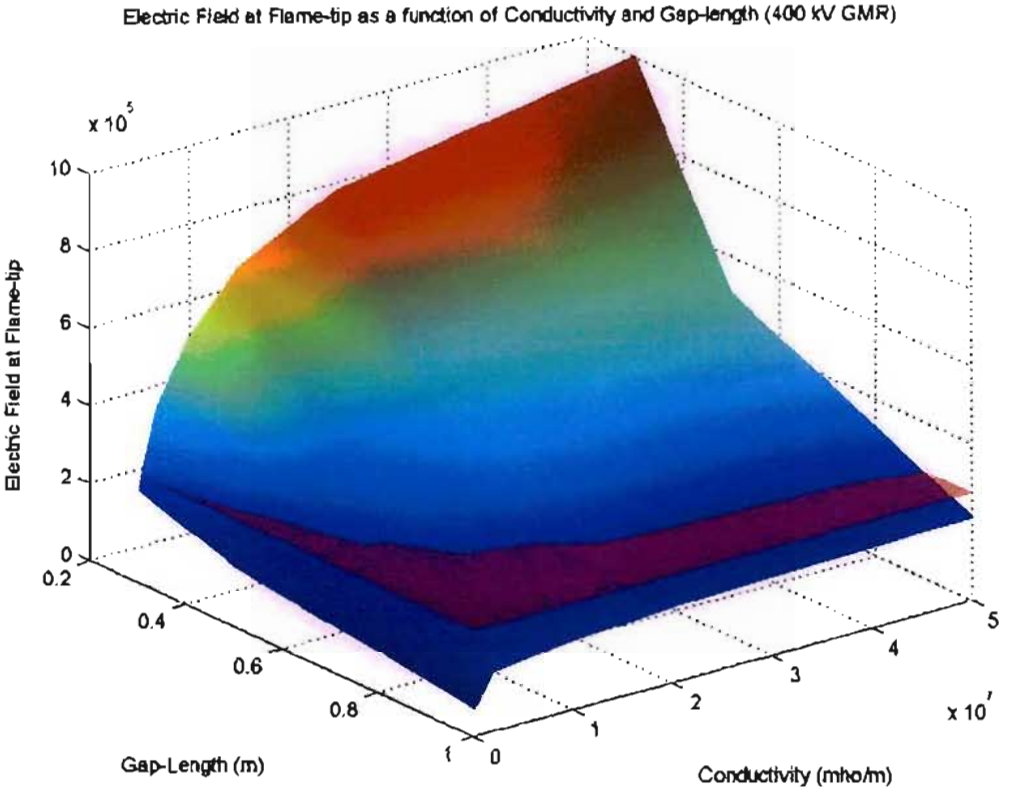

Figure 4.15: Electric field strength at flame tip as a function of conductivity: 400kV (GMR). The corona sustenance threshold is shown as a red semi-transparent horizontal plane.

4.6.3(d) 400 kV – Twin Bundle Conductor

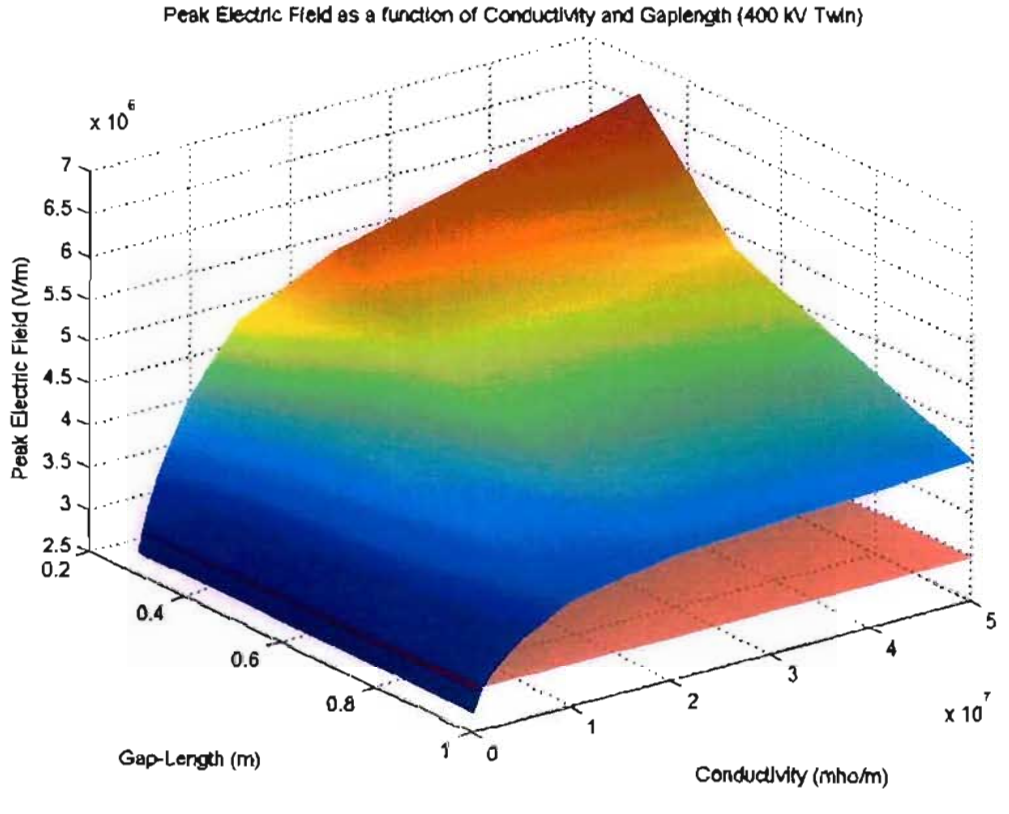

Figure 4.16: Peak Electric field strength at conductor surface as a function of conductivity: 400kV (Twin Bundle conductors). The corona threshold field is shown as a red semi-transparent horizontal plane.

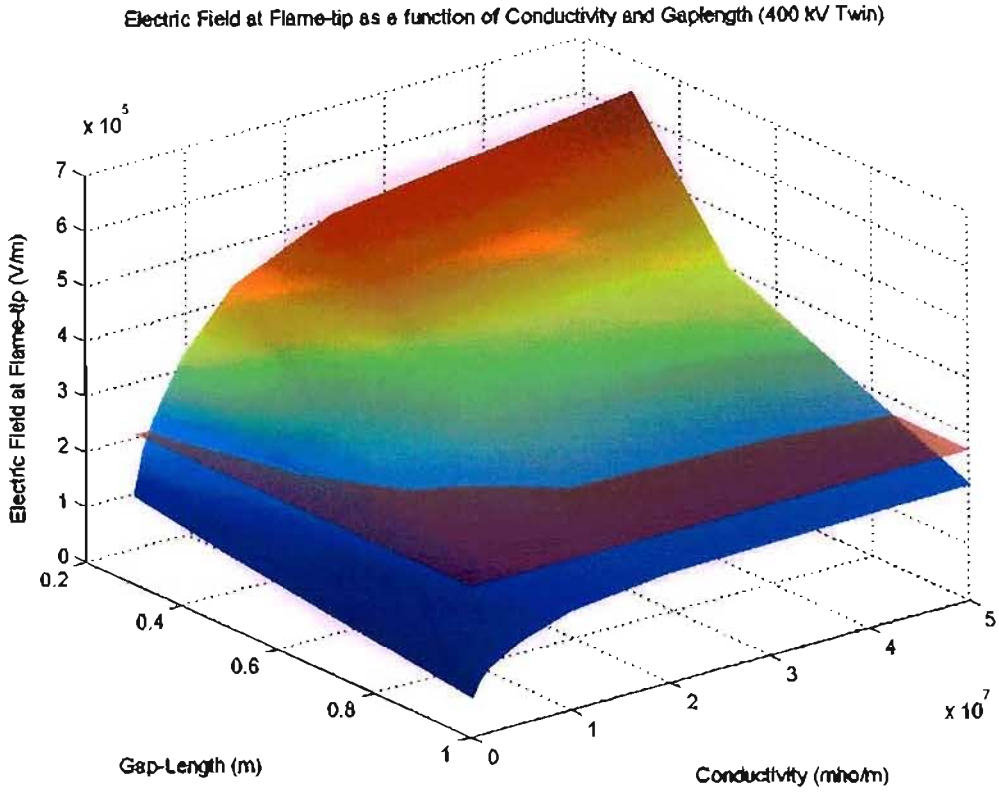

Figure 4.17: Electric field strength at flame tip as a function of conductivity: 400kV (Twin Bundle conductors). The corona sustenance threshold is shown a red semi-transparent horizontal plane.

4.6.4 Three-Dimensional Results

The three-dimensional results are very similar to those obtained for the two-dimensional simulations. The observations and analysis of these would also follow the same structure as performed above. Hence the three-dimensional results are presented in Appendix 7.

4.6.5 Results Summary

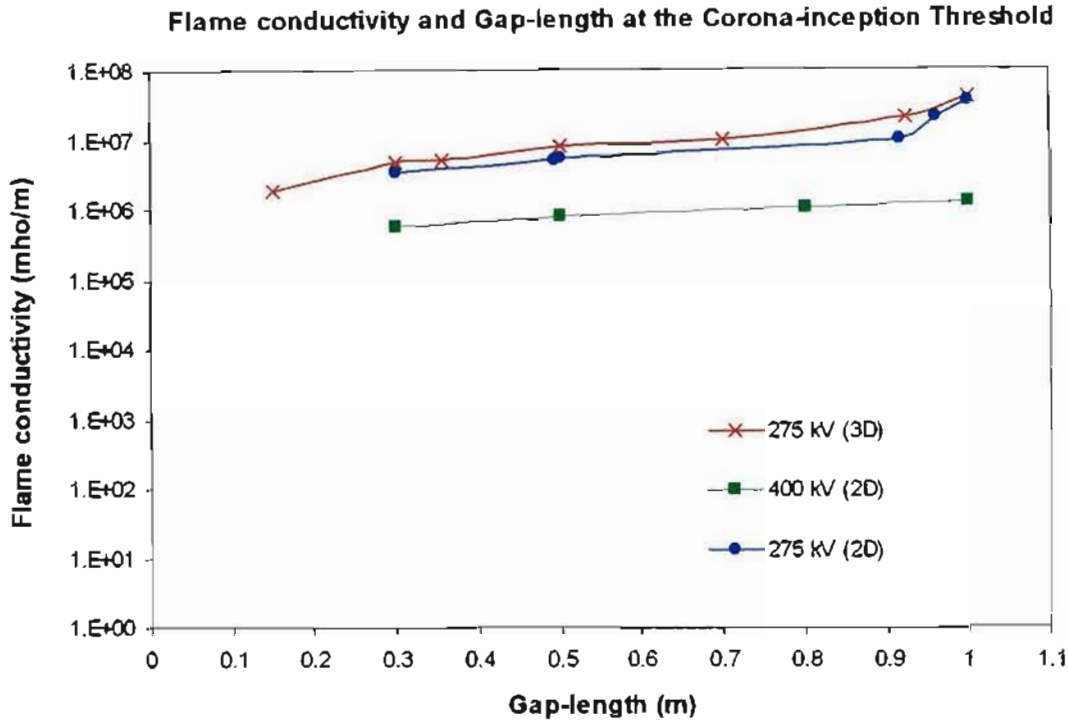

Figure 4.26: Values of flame conductivity and flame tip to conductor gap-length at the corona inception threshold defined by Peek's law

Figure 4.26 shows the values of flame conductivity and gap-length for which the corona inception criterion according to Peek's law is met. Each line represents the inception threshold for a particular case covered in the simulations with every point on and above the line resulting in corona inception. The three-dimensional 400 kV twin conductor case is not represented here since the entire domain of flame conductivity and gap-length simulated for yields electric field strengths that lie above the corona inception threshold. There is a deviation between the three-dimensional and two-dimensional cases as can be seen in Figure 4.26. Amongst other things discretization of the surface may result in errors. FEMLAB® also uses different solving techniques for two and three-dimensional problems.

Figure 4.2.7 shows the values of flame conductivity and gap-length for which the corona sustenance threshold is achieved. It can be seen from these curves that there is not much difference between the two-dimensional and three-dimensional results.

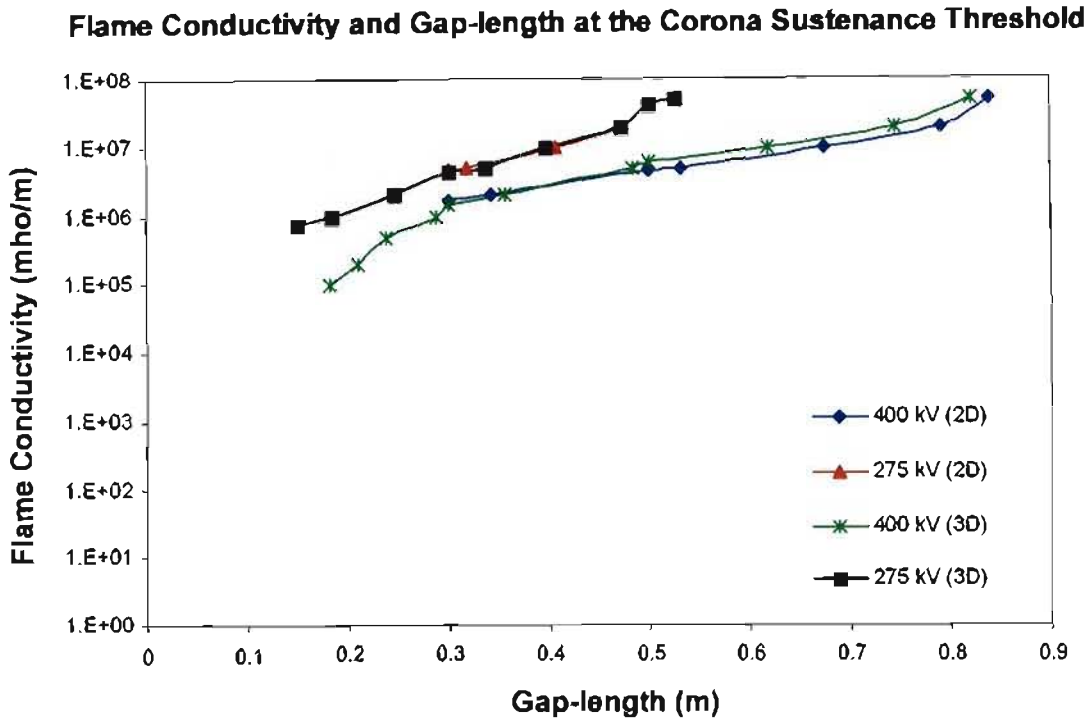

Figure 4.27: Values of flame conductivity and flame tip to conductor gap-length at the corona sustenance threshold

4.7 Conclusion

This chapter has illustrated the use of the simulation software, FEMLAB®, as a tool capable of providing electric field maps of various flame conductor geometries in both 3D and 2D. This finite element analysis package enables the solution of the electric field distribution in a gap taking both permittivity and conductivity into account. These results were used in conjunction with the criteria for flashover as described in section 4.6.2 (corona inception and sustenance) to ascertain whether flashover would be probable.

The general trend of all cases is that electric field intensity increases with an increase in conductivity and a decease in air-gap length. However, saturation with respect to conductivity is easily noticeable.

For each specific case simulated, three-dimensional surface plots are used to summarise the results and further make comparisons with the criteria for flashover. Finally summaries of the corona inception and sustenance boundaries were presented in Figure 4.26 and 4.27 for both 2D and 3D results.

The Geometric Mean Radius concept has been used and electric field plots show considerable deviation from the actual bundled conductor transmission line. The electric field strength at the conductor surface is ~2 times greater for the bundled-twin conductor case.

The probability of flashover for FIF is very dependant on flame conductivity and the size of the air-gap that is created between flame and conductor, as is evident in the results presented by this chapter. This ties up well with field observations which claim that flashover is erratic and cannot be predicted by a mere visual of the flame. A flame that reaches very near the conductor often does not cause flashover. This may be attributed to the fact that FIF is dependant on flame conductivity as well. It is confidently concluded that the simulations support a theoretical model that suggests that the conductivity of the flame is an important factor in the breakdown process.

Simulations showed field enhancement factors of ~1.4 due to stranding of the Zebra and Dinosaur conductors.

Using the two-factor theory for corona inception and streamer sustenance, it is shown that:

(a) For a 400kV line with the flame 0.3m away, the flame conductivity required is ~1.5 $x10^{6}$ mho/m for flashover to occur. This simulated conductivity value corresponds to a real value of ~5.27 $x10^{-9}$mho/m

(b) For a flame 0.3m away from a 275kV line, the flame conductivity required is ~4.6 $x10^{6}$ mho/m for flashover to occur. This simulated conductivity value corresponds to a real value of ~1.9 $x10^{-8}$mho/m

Chapter 5

Experimental Investigation Into Fire-Induced Flashover and Particle Induced Flashover of Transmission Lines

5.1 Introduction

The chapter documents an experimental investigation of FIF. The objective and approach of the experiments are discussed. Thereafter the experimental apparatus and procedure are detailed and finally the results and findings are presented.

The importance of the experimental study is to ascertain some basic characteristics of FIF. The effect of flame geometries and particle sizes that are present beneath a transmission line during FIF forms the backbone of the importance for experimentation. This experimental study is also used to support the simulative study discussed in chapter 4.

Cost and time often place severe restrictions on the scope of experimental work. In this study limitations were also present due to the following:

(a) Controllability of the fire
(b) Repeatability of experimental conditions
(c) Lack of control of larger flames
(d) Upper limit to test AC voltage
(e) Upper limit to air-gap size as a direct result of limit on test voltage
(f) Safety

Thus all experimental work was conducted within defined limits due to the above-mentioned restrictions.

Sadurski and Reynders [11] have previously conducted lab-scale experimentation of FIF. This study shares some similarities with [11], however significant differences are also present. An important difference is that this study focuses on the effect of flame geometry. It also is aimed at quantifying the exact significance particles have apart from merely decreasing the effective air-gap size. Current and voltage waveform recordings were also taken.

5.2 Experimental Approach

This experimental study can be sub-divided into three subsections, namely:

(1) Effect of Flame Geometry (Experiment 1 to 4),

(2) Effect of Particles in the air-gap (Experiment 5), and

(3) Actual FIF (Experiment 6)

Six experiments were performed in this study. They are as follows:

(1) Flashover test: Rod-Plane breakdown characteristics

(2) Flame geometry investigations: Simulation of thin flames

(3) Flame geometry investigations: Simulation of laminar flames parallel to the conductor

(4) Flame geometry investigations: Simulation of laminar flames perpendicular to the conductor

(5) Particles in an air-gap above simulated flame – effect of particles on air insulation strength reduction

(6) FIF – Effect of gap size.

5.3 Basic Experimental Setup

All experiments were conducted on the concrete deck-roof of the High Voltage Laboratory at the University of Natal, Durban campus. The high voltage test transformer is located inside the lab on the ground floor. A connection was made to the transmission line via a bushing through the concrete roof. Section 5.4.2 describes the basic apparatus used in all experiments. Specific apparatus will be described in detail in association with the experimental procedure and results.

5.3.1 High Voltage Alternating Current Source

The circuit diagram in Figure 5.1 illustrates the 50Hz voltage source used during measurements. A Brentford 200kVA, 400V AC voltage regulator was used for voltage control of the high voltage output to the transmission line. The 200kVA cascaded transformer test set had a turns ratio of 1:615. The water column resistor of value ~100kΩ was connected in series to provide a current limiting function.

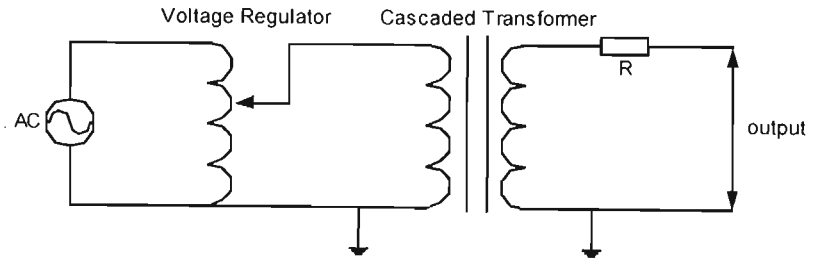

Figure 5.1 High Voltage AC source used for experiments (50Hz)

5.3.2 Basic Apparatus

The three different sections of experiments all used the same basic apparatus but with relevant modifications. The basic apparatus is sketched in Figure 5.2.

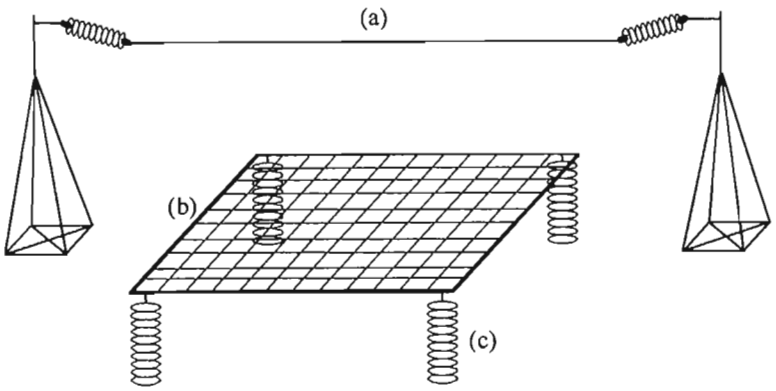

Figure 5.2 Basic experimental apparatus

The basic experimental apparatus contains the following components:

(a) High voltage transmission line

The transmission line was strung using all aluminum Mosquito conductor (7 strands, each having 2.59 mm diameter giving an approximate overall diameter of 7.80 mm). The complete physical characteristics of this conductor are tabulated in Appendix 2. Height adjustable tower masts were used to elevate the Mosquito conductor. Silicon rubber insulator strings were used to suspend the conductor from the mast.

(b) Earth grid elevated above ground and insulated

The galvanized earth grid is made of 25 mm x 50 mm expanded wire mesh (2 mm thick) welded onto an angle iron frame of 2400 mm x 2400 mm. The main reason for using a mesh is to allow a flame to pass through. In this way, the burner can be placed underneath the earth mesh and thus be protected from the flashover arc.

(c) Post insulators used to elevate the earth grid and keep it insulated from ground

A string of post insulators, each 220 mm high, were used to create an elevation of the earth grid from the ground. This allowed the measurement of currents to ground via a 47 Ω resister, and also provided enough space for the burner to be positioned underneath the earth mesh.

5.4 Experiment 1: Rod-Plane Breakdown Characteristics

The objective of this experiment was two fold:

(1) Since this was the first flashover experiment, using the basic experimental setup shown in Figure 5.2, it was a test of the functional capabilities of the basic experimental setup and its insulation withstand ability.

(2) To record some data that other measurements can be compared back to and to get and indication of the validity of the measurements.

5.4.1 Experimental setup and procedure

Figure 5.3 captures the experimental setup used in Experiment 1. An 8mm brass electrode with a hook on one end was hung from the transmission line. This formed the rod plane configuration.

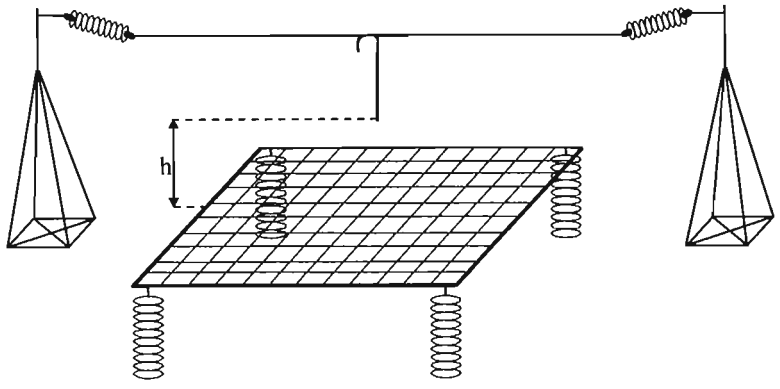

Figure 5.3 Rod-plane setup used in Experiment 1. The gap length shown as 'h'

Without the rod electrode in place the transmission line was energized and the voltage was slowly raised to 160kV rms. This condition was held for one minute to assess the ability of the apparatus's insulation withstand under 50Hz power frequency voltage. Thereafter the rod electrode was put in place and flashover testing of two different gap lengths were carried out. Each test was done five times and the average value of the voltage measurements were taken as the flashover voltage. Thereafter this value was corrected for standard pressure and temperature conditions. This measurement technique was followed for most of the experimental study.

5.4.2 Results

The results are displayed in Table 5.1. These values compare favorably with those obtained by Taylor [56].

Table 5.1 Results of Rod-plane flashover testing.

Gap Length (mm)	Flashover Voltage rms (kV) (corrected to STP)
150	68.96
180	73.25

The average standard deviation is less than 2.1%.

Summary of results:

(1) The insulation withstand of the experimental setup which includes the transmission line and bushing through the roof of the lab is in order.

(2) Reference points for measurement of breakdown characteristics of the rod plane gap have been attained.

(3) Close correlation with the work of Taylor [56] signifies measurement validity.

5.5 Experiment 2, 3 and 4: Flame Geometry Investigations

Field observations have shown flames of different geometries and orientations [57]. Harvesting fires are most often burnt "into the wind" as a general practice and the point of first ignition is almost always the crop edge. Depending on wind direction, these fires may have various orientations with reference to the transmission line. Flames that reach high above the rest of the fire often engulfing the conductor may have different geometries in the vicinity the conductor.

The aim of experiments 2, 3 and 4 are to investigate the effect localized flame geometry has on flashover voltage. Experiment 2 uses a brass rod electrode (8mm diameter) in contact with the earth mesh to simulate a flame that rises high above the rest of the fire and is very narrow when near the conductor. Experiment 3 and 4 uses a sheet of aluminum (2m x 1m x 2mm), which is in contact with earth to simulate a flame that has the geometry of a laminar. In experiment 3, the laminar is parallel to and beneath the transmission line while in experiment 4, the laminar is perpendicular to the transmission line.

5.5.1 Experimental setup and procedure

The experimental setup for experiments 2, 3 and 4 are shown in Figures 5.4, 5.5 and 5.6 respectively.

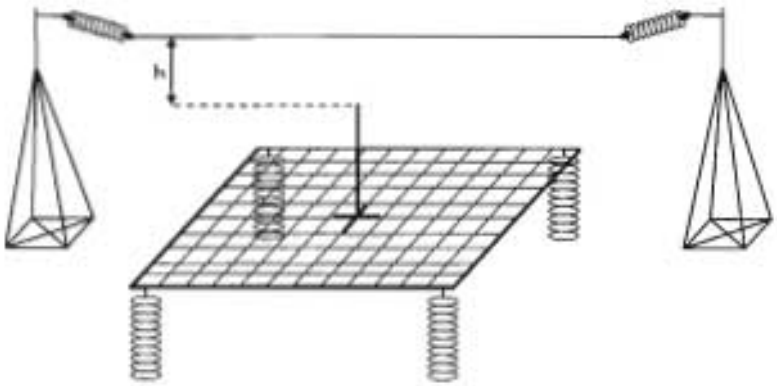

Figure 5.4 Apparatus used in experiment 2

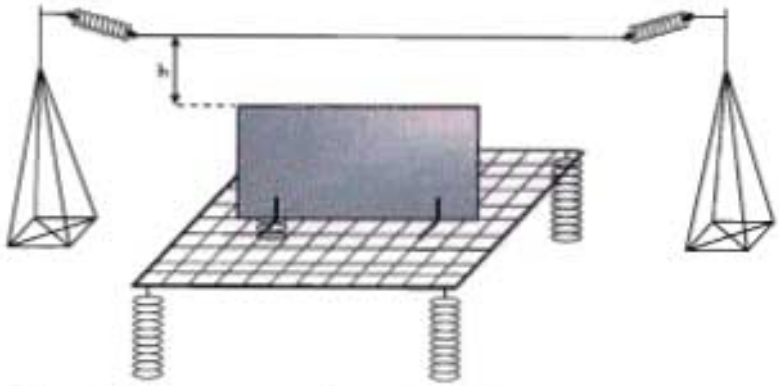

Figure 5.5 Apparatus used in experiment 3

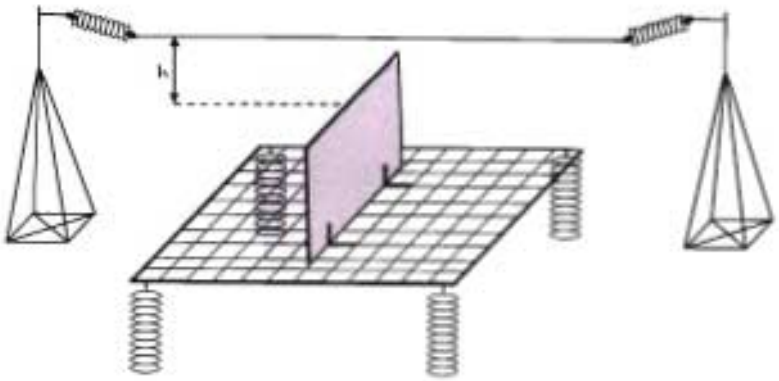

Figure 5.6 Apparatus used in experiment 4

The procedure followed for all three experiments were the same. Once again an average value of five measured flashover voltages was taken as the flashover voltage. These tests were repeated for various gap-lengths *h*. (see Figure 5.4, 5.4 and 5.6)

5.5.2 Results

The results obtained in experiments 2, 3 and 4 are presented graphically with flashover voltage as a function of gap length *h* in Figure 5.7.

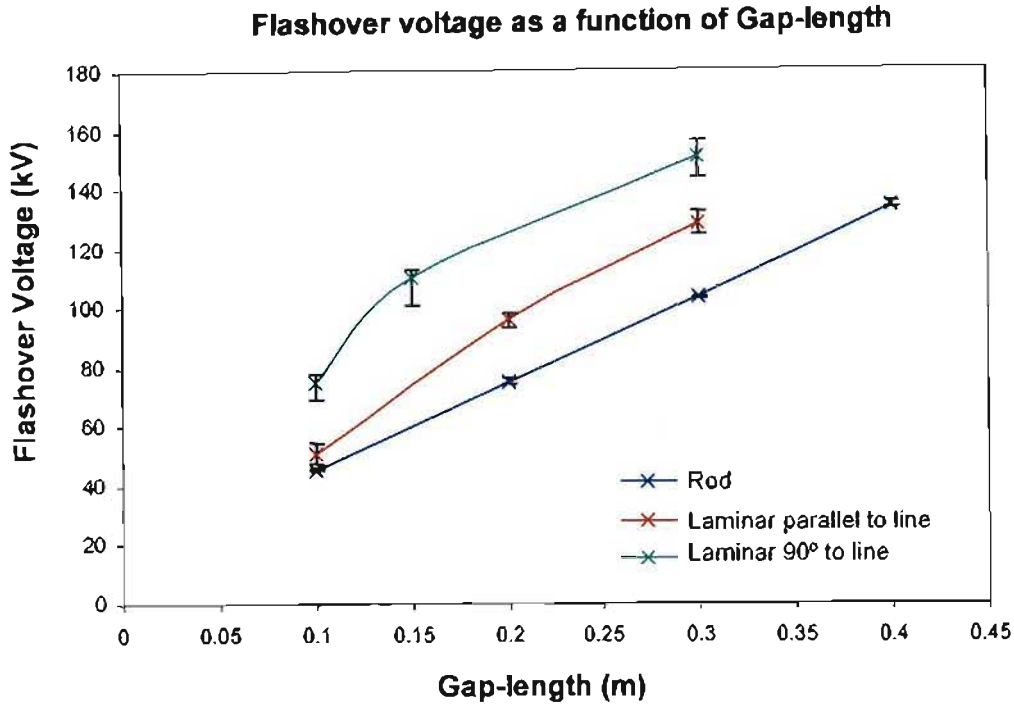

Figure 5.7 Results of flame geometry experiments where the flame is simulated with a metal plate – Flashover voltage as a function of gap-length

The average standard deviations of the measured values were as follows:

(1) Rod (experiment 2) – less than 1%

(2) Laminar parallel to line (experiment 3)– 4.2%

(3) Laminar 90° to line (experiment 4)– 4.5%

The results in Figure 5.7 show that there is a general trend in that flashover voltages increases as gap-length increases. The rod plane gap has the lowest flashover voltage values while the laminar 90°to the line has the highest. This can be attributed to the 'edge effect'. During experiments the arc always burnt between the conductor and one of the outer most edges of the parallel laminar. The flashover voltages are lower for those geometries that have sharp edges near the conductor. When the laminar is perpendicular to the conductor, the edges are the furthest away from the conductor. For gap sizes larger than 150mm there is approximately a

30% reduction in flashover voltage for the rod configuration as compared to the crossed laminar configuration. These findings show that a flame that comes close to the conductor with a sharp pointed tip has a greater possibility of causing a flashover as compared to a flame that is spread out.

The scatter bars also show that there is a smaller spread in the results for geometries with sharp edges near the conductor.

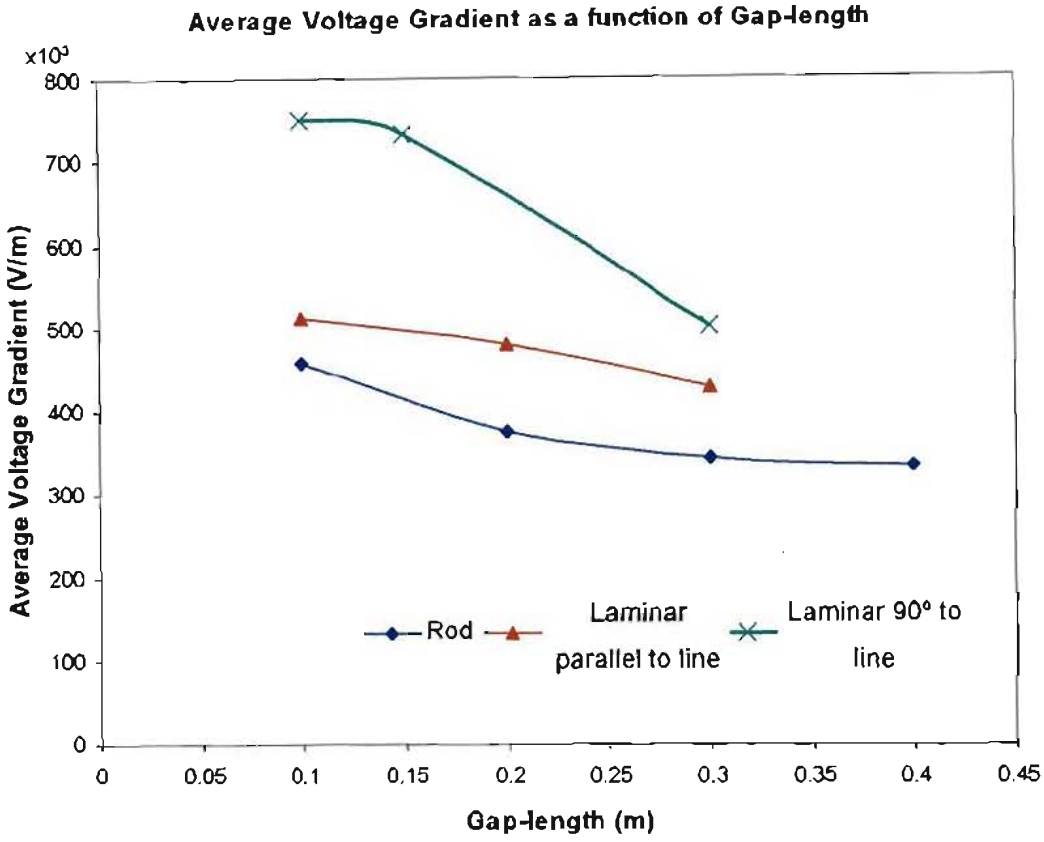

Figure 5.8 Average voltage gradient as a function of gap-length for flame geometry experiments

Figure 5.8 shows the average voltage gradient (E_{avg}) as a function of gap-length. At a gap-length of 100mm E_{avg} for the parallel laminar is 68% of the E_{avg} value for the crossed laminar while at 300mm, E_{avg} for the parallel laminar is 85% of E_{avg} for the crossed laminar. Thus there is a steeper fall in the crossed laminar value than there is in the parallel laminar value. This illustrates that the edge effect has a greater impact for smaller gaps.

5.6 Experiment 5: Particles in an Air-gap above a simulated flame

The aim of experiment 5 is to gain insight on how particles in an air-gap between flame and conductor change the insulating properties of the air-gap. The effect of particle type and size were also part of the objectives.

5.6.1 Experimental setup and procedure

Two different types of particles were used in this experiment namely:

(a) Brass cylindrical rods of 5mm diameter

(b) Graphite filled pencils of 2mm diameter graphite

All particles were mid-gap particles suspended from the conductor using nylon thread. Figure 5.9 shows a sketch of the experimental setup.

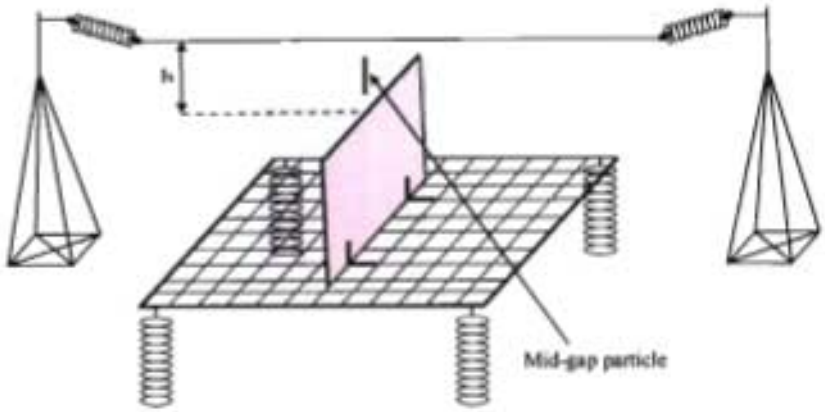

Figure 5.9 Mid-gap particle setup used in Experiment 5. The gap length shows as 'h'

5.6.2 Results

Figure 5.10 presents the results of experiments with particles graphically with flashover voltage as a function of particle size for 300 mm and 500 mm air-gaps. These results were obtained using the graphite filled pencil-particle

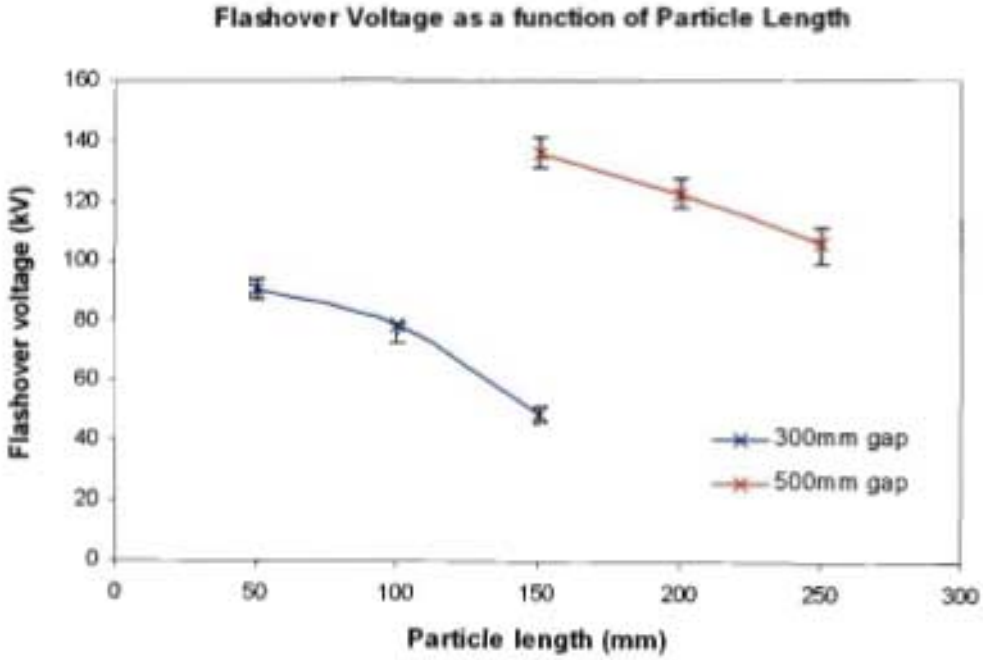

Figure 5.10 Results of experiments with particles – Flashover voltage as a function of particle size for gap lengths of 300mm and 500mm

It is noticeable that as particle size increases, flashover voltage decreases. The scatter bars are smaller for a smaller gap size. The graphite rod has a slightly more significant effect as compared to the brass rod. This can be attributed to the fact that the graphite rod has a smaller diameter as compared to the brass rod.

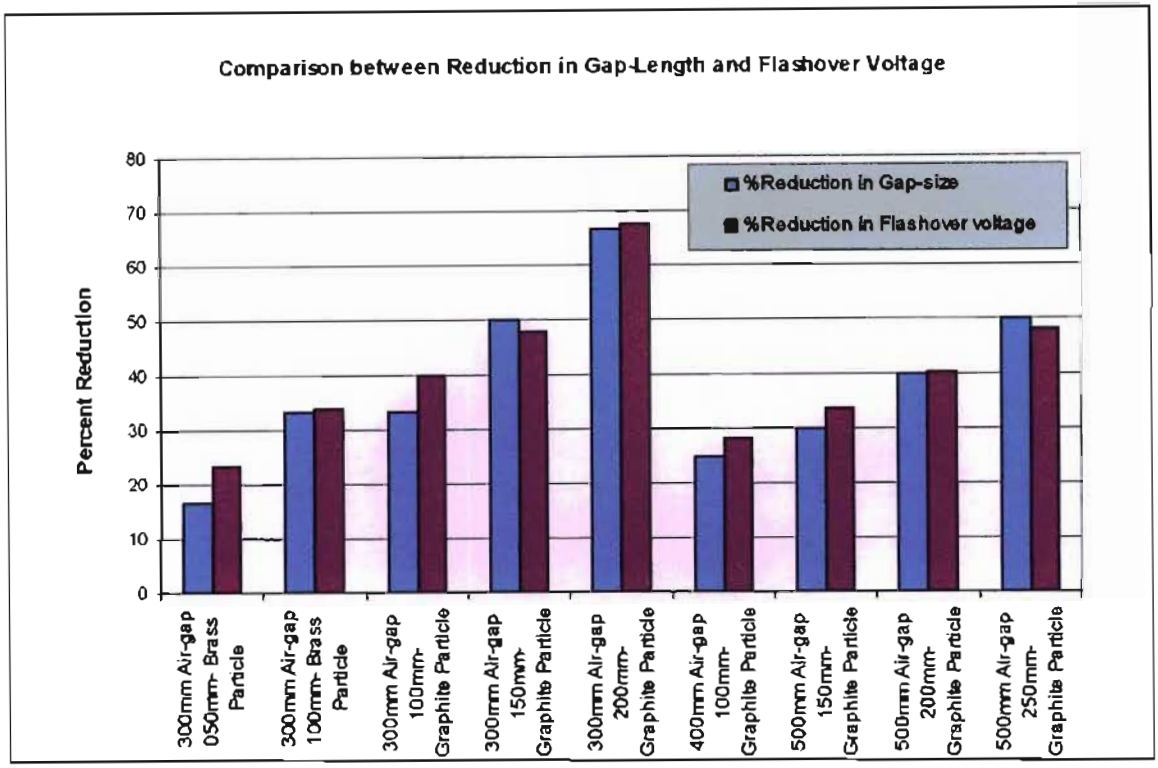

Figure 5.11 Results of experiments with particles – Comparison between reduction in gap-length due to the presence of a particle and Flashover voltage

Figure 5.11 shows a comparison between the effective reduction of air-gap size due to the presence of particles and the corresponding reduction in flashover voltage. It is noted that there is no significant difference. The maximum difference in flashover voltage reduction as compared to gap size reduction is approximately 6%. Also, smaller particles (relative to gap size) have a more significant effect in reducing flashover voltages relative to the percentage of the air-gap that the particle itself short circuits. When the particle size is greater than approximately half the gap size, the resulting effect of the particle becomes less than if the gap had to be decreased by the respective particle length.

It can thus be concluded with confidence, that the presence of particles have no significant effect in the reduction of flashover voltage, over and above the effective reduction in gap-length due to the conductive particle 'shorting out' a part of the air-gap.

5.7 Experiment 6: FIF – Effect of Gap Size

The aim of experiment 6 is to investigate the effect of air-gap length on flashover voltage for FIF. A hot air balloon burner was placed under the earth grid with the flame burning through the grid rising up towards the conductor.

5.7.1 Experimental setup and procedure

The hot air balloon burner uses Liquid Petroleum Gas (LPG) commonly called Handygas. It is equipped with a pilot flame, which is rather small and is simply used as an ignition source for the primary burner. The primary burner is controlled via a solenoid valve with electric throttle.
In order to measure currents that flow through the flame to earth, a 47 Ω resister is inserted in series with the earth connection. Thus by monitoring the voltage across this resister, current can be calculated. Figure 5.12 shows a sketch of the overall setup also showing the measurement resister.

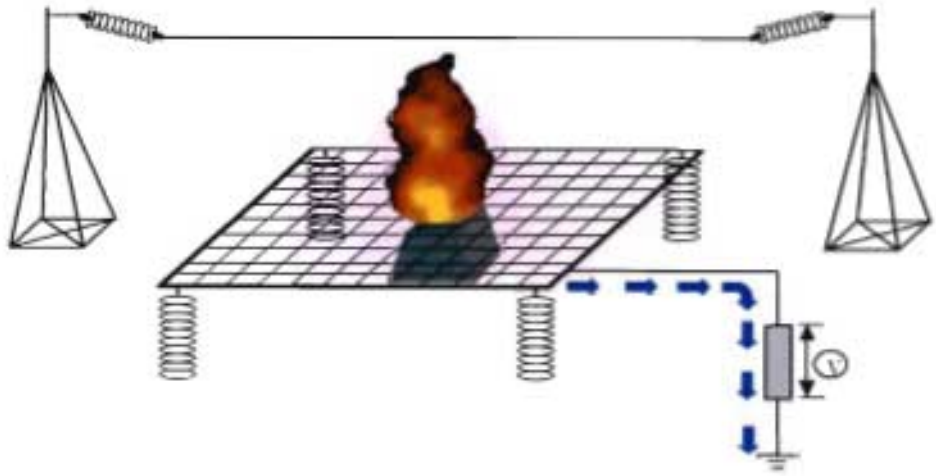

Figure 5.12 Experimental setup for FIF experiments

Figure 5.13 Picture of experimental setup for FIF experiments

Figure 5.13 shows a picture of the experimental setup with a flame burning through the earth grid and engulfing the conductor.

The experimental procedure was as follows:

(1) The appropriate gap size was set.

(2) The burner was turned on, with the flame engulfing the conductor.

(3) The transmission line voltage was ramped up slowly to roughly establish the approximate flashover voltage.

(4) The transmission line voltage was then set at discrete voltage levels around the value measured in (3).

(5) Flashover evaluation was done with a total of ten attempts per voltage level with each attempt sustaining a flame for five seconds.

(6) The number of flashovers out of the ten attempts was recorded.

(7) Steps (4) to (6) were repeated for other selected voltage levels in order to establish $V_{50\%}$.

5.7.2 Results

Figure 5.14 presents the results of the FIF experiments in the form of $V_{50\%}$ as a function of gap-length. $V_{50\%}$ is defined as the voltage at which five flashovers are achieved out of ten attempts and is commonly referred to as the 50% flashover probability threshold. In Figure 5.14, it can be

seen that there is some degree of non-linearity present. The 90% confidence interval is between 2.4 and 7.6 flashovers out of 10 attempts.

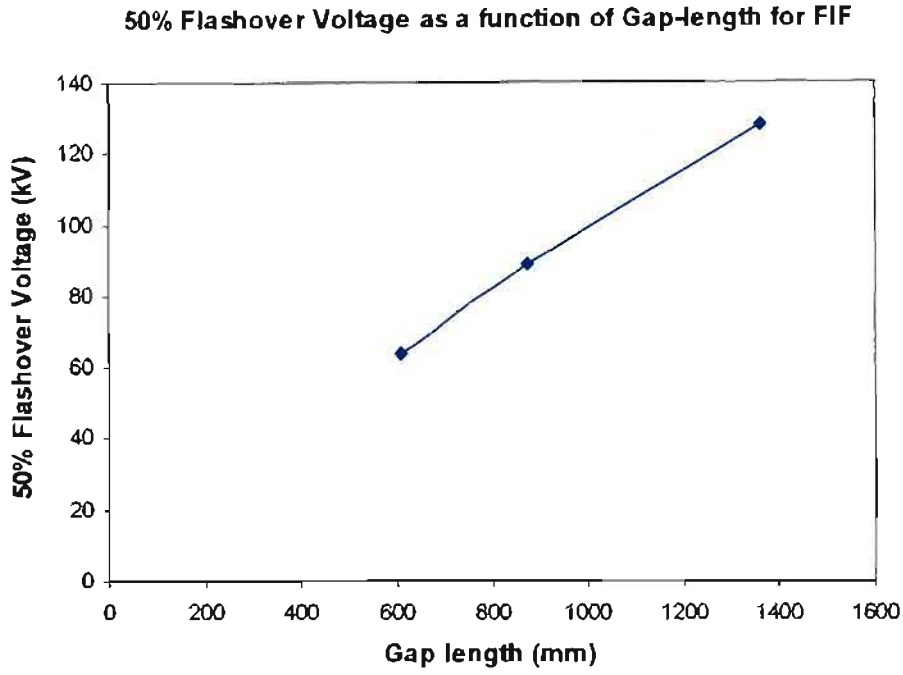

Figure 5.14 Graph of 50% flashover voltage as a function of gap-length – FIF experiments

To evaluate this non-linear behavior, a closer look at the average voltage gradient E_{avg} is required. Figure 5.15 displays E_{avg} as a function of gap-length. There is a definite trend of a decrease in average voltage gradient as gap-length increases. E_{avg} decreases by 10 % between gap-lengths of 610 mm and 1360 mm.

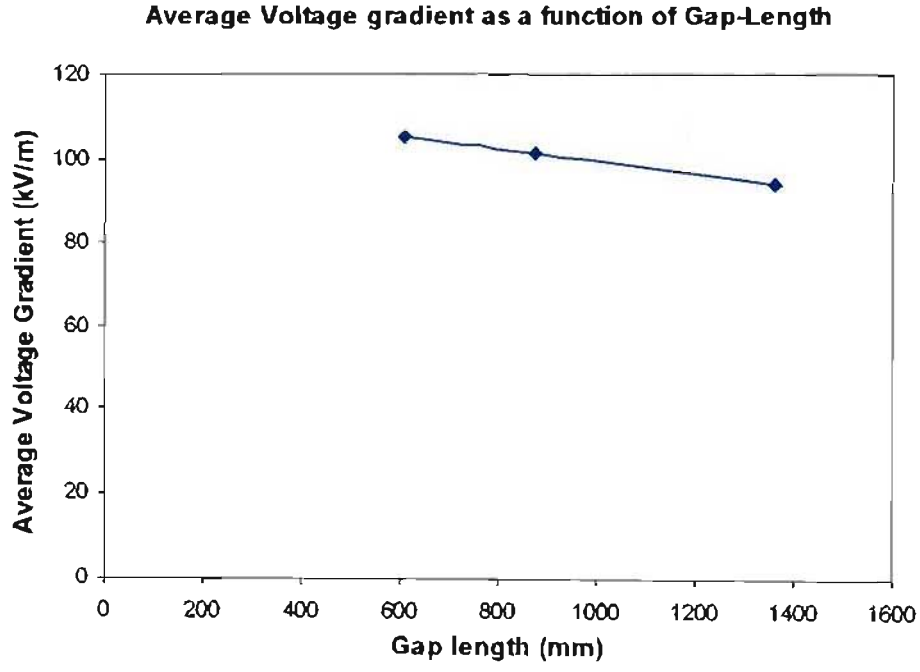

Figure 5.15 Graph of Voltage gradient at 50% flashover voltage as a function of gap-length - FIF experiments

Sadurski and Reynders measured an average value for E_{avg} of 110kV/m for gaps up to 1200mm [11], [58]. For these results E_{avg} has a range of 94.31kV/m to 105.13kV/m for gap-lengths between 610mm and 1360mm. This compares well with Sadurski and Reynders.

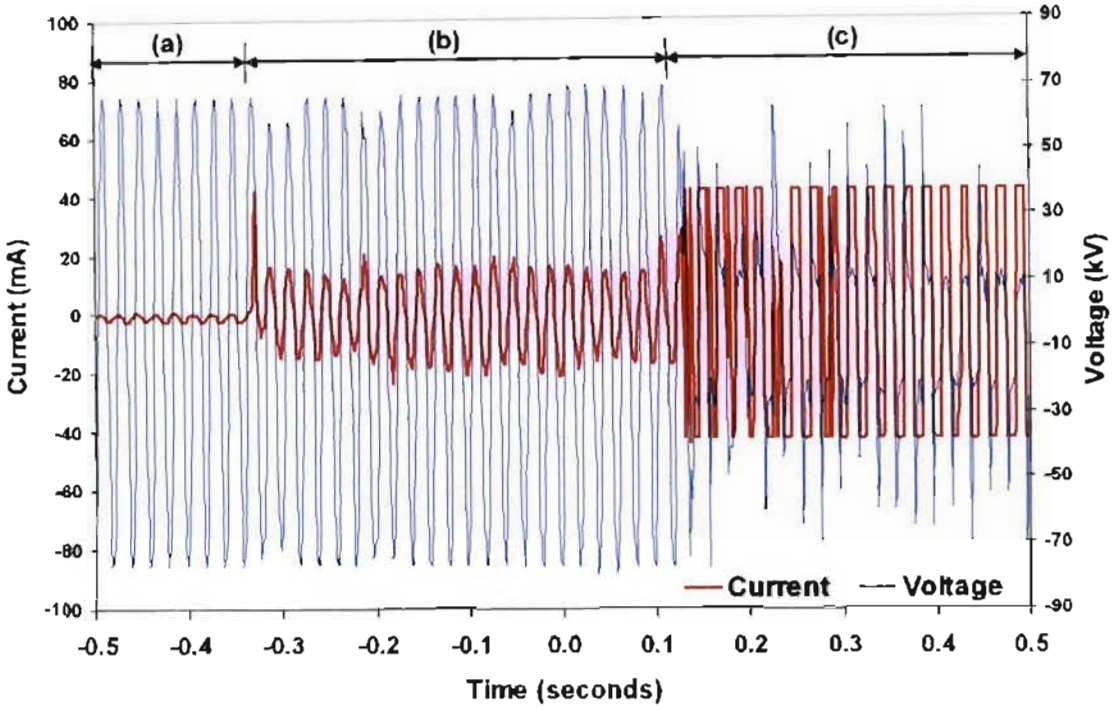

Figure 5.16 Voltage and current waveform recordings for a FIF

Figure 5.16 shows a typical recording of voltage and current waveforms of interest during the FIF experiments. The voltage waveform (blue) represents the transmission line voltage and the current waveform (red) represents the current that flows through the flame to earth. The transmission line voltage was measured with the aid of a measurement capacitive divider and a voltage attenuator having input to output ratios of 851:1 and 20:1 respectively. The current measurement is derived from the voltage measured across the 47 Ω resistor (with surge protection) as described in section 5.7.1. The voltage at the conductor and resistor were monitored on separate channels of a dual trace storage oscilloscope using the same time base as shown in Figure 5.16. This enabled the continuous measurement of current through the flame at different stages in the breakdown process. The voltage waveform in Figure 5.16 has an rms value of 50.7 kV.

There are three distinct phases that were recorded. Firstly, there is a stage where the current can be classified as being capacitive. In this region the current leads the voltage by approximately 90°(Figure 5.16(a)). There is a second stage, which can be called the flame conduction region (Figure 5.16(b)). This is characterized by a high impedance flame conducting a current that is resistive and in phase with the voltage. At this point the flame has crossed the gap and the capacitance is eliminated. Due to the current flow through the flame there is some degree of

ohmic heating. The power dissipated is approximated as being slightly greater than 722 watts, which is rather insignificant when considering the energy released due to the exothermic reaction of the flame. The third stage is the flashover component, where the current increases to a value limited by the external impedance and the voltage collapses rapidly (Figure 5.16(c)).

At a flame height of 540mm, recordings of current and voltage show an effective flame resistance of 4.09MΩ with a standard deviation of 0.69MΩ. These values allow an estimated flame conductivity of 6.73×10^{-7} mho/m. Important to note is that these values are characteristic of a clean flame while in the high resistance state. Lanoie and Mercure [8] reported flame conductivity between 2×10^{-6} and 1.43×10^{-5} mho/m when burning spruce trees. A voltage gradient less than 33kV/m was recorded under their experimental conditions. There appears to be a relation between voltage gradient required for flashover and flame conductivity when the work of Lanoie and Mercure [8] is considered in conjunction with the current investigation.

There was a high level of audible noise emanating from corona discharges while voltage levels were above 10kV and the flame tips were in contact with the conductor.

5.8 Conclusion

This chapter has document the experimental investigation conducted as part of the research into FIF. Due to the restrictions that are present with respect to this type of investigation the study was carried out within defined limitations. There are six experiments within three defined topics:

(a) Effect of flame geometry,
(b) Effect of particles, and
(c) Effect of gap-length on FIF.

The flame geometry findings show that a flame that comes close to the conductor with a sharp pointed tip has a greater possibility of causing a flashover as compared to a flame that is spread out. The standard deviation for geometries with sharp edges is also generally lower.

Particles have a reducing effect on air insulation strength. This is mainly due to the fact that the particle reduces the effective air-gap size. No significant effect over and above this is seen. For particle sizes between 50 and 250mm, the smaller particles have a more significant flashover voltage reducing effect relative to particle size.

For gaps spanned by clean LPG flames $V_{50\%}$ increases as gap-length increases with some degree of non-linearity. Flame resistances and conductivity was approximated from measured currents

and voltages. In the resistive region the ohmic heating due to the current conduction through the flame is approximated as being slightly greater than 700 watts.

Chapter
6

Discussion

FIF has a negative effect on transmission line reliability and quality of supply. This study has introduced a new theory called the flame conductivity theory in order to explain the mechanism of flashover. FIF is not only confined to South Africa and Eskom but research initiatives have been made around the world. These are either lab-scale or field investigations. This study focuses on both simulation and experimental investigations.

At present there are still three main theories about the mechanism of flashover. The third being the flame conductivity theory which is an outcome of this thesis. The first theory is the reduced air density theory, which states that the lack of air insulation strength is caused by the reduced air density, which is a direct result of the high temperatures. There is some degree of truth in this however a claim that reduced air density alone is responsible for the breakdown is arguable according to the standards of the IEEE.

The second theory is the particle initiated flashover theory. The results of the experimental investigation on particles show that the presence of particles have no significant effect in the reduction of flashover voltage, over and above the effective reduction in gap-length due to the conductive particle 'shorting out' a part of the air-gap. It was also noted that smaller particles (relative to gap size) have a more significant effect in reducing flashover voltages relative to the percentage of the air-gap that the particle itself short circuits. When the particle size is greater than approximately half the gap size, the resulting effect of the particle becomes less significant than if the gap had to be decreased by the respective particle length.

Chapter two has taken us from the basic concepts of the kinetic theory of gases through to the concepts of Townsend's coefficients and Meeks streamer theory. This has resulted in a better understanding of the streamer and leader type breakdown of air gaps. The different mechanisms of ionisation and electron recombination have been discussed. The phenomena of corona and the leader mechanism with its observed properties have been presented. This chapter provides the background required to familiarise oneself with the theory of air insulation breakdown.

Bush, grass and cane fires do not specifically fall under either premixed or diffusion flames. They can be categorized as having some characteristics of both. An important consideration that

comes out of chapter 3 is that hydrocarbon flame temperatures can be in the range of 1000°C to 3500°C. These severe temperatures will however greatly affect the degree of ionisation as described by Saha. Thus the conductivity of the flame will increase with this increased ionisation. In the high temperature combustion of hydrocarbons the majority of the enthalpy of the reaction is released rapidly in a narrow reaction zone leading to the production of very high temperatures. There are a large number of ions present in the hydrocarbon flame with ion concentrations reaching values in the order of 10^{18}. Basically, there are three sources of ions. Firstly, due to the chemi-ionisation process involved in hydrocarbon combustion, secondly, due to thermal-ionisation resultant of the high temperature flame, and lastly, due to photo-ionisation.

Often electric fields change the heat release rate of flames depending on orientation and the substances that are being combusted. This allows us to believe more easily that the flame could possibly get very hot at times, and thus becoming very conductive. The possibility of having a highly conductive flame, even for a very short time becomes apparent. This is the basis for the flame conductivity theory. It is believed that the flame channel itself becomes very conductive and allows most of the voltage to appear across the air-gap between the flame tip and conductor. This causes an enhanced electric field in the air-gap itself. Often the enhanced field is sufficient to engage corona inception and sustenance throughout the gap. Flashover is the result.

Chapter 4 has illustrated the use of the simulation software, FEMLAB®, as a tool capable of providing electric field maps of various flame conductor geometries in both 3D and 2D. These results were used in conjunction with the criteria for flashover (corona inception and sustenance) to ascertain whether flashover would be probable on the 275 kV and 400 kV transmission lines for various fire conditions. The general trend shows that electric field intensity, increases with an increase in conductivity or a decease in air-gap length. For each specific case simulated, three-dimensional surface plots are used to summarise the results and further make evaluations with the criteria for flashover. Finally summaries of the corona inception and sustenance boundaries were presented.

The Geometric Mean Radius concept has been used and electric field plots show considerable deviation from the actual bundled conductor transmission line. The electric field strength at the conductor surface is ~2 times greater for the bundled-twin conductor case.

The probability FIF is very dependant on flame conductivity and the size of the air-gap that is created between flame and conductor, as is evident in the results presented. This ties up well with field observations, which claim that flashover is erratic and cannot be predicted by a mere visualisation of the flame. A flame that reaches very near the conductor often does not cause

flashover. It is believed that this may be attributed to the fact that FIF is dependant on flame conductivity as well. It is confidently concluded that the simulations support a theoretical model that suggests that the conductivity of the flame is an important factor in the breakdown process.

Simulations showed field enhancement factors of ~1.4 due to stranding of the Zebra and Dinosaur conductors. Using the two-factor theory for corona inception and streamer sustenance, it is shown that for a 400kV line with the flame 0.3m away, the flame conductivity required for flashover to occur is ~1.5 $x10^{6}$ mho/m. This simulated conductivity value corresponds to a real value of ~5.27 $x10^{-9}$mho/m. It has also been shown that for a flame 0.3m away from a 275kV line, the flame conductivity required for flashover to occur is ~4.6 $x10^{6}$ mho/m. This simulated conductivity value corresponds to a real value of ~1.9 $x10^{-8}$mho/m.

Chapter 5 has documented the experimental investigation conducted as part of the research into FIF. The investigation on flame geometry shows that a flame close to the conductor with a sharp pointed tip has a greater possibility of causing a flashover as compared to a flame that is spread out. Particles have a reducing effect on air insulation strength. This is mainly due to the fact that the particle reduces the effective air-gap size. No significant effect over and above this is seen. For particle sizes between 50 and 250mm, smaller particles have a more significant flashover voltage reducing effect relative to particle size.

For gaps spanned by clean LPG flames, the 50% flashover probability voltage increases as gap-length increases with some degree of non-linearity. Flame resistances and conductivity were approximated from measured currents and voltages. In the resistive region the ohmic heating due to the current conduction through the flame is approximated as being slightly greater than 700 watts.

Sadurski and Reynders measured an average value for the mean voltage gradient through the flame as 110kV/m for gaps up to 1200mm. The results in this thesis have a range between 94.31kV/m and 105.13kV/m for gap-lengths between 610mm and 1360mm. This compares well with Sadurski and Reynders. At a flame height of 540mm, recordings of current and voltage show an effective flame resistance of 4.09MΩ. These values allow an estimated flame conductivity of $6.73x10^{-7}$ mho/m. Important to note is that these values are characteristic of a clean flame while in the high resistance state. Lanoie and Mercure [50] have reported flame conductivity between $2x10^{-6}$ and $1.43x10^{-5}$ mho/m when burning spruce trees. A voltage gradient less than 33kV/m was recorded under their experimental conditions. There appears to be a relation between voltage gradient required for flashover and flame conductivity when the work of Lanoie and Mercure [50] is considered in conjunction with the current investigation.

Chapter
7

Conclusion

This thesis has investigated fire induced flashover and the relative role of particles and the flame conductivity on the overall complex flashover mechanism. The major outcome of this study is the introduction of a new theory called the flame conductivity theory, which is used to explain the mechanism of flashover. The major conclusions drawn from the investigation are listed below. From the simulative study, the following may be highlighted:

(1) Accurate modeling of the twin conductor geometry (including stranding) provided electric field information that was used to predict how close a flame has to approach a conductor before flashover becomes feasible.

(2) The flame conductivity is an important simulation parameter in determining the electric field between the flame tip and the conductor. The geometric shape of the flame is also an important parameter.

(3) It is evident from the simulations that for a 400kV line with the flame 0.3m away, the flame conductivity required is ~1.5 $x10^{6}$ mho/m for flashover to occur. This simulated conductivity value corresponds to a real value of ~5.27 $x10^{-9}$mho/m. It has also been shown that for a flame 0.3m away from a 275kV line, the flame conductivity required is ~4.6 $x10^{6}$ mho/m for flashover to occur. This simulated conductivity value corresponds to a real value of ~1.9 $x10^{-8}$mho/m.

(4) While implementing the concept of Geometric Mean Radius (representing a twin conductor configuration with a single conductor equivalent) within the Finite element method, electric field plots show that the electric field strength at the conductor surface is approximately half of the electric field achieved for the bundled-twin conductor case. Twin conductors therefore need to be modeled accurately.

Following from the simulations, the conclusions drawn from the experimental investigation are as follows:

(1) The results of the experimental investigation on particles show that the presence of particles on the reduction of the flashover voltage is due to the reduction in air gap size caused by the conductive particle shorting out a part of the air-gap.

(2) Experiments show that smaller particles (relative to the original air gap size) have a more significant effect in reducing flashover voltages than larger particles.

(3) When the particle size is greater than approximately half the gap size, the resulting effect of the particle becomes less significant than if the gap had to be decreased by the respective particle length.

(4) Experimental data using a gas burner has confirmed, for gaps up to 1.3m, the average flashover gradients obtained by previous researchers for smaller gaps where conductor engulfment occurs.

(5) Current and voltage recordings indicate a significant time period during which resistive current flow to earth occurs through the flame prior to flashover.

Chapter
8

Recommendations for Further Work

8.1 General

Work has been done during this research initiative in order to get a better understanding of FIF, resulting in many pieces of ring-fenced information. To use this work as a springboard for further work would add greater value to the understanding of FIF. With this in mind, this chapter is dedicated to the ideas that are present at the culmination of this thesis.

8.2 Simulative Research

In this study simulations were carried out with flames having a constant conductivity value throughout the flame. Saha has shown that the conductivity of a plasma is related to its temperature. When considering a flame, the temperature generally is greater towards the middle (combustion zone) and is known to decrease when moving away from the combustion zone. Thus the conductivity is anisotropic. There would be some merit in observing the effect of an anisotropic flame on electric field stresses.

8.3 Experimental Investigations

Wind is said to play an important role in FIF according to field observations. This is believable since it is anticipated that wind would impact on the physical properties of the flame. Thus an experimental investigation with the aim to discover the dependence of FIF on wind speed and direction would be useful.

The dependence of FIF on the horizontal length of fire beneath a transmission line would make an interesting investigation.

Within a flame, there are three sources of ions:

(1) The ions taking part in the combustion chemi-ionisation processes
(2) The ions created due to thermal ionisation
(3) The ions created due to ultra violet radiation emanating from the emission spectra of substances present in the flame.

It would be of some value if different ultra violet producing substances could be added to the fire to investigate the effect ultra violet radiation within a flame has on flashover voltage.

References

1. Cowan P M, Dunn J A., Naidoo P and Masters J, *Sugar cane fire induced transmission line flashovers*, Electron, 1991. January: p. 12-15.

2. Evert C R and de Klerk P J *Corona noise as a diagnostic tool.* in *Proceedings of the 4th International Conference on Properties and Applications of Dielectric Materials.* 1994.

3. Gale P F, Taylor P V, Naidoo P, Hitchin C and Clowes D, *Travelling wave fault locator experience on Eskom's Transmission network.* in *Developments in the Power System Protection Conference.* 2001.

4. Vosloo W L, H.J.P.a.B.A.C., *A Laboratory Investigation into the effect of sugar cane fires on corona noise.*

5. Sukhnandan A and Hoch D A, *An Investigation of Fire Induced Flashovers of Transmission Lines.* in *Proceedings of the 13th anual South African Universities Power Engineering Conference.* 2004. University of Stellenbosch.

6. Meek, *Inaugural Address-The Vital Spark.* IEE Proceedings, 1969. 116(1): p. 1-11.

7. Fonseca J R, Tan A L, Monassi V, Junqueira W S, Silva R P, Assuncao L A R and Melo M O C, *Effects of agricultural fires on the performance of overhead transmission lines.* IEEE Transactions on Power Delivery, 1990. 5(2).

8. Lanoie R and Mercure H, *Influence of Forest fires on Power Line Insulation.* in *Sixth International Symposium on High Voltage Engineering.* 1989. New Orleans, LA,USA.

9. Naidoo P and Swift D A, *Large Particle Initiated Breakdown of an Atmospheric Air gap: Relating to AC Power Line Faults Caused by Sugar Cane Fires.* in *8th International Symposium on High Voltage Engineering.* 1993. Yokohama, Japan.

10. Benard L and von Elbe G, *Combustion, flames and explosion of gases.* 1987, Orlando: Academic press.

11. Sadurski K J and Reynders J P, *High Voltage AC breakdown in Presence of Fires.* in *Sixth International Symposium on High Voltage Engineering.* 1989. New Orleans, LA, USA.

12. Baldo G, Diaz R R and Pesavento G, *Discharge Mechanisms in Presence of Flames.* in *8th International Symposium on High Voltage Engineering.* 1993. Yokohama, Japan.

13. Deno D W and Zaffanella L E, *Transmission Line reference book 345KV and above.* 2ed. 1982, Palo Alto, California: EPRI. 384-388.

14. Diesendorf W, *Insulation co-ordination in high voltage electric power systems.* ISBN 0408 70464 0 ed. 1974: Butterworth and Co.

15. Allen N L, Lam D S K and Greaves D A, *Tests on the breakdown of air at elevated temperatures in non-uniform electric fields.* IEE Proceedings - Sci. Meas. Technol., 2000. 147(6).

16. Allen N L, Mikropoulous P N, *Dynamics of streamer propagation in air.* Journal of Physics D: Applied Physics, 1999. 32.

17. Pedersen A, *Calculation of Spark Breakdown or Corona Starting Voltages In Nonuniform Fields.* IEEE Transactions on Power Apparatus and Systems, 1967. PAS-86(2): p. 200-205.

18. Sukhnndan A and Hoch D A. *Fire induced Flashover of Transmission Lines: Theoretical Models.* in *Proceedings of the IEEE Africon Conference.* 2002. George South Africa: IEEE.

19. Allen N L and Gaffar A, *Temperature and density effects on streamer propagation in air.* in *8th International Symposium on High Voltage Engineering.* 1993. Yokohama, Japan.

20. Forster E O, *The Search For Universal Features of Electrical breakdown in Solids , Liquids and Gases.* IEEE Transactions on Electrical Insulation, 1982. EI-17(6): p. 517-521.

21. Hutzler B and Hutzler-Barre D, *Leader Propagation Model for Predetermination of switching Surge Flashover Voltage of Large Air Gaps.* IEEE Transactions on Power Apparatus and Systems, 1978. PAS-97(4): p. 1087-1096.

22. Radtke R and Gunther K, *Electrical Conductivity of highly ionized dense hydrogen plasma: I Electrical measurements and diagnostics.* Journal of Physics D: Applied Physics, 1976. 9.

23. Kuffel and Zaengl W S, *High voltage engineering.* ISBN 0-08-024213-8 ed. 1984: A. Wheatman and Co.

24. Goldman M, *Corona Discharges and their Applications.* IEE Proceedings, 1981. 128 Part A (4): p. 298-302.

25. Hileman A R, *Transmission line insulation coordination - Twenty-eight Bernard Price Memorial Lecture.* The transactions of the SA institute of electrical engineers, 1980. June: p. 145-157.

26. Aleksandrov N L, Bazelyan E M, Kochetov I V and Dyatko N A, *The ionization kinetics and electric field in the leader channel in long air gaps.* Journal of Physics D: Applied Physics, 1997. 30: p. 1616-1624.

27. Pedersen T and Brown R C, *Simulation of Electric Fields in Premixed Methane Flames.* Combustion and Flame, 1993. 94: p. 433-448.

28. Domens P, Gilbert A, Dupuy J and Hutzler B, *Propagation of the positive streamer-leader syatem in a 16.7m rod-plane gap.* Journal of Physics D: Applied Physics, 1991. 24: p. 1748-1757.

29. Bondiou A and Gallimberti I, *Theoretical modeling of the development of the positive-spark in long air gaps.* J.Phys. D: Appl. Phys, 1994. 27: p. 1252-1266.

30. Rizk F A M, *Switching impulse Strength of air insulation: Leader inception criterion.* IEEE Transactions on Power Delivery, 1989. 4(4): p. 2187-2194.

31. Baldo G, Gallimbeti I, Gracia H N, Hutzler B, Jouaire J and Simon M F, *Breakdown Phenomena of Long Gaps Under Switching Impulse Conditions Influence of Distance and Voltage Level.* IEEE Transactions on Power Apparatus and Systems, 1975. PAS-94(4): p. 1131-1139.

32. Gracia H N and Hutzler B, *Electrical Breakdown in long air gaps - The Final Jump.* : p. 206-210.

33. Boutlendji J, Allen I, *Dielectric strength of air insulation for coordination of minimum clearances of overhead lines: a review.* IEE Proceedings Science, Measurement and Technology, 1994. 141(6): p. 449-461.

34. Carrara G and Thione L, *Switching Surge Strength of Large Air Gaps: A Physical Approach.* IEEE Transactions on Power Apparatus and Systems, 1976. PAS-95(2): p. 512-521.

35. Waters R T, *Breakdown in nonuniform fields.* IEE Proceedings, 1981. 128(Part A No 4): p. 319-325.

36. Allen N L and Ghaffar A, *The variation with temperature of positive streamer properties in air.* Journal of Physics D: Applied Physics, 1995. 28: p. 338-343.

37. Gilbert A and Bastien F, *Fine structure of streamers.* Journal of Physics D: Applied Physics, 1989. 22.

38. Rizk F A M, *A Model for switching impulse leader inception and breakdown of long air-gaps.* IEEE Transactions on Power Delivery, 1989. 4(1): p. 596-606.

39. Goelian N, Lalande P, Bondiou-Clergerie A, Bacchiega G L, Gazzani A and Gallimberti I, *A simplified model for the simulation of positive-spark development in long air gaps.* Journal of Physics D: Applied Physics, 1997. 30: p. 2441-2452.

40. Rizk F A M. *An Overview of Recent High Voltage Engineering Research in Canada.* in *10th International Symposium on High Voltage Engineering.* 1997. Montreal, Quebec,

Canada: ISH.

41. Tobazéon R, *Liquid Breakdown and its Relation to Gas Breakdown*, Laboratoire d'Electrstatique et de Materiaux Dielectriques: Grenoble Cedex France.

42. Rizk F A M, *Critical switching impulse breakdown of long bundle conductor gaps.* IEEE Transactions on Power Delivery, 1996. 11(1): p. 373-381.

43. Mousa A M, *Protecting firemen against fire-induced flashovers.* IEEE Transactions on Power Delivery, 1990. 5(1).

44. Bradley J N, *Flame and Combustion Phenomena.* 1965, London, Methuen.

45. Palmer H B and Beer J M, *Combustion, flames and explosion of gases.* 3 ed. 1987, Orlando: Academic press.

46. Williams F A, *Combustion*, in *Encyclopedia of Physical Science and Technology.* 1987, Academic Press Inc.

47. Karlovitz B, *Flames Augmented by Electrical Power.* in *International Union of Pure and Applied Chemistry: Radioactivation Analysis Symposium.* 1962. Vienna, Austria: Pergamon Press

48. Krumm P, *Playing with Fire: A probe into the bounded-plasma properties of a Laboratory Flame*, , University of Natal: Durban, South Africa.

49. Brauer J R, *What Every Engineer should know about finite element analysis.* 1988, Marcel Dekker: New York. 219.

50. Fristom R M and Westenberg A A, *Flame Structure.* 1965: New York: McGraw Hill.

51. COMSOL Inc: *Femlab User's guide and introduction,* 2001, COMSOL AB.

52. COMSOL Inc: *Femlab Electromagnetics Module,* 2001, COMSOL AB.

53. Sodha M S, Sagoo M S, Chandra A and Ghatak A K, *Electrical Properties of rich Hydrocarbon flames.* Journal of Applied Physics, 1975. 46(9).

54. Larsson A, *The Effect of a Large series resistance on the streamer to spark transition in dry air.* Journal of Physics D: Applied Physics, 1998. 31: p. 1100-1108.

55. Rizk F A M, *Effect of Floating Conducting Objects on Critical Switching Impulse Breakdown of Air Insulation.* IEEE Transactions on Power Delivery, 1995. 10(3): p. 1360-1367.

56. Taylor P, *Case study into bird streamer caused transient earth faults on a 275 kV transmission grid*, in *School of electrical engineering.* 2001, University of Natal: Durban. p. 123.

57. *Prescribed Burning*, in http://www.kentuckyhunting.com/habitat/burning.html. 2002.

58. Sadurski K J, *Effect of bush, grass and cane fires below Transmission Lines*, 1977, Electricity Supply Commission, New Works Department, Electrical Research Division: Johannesburg.

59. Cigre SC33, *Guidelines for the evaluation of the dielectric strength of external insulation,* Cigre, Paris, 1992.

Appendix 1

Concept of Gap Factor

The gap factor for a particular geometry is given the symbol k and is defined as:

$$k = \frac{V_{50\%}(config)}{V_{50\%}(rod - plane)}$$

The rod-plane gap, which is regarded as the reference gap since it gives the lowest spark over voltage of all configurations, yields a k value of one [2].

Appendix 2

Transmission Line Parameters – 275 kV

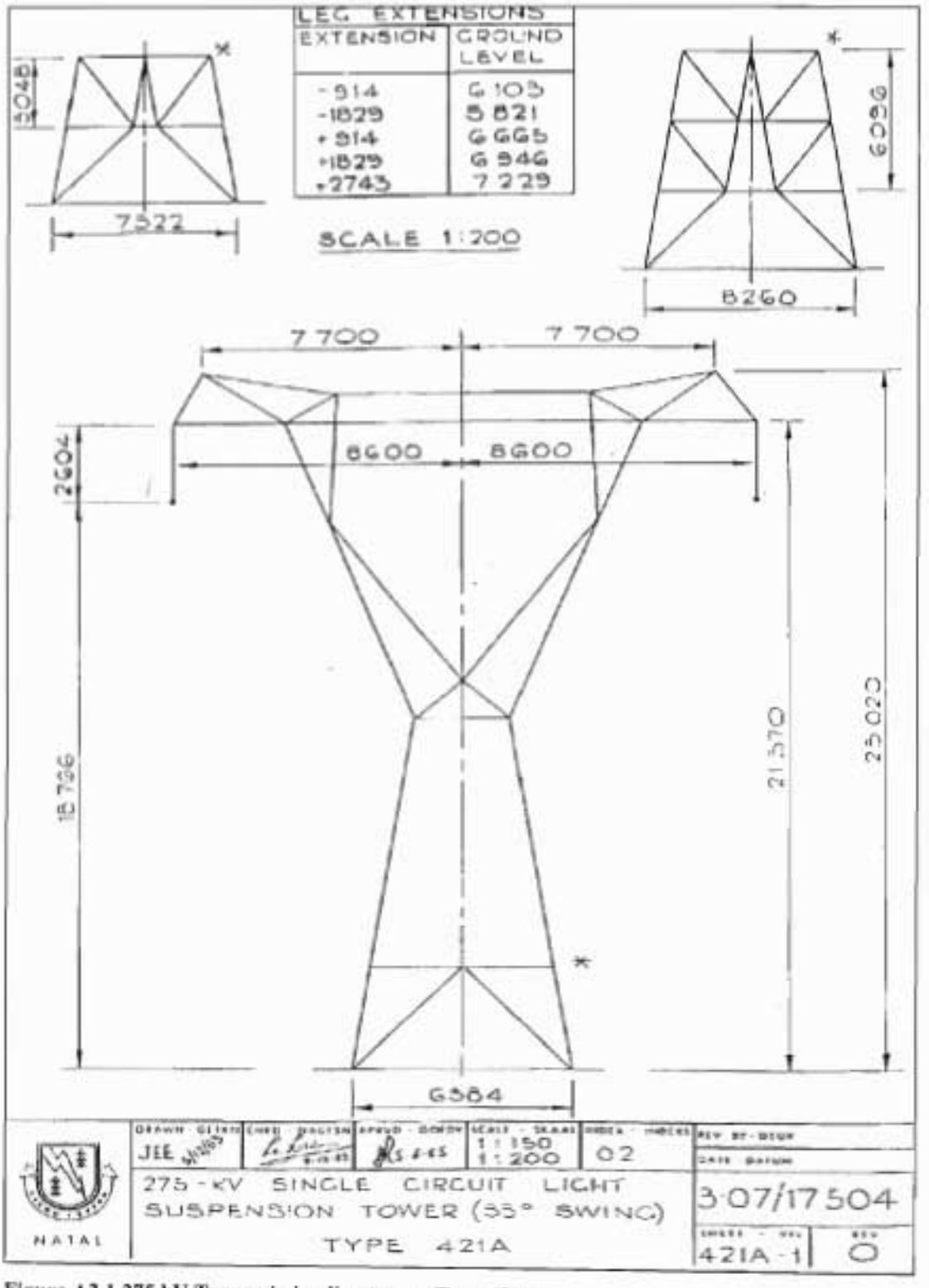

Figure A2.1 275 kV Transmission line tower -Type 421A

54(12+18+24)+7(1+6)

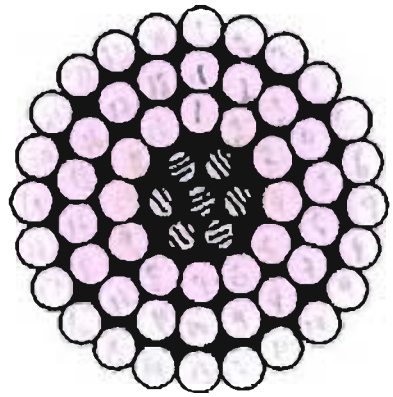

Figure A2.2 Cross-section of the Zebra conductor

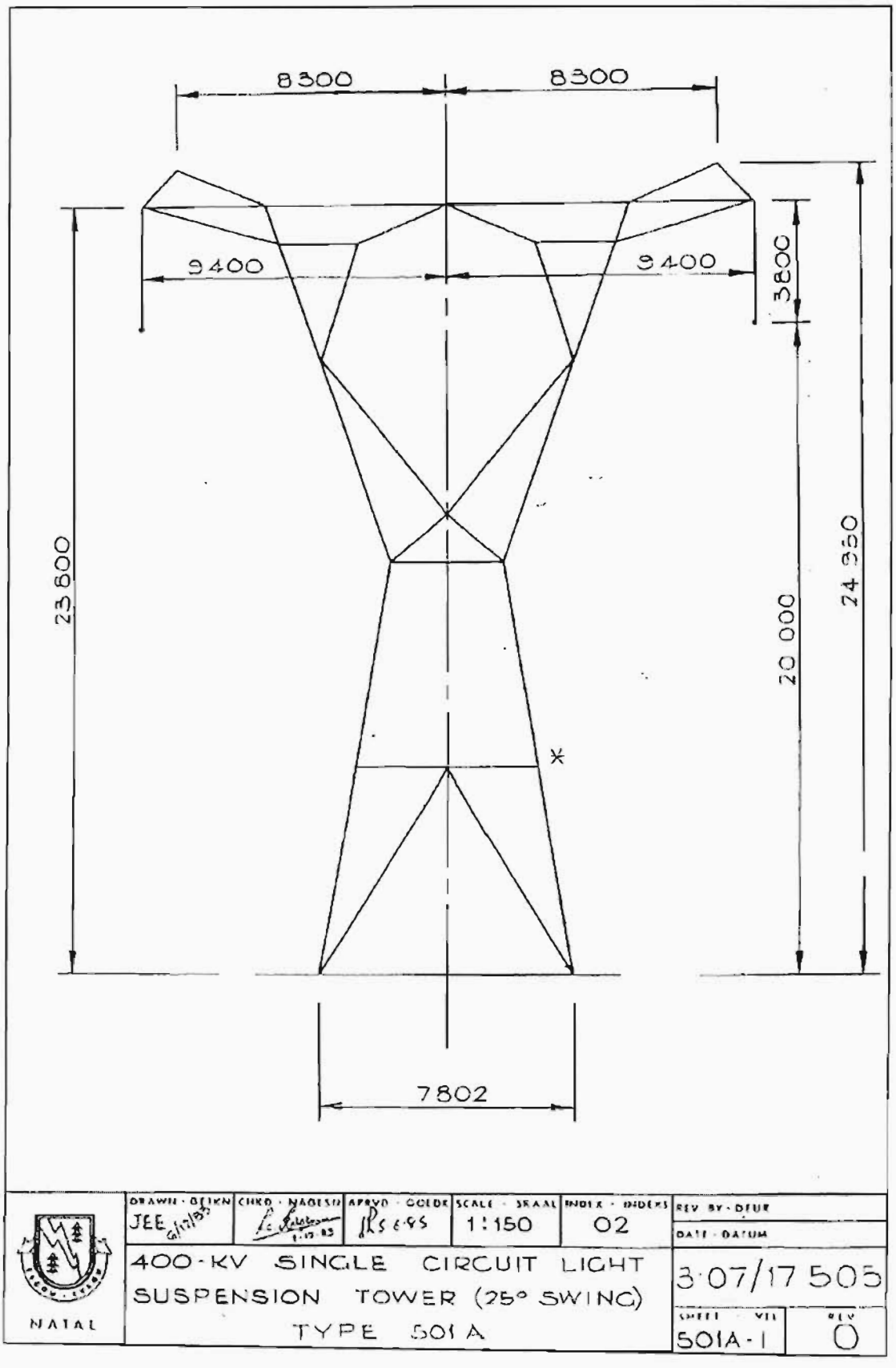

Figure A2.3: 400 kV Transmission line tower -Type 501A

TRANSMISSION LINES
CONDUCTORS & EARTHWIRES
CHARACTERISTICS

DURBAN DISTRIBUTOR
INLAND

NOTES

D.C.R. | M.J.P | J.R | NTS | C.3

3077/14760

DATE 27/05/93

A2-4

Appendix 3

Concept of Geometric Mean Radius (GMR)

The "GMR", ds, is the radius of an equivalent conductor in the form of an infinitely thin walled hollow circular tube, producing the same flux, ϕ, from the same current.

For practical conductors of laid up strands of equal round wires, GMR is as illustrated in table A3.1.

Table A3.1 Value of Geometric Mean Radius for stranded conductors.

Number of Strands	GMR = (ds)
1	0.779 r
3	0.680 r
7	0.726 r
19	0.758 r
37	0.768 r
61	0.772 r
91	0.774 r
∞ (Infinitely fine stranding)	0.779 r

Twin Bundle conductors:

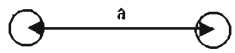

$$GMR = \sqrt{ds * a}$$

Where *ds* is as in table A3.1 and,

a is the distance between conductor centers in meters.

Table A3.2 shows the values of GMR for the two conductors relevant to this study.

Table A3.2 Values of GMR for Twin bundled conductors.

Conductor	Value of GMR
Dinosaur (400 kV)	78.64 mm
Zebra (275 kV)	61.18 mm

Appendix 4

Corona Inception Values

The Corona inception values of electric field strength for the various conductors used in simulations are listed in table A4.1.

Table A4.1 Values of electric field strength for corona inception for various conductors according to Peek's Law [49].

Condctor	Corona Inception Electric field strength (kV/m)
Zebra	3035
GMR Zebra (Twin bundle)	2684
Dinosaur	2974
GMR Dinosaur (Twin bundle)	2647

Appendix 5

Results of Two - Dimensional Simulations

Table A5.1: Results of 275kV - Geometric Mean Radius (GMR) : Peak Electric Field at conductor

Air Gap Length	0.3m	0.5m	1m
Conductivity (mho/m)	Peak Electric Field (V/m)	Peak Electric Field (V/m)	Peak Electric Field (V/m)
1.00E+05	7.10E+05	7.00E+05	7.00E+05
2.00E+05	7.30E+05	7.15E+05	7.05E+05
5.00E+05	7.75E+05	7.50E+05	7.20E+05
1.00E+06	8.50E+05	8.00E+05	7.50E+05
2.00E+06	9.70E+05	8.75E+05	7.90E+05
5.00E+06	1.20E+06	1.03E+06	8.70E+05
1.00E+07	1.41E+06	1.15E+06	9.40E+05
2.00E+07	1.61E+06	1.27E+06	9.75E+05
5.00E+07	1.80E+06	1.37E+06	1.03E+06

Table A5.2: Results of 275kV - Geometric Mean Radius (GMR) : Voltage at flame-tip

Air Gap Length	0.3m	0.5m	1m
Conductivity (mho/m)	Voltage at flame tip (V)	Voltage at flame tip (V)	Voltage at flame tip (V)
1.00E+05	1.55E+05	1.31E+05	1.00E+05
2.00E+05	1.52E+05	1.30E+05	9.90E+04
5.00E+05	1.45E+05	1.25E+05	9.30E+04
1.00E+06	1.35E+05	1.15E+05	8.50E+04
2.00E+06	1.25E+05	1.00E+05	7.00E+04
5.00E+06	1.00E+05	7.20E+04	5.00E+04
1.00E+07	6.50E+04	5.00E+04	3.30E+04
2.00E+07	4.20E+04	3.80E+04	2.00E+04
5.00E+07	2.00E+04	1.50E+04	9.00E+03

Table A5.3: Results of 275kV - Geometric Mean Radius (GMR) : Electric field at flame-tip

Air Gap Length	0.3m	0.5m	1m
Conductivity (mho/m)	Electric field at flame Tip (V/m)	Electric field at flame Tip (V/m)	Electric field at flame Tip (V/m)
1.00E+05	1.60E+05	1.00E+05	5.00E+04
2.00E+05	1.70E+05	1.05E+05	5.50E+04
5.00E+05	2.00E+05	1.20E+05	6.00E+04
1.00E+06	2.25E+05	1.40E+05	7.00E+04
2.00E+06	2.80E+05	1.60E+05	8.00E+04
5.00E+06	3.88E+05	2.13E+05	1.00E+05
1.00E+07	4.60E+05	2.50E+05	1.15E+05
2.00E+07	5.45E+05	2.80E+05	1.25E+05
5.00E+07	6.15E+05	3.10E+05	1.35E+05

Table A5.4: Results of 275kV – Twin Conductor : Peak Electric Field at conductor

Air Gap Length	0.3m	0.5m	1m
Conductivity (mho/m)	Peak Electric Field (V/m)	Peak Electric Field (V/m)	Peak Electric Field (V/m)
1.00E+05	1.54E+06	1.54E+06	1.53E+06
2.00E+05	1.57E+06	1.56E+06	1.54E+06
5.00E+05	1.65E+06	1.62E+06	1.58E+06
1.00E+06	1.77E+06	1.72E+06	1.63E+06
2.00E+06	1.98E+06	1.86E+06	1.72E+06
5.00E+06	2.38E+06	2.15E+06	1.88E+06
1.00E+07	2.75E+06	2.40E+06	2.11E+06
2.00E+07	3.12E+06	2.62E+06	2.12E+06
5.00E+07	3.47E+06	2.81E+06	2.20E+06

Table A5.5: Results of 275kV – Twin Conductor : Voltage at flame-tip

Air Gap Length	0.3m	0.5m	1m
Conductivity (mho/m)	Voltage at flame tip (V)	Voltage at flame tip (V)	Voltage at flame tip (V)
1.00E+05	1.50E+05	1.30E+05	1.00E+05
2.00E+05	1.45E+05	1.25E+05	9.90E+04
5.00E+05	1.40E+05	1.22E+05	9.40E+04
1.00E+06	1.32E+05	1.15E+05	8.50E+04
2.00E+06	1.15E+05	1.00E+05	7.20E+04
5.00E+06	9.00E+04	7.50E+04	5.00E+04
1.00E+07	6.50E+04	5.20E+04	3.30E+04
2.00E+07	4.50E+04	3.20E+04	2.00E+04
5.00E+07	2.00E+04	1.50E+04	1.00E+04

Table A5.6: Results of 275kV – Twin Conductor : Electric field at flame-tip

Air Gap Length	0.3m	0.5m	1m
Conductivity (mho/m)	Electric field at flame Tip (V/m)	Electric field at flame Tip (V/m)	Electric field at flame Tip (V/m)
1.00E+05	1.25E+05	8.00E+04	5.00E+04
2.00E+05	1.35E+05	8.50E+04	5.00E+04
5.00E+05	1.50E+05	1.00E+05	6.00E+04
1.00E+06	1.65E+05	1.20E+05	7.00E+04
2.00E+06	2.10E+05	1.45E+05	8.00E+04
5.00E+06	2.80E+05	1.85E+05	1.00E+05
1.00E+07	3.30E+05	2.20E+05	1.20E+05
2.00E+07	4.00E+05	2.50E+05	1.25E+05
5.00E+07	4.30E+05	2.80E+05	1.30E+05

Table A5.7: Results of 400kV - Geometric Mean Radius (GMR) : Peak Electric Field at conductor

Air Gap Length	0.3m	0.5m	1m
Conductivity (mho/m)	Peak Electric Field (V/m)	Peak Electric Field (V/m)	Peak Electric Field (V/m)
1.00E+05	8.40E+05	8.25E+05	8.30E+05
2.00E+05	8.65E+05	8.45E+05	8.40E+05
5.00E+05	9.35E+05	8.90E+05	8.60E+05
1.00E+06	1.04E+06	9.55E+05	9.00E+05
2.00E+06	1.20E+06	1.06E+06	9.57E+05
5.00E+06	1.53E+06	1.28E+06	1.07E+06
1.00E+07	1.85E+06	1.45E+06	1.15E+06
2.00E+07	2.14E+06	1.61E+06	1.23E+06
5.00E+07	2.41E+06	1.75E+06	1.28E+06

Table A5.8: Results of 400kV - Geometric Mean Radius (GMR) : Voltage at flame-tip

Air Gap Length	0.3m	0.5m	1m
Conductivity (mho/m)	Voltage at flame tip (V)	Voltage at flame tip (V)	Voltage at flame tip (V)
1.00E+05	2.45E+05	2.00E+05	1.55E+05
2.00E+05	2.30E+05	2.00E+05	1.52E+05
5.00E+05	2.25E+05	1.90E+05	1.45E+05
1.00E+06	2.10E+05	1.75E+05	1.30E+05
2.00E+06	1.90E+05	1.55E+05	1.10E+05
5.00E+06	1.45E+05	1.15E+05	8.00E+04
1.00E+07	1.08E+05	8.00E+04	5.20E+04
2.00E+07	7.00E+04	5.00E+04	3.20E+04
5.00E+07	3.40E+04	2.50E+04	1.50E+04

Table A5.9: Results of 400kV - Geometric Mean Radius (GMR) : Electric field at flame-tip

Air Gap Length	0.3m	0.5m	1m
Conductivity (mho/m)	Electric field at flame Tip (V/m)	Electric field at flame Tip (V/m)	Electric field at flame Tip (V/m)
1.00E+05	2.35E+05	1.50E+05	7.00E+04
2.00E+05	2.50E+05	1.55E+05	7.50E+04
5.00E+05	2.90E+05	1.75E+05	8.00E+04
1.00E+06	3.45E+05	2.05E+05	1.05E+05
2.00E+06	4.35E+05	2.50E+05	1.50E+05
5.00E+06	5.90E+05	3.25E+05	1.60E+05
1.00E+07	7.40E+05	3.85E+05	1.75E+05
2.00E+07	8.70E+05	4.50E+05	1.92E+05
5.00E+07	1.00E+06	5.00E+05	2.10E+05

Table A5.10: Results of 400kV – Twin Conductor : Peak Electric Field at conductor

Air Gap Length	0.3m	0.5m	1m
Conductivity (mho/m)	Peak Electric Field (V/m)	Peak Electric Field (V/m)	Peak Electric Field (V/m)
1.00E+05	1.85E+06	1.85E+06	1.84E+06
2.00E+05	1.90E+06	1.88E+06	1.86E+06
5.00E+05	2.00E+06	1.95E+06	1.91E+06
1.00E+06	2.16E+06	2.07E+06	1.99E+06
2.00E+06	2.43E+06	2.28E+06	2.11E+06
5.00E+06	2.98E+06	2.67E+06	2.32E+06
1.00E+07	3.50E+06	3.01E+06	2.51E+06
2.00E+07	3.88E+06	3.32E+06	2.65E+06
5.00E+07	4.45E+06	3.60E+06	2.78E+06

Table A5.11: Results of 400kV – Twin Conductor : Voltage at flame-tip

Air Gap Length	0.3m	0.5m	1m
Conductivity (mho/m)	Voltage at flame tip (V)	Voltage at flame tip (V)	Voltage at flame tip (V)
1.00E+05	2.25E+05	2.05E+05	1.57E+05
2.00E+05	2.20E+05	1.95E+05	1.55E+05
5.00E+05	2.15E+05	1.87E+05	1.45E+05
1.00E+06	2.00E+05	1.75E+05	1.33E+05
2.00E+06	1.80E+05	1.53E+05	1.13E+05
5.00E+06	1.40E+05	1.14E+05	8.00E+04
1.00E+07	1.02E+05	8.00E+04	5.40E+04
2.00E+07	6.60E+04	5.00E+04	3.10E+04
5.00E+07	3.20E+04	2.40E+04	1.50E+04

Table A5.12: Results of 400kV – Twin Conductor : Electric field at flame-tip

Air Gap Length	0.3m	0.5m	1m
Conductivity (mho/m)	Electric field at flame Tip (V/m)	Electric field at flame Tip (V/m)	Electric field at flame Tip (V/m)
1.00E+05	1.60E+05	1.30E+05	7.20E+04
2.00E+05	1.75E+05	1.40E+05	7.00E+04
5.00E+05	2.00E+05	1.50E+05	8.00E+04
1.00E+06	2.40E+05	1.80E+05	1.00E+05
2.00E+06	2.90E+05	2.00E+05	1.18E+05
5.00E+06	3.90E+05	2.80E+05	1.50E+05
1.00E+07	4.90E+05	3.20E+05	1.80E+05
2.00E+07	5.70E+05	3.70E+05	2.00E+05
5.00E+07	6.40E+05	4.00E+05	2.10E+05

Table A5.13: Results of 275kV - Geometric Mean Radius (GMR) : Peak Electric Field at conductor

Air Gap Length	0.15m	0.3m	0.5m	1m
Conductivity (mho/m)	Peak Electric Field (V/m)	Peak Electric Field (V/m)	Peak Electric Field (V/m)	Peak Electric Field (V/m)
1.00E+05	7.80E+05	7.20E+05	7.60E+05	7.30E+05
2.00E+05	8.20E+05	7.30E+05	7.70E+05	7.35E+05
5.00E+05	9.10E+05	7.75E+05	8.00E+05	7.50E+05
1.00E+06	1.04E+06	8.40E+05	8.42E+05	7.70E+05
2.00E+06	1.25E+06	9.40E+05	9.10E+05	8.10E+05
5.00E+06	1.70E+06	1.14E+06	1.05E+06	8.75E+05
1.00E+07	2.15E+06	1.32E+06	1.16E+06	9.25E+05
2.00E+07	2.60E+06	1.49E+06	1.27E+06	9.70E+05
5.00E+07	3.10E+06	1.65E+06	1.35E+06	1.00E+06

Table A5.14: Results of 275kV - Geometric Mean Radius (GMR) : Electric field at flame-tip

Air Gap Length	0.15m	0.3m	0.5m	1m
Conductivity (mho/m)	Electric field at flame Tip (V/m)	Electric field at flame Tip (V/m)	Electric field at flame Tip (V/m)	Electric field at flame Tip (V/m)
1.00E+05	3.70E+05	1.80E+05	1.00E+05	5.00E+04
2.00E+05	4.00E+05	1.80E+05	1.10E+05	5.50E+04
5.00E+05	4.60E+05	2.10E+05	1.20E+05	6.00E+04
1.00E+06	5.50E+05	2.40E+05	1.40E+05	7.00E+04
2.00E+06	7.00E+05	3.00E+05	1.70E+05	8.00E+04
5.00E+06	1.00E+06	4.00E+05	2.10E+05	1.00E+05
1.00E+07	1.30E+06	4.75E+05	2.50E+05	1.20E+05
2.00E+07	1.60E+06	5.50E+05	2.80E+05	1.25E+05
5.00E+07	1.90E+06	6.30E+05	3.00E+05	1.25E+05

Table A5.15: Results of 275kV – Twin Conductor : Peak Electric Field at conductor

Air Gap Length	0.15m	0.3m	0.5m	1m
Conductivity (mho/m)	Peak Electric Field (V/m)	Peak Electric Field (V/m)	Peak Electric Field (V/m)	Peak Electric Field (V/m)
1.00E+05	1.65E+06	1.51E+06	1.54E+06	1.63E+06
2.00E+05	1.70E+06	1.54E+06	1.56E+06	1.64E+06
5.00E+05	1.80E+06	1.61E+06	1.61E+06	1.67E+06
1.00E+06	1.97E+06	1.71E+06	1.69E+06	1.71E+06
2.00E+06	2.21E+06	1.87E+06	1.80E+06	1.79E+06
5.00E+06	2.78E+06	2.20E+06	2.05E+06	1.91E+06
1.00E+07	3.32E+06	2.50E+06	2.25E+06	2.02E+06
2.00E+07	3.90E+06	2.80E+06	2.43E+06	2.11E+06
5.00E+07	4.50E+06	3.10E+06	2.60E+06	2.19E+06

Table A5.16: Results of 275kV – Twin Conductor : Electric field at flame-tip

Air Gap Length	0.15m	0.3m	0.5m	1m
Conductivity (mho/m)	Electric field at flame Tip (V/m)	Electric field at flame Tip (V/m)	Electric field at flame Tip (V/m)	Electric field at flame Tip (V/m)
1.00E+05	2.20E+05	1.25E+05	1.00E+05	5.00E+04
2.00E+05	2.40E+05	1.40E+05	1.00E+05	5.10E+04
5.00E+05	2.50E+05	1.50E+05	1.10E+05	5.20E+04
1.00E+06	3.00E+05	1.75E+05	1.20E+05	7.00E+04
2.00E+06	3.80E+05	2.10E+05	1.50E+05	8.00E+04
5.00E+06	5.00E+05	2.90E+05	1.90E+05	1.00E+05
1.00E+07	6.50E+05	3.20E+05	2.20E+05	1.10E+05
2.00E+07	8.00E+05	4.00E+05	2.50E+05	1.20E+05
5.00E+07	9.00E+05	4.50E+05	2.80E+05	1.20E+05

Table A5.19: Results of 400kV - Geometric Mean Radius (GMR) : Peak Electric Field at conductor

Air Gap Length	0.15m	0.3m	0.5m	1m
Conductivity (mho/m)	Peak Electric Field (V/m)	Peak Electric Field (V/m)	Peak Electric Field (V/m)	Peak Electric Field (V/m)
1.00E+05	9.10E+05	9.00E+05	8.60E+05	8.80E+05
2.00E+05	9.60E+05	9.25E+05	8.70E+05	8.90E+05
5.00E+05	1.08E+06	9.90E+05	9.12E+05	9.10E+05
1.00E+06	1.27E+06	1.08E+06	9.70E+05	9.40E+05
2.00E+06	1.59E+06	1.24E+06	1.06E+06	9.80E+05
5.00E+06	2.25E+06	1.54E+06	1.24E+06	1.08E+06
1.00E+07	2.95E+06	1.82E+06	1.39E+06	1.15E+06
2.00E+07	3.72E+06	2.10E+06	1.53E+06	1.21E+06
5.00E+07	4.60E+06	2.35E+06	1.66E+06	1.27E+06

Table A5.21: Results of 400kV - Geometric Mean Radius (GMR) : Electric field at flame-tip

Air Gap Length	0.15m	0.3m	0.5m	1m
Conductivity (mho/m)	Electric field at flame Tip (V/m)	Electric field at flame Tip (V/m)	Electric field at flame Tip (V/m)	Electric field at flame Tip (V/m)
1.00E+05	5.70E+05	2.70E+05	1.60E+05	7.50E+04
2.00E+05	6.10E+05	2.80E+05	1.60E+05	8.00E+04
5.00E+05	7.20E+05	3.20E+05	1.80E+05	9.00E+04
1.00E+06	8.60E+05	3.75E+05	2.15E+05	1.00E+05
2.00E+06	1.12E+06	4.60E+05	2.55E+05	1.20E+05
5.00E+06	1.62E+06	6.25E+05	3.30E+05	1.50E+05
1.00E+07	2.18E+06	7.60E+05	3.95E+05	1.75E+05
2.00E+07	2.78E+06	9.00E+05	4.50E+05	1.90E+05
5.00E+07	3.45E+06	1.00E+06	4.90E+05	2.00E+05

Table A5.22: Results of 400kV – Twin Conductor : Peak Electric Field at conductor

Air Gap Length	0.15m	0.3m	0.5m	1m
Conductivity (mho/m)	Peak Electric Field (V/m)	Peak Electric Field (V/m)	Peak Electric Field (V/m)	Peak Electric Field (V/m)
1.00E+05	2.05E+06	2.01E+06	2.07E+06	2.12E+06
2.00E+05	2.10E+06	2.05E+06	2.10E+06	2.15E+06
5.00E+05	2.22E+06	2.14E+06	2.17E+06	2.20E+06
1.00E+06	2.45E+06	2.28E+06	2.27E+06	2.26E+06
2.00E+06	2.78E+06	2.51E+06	2.40E+06	2.36E+06
5.00E+06	3.50E+06	3.00E+06	2.72E+06	2.55E+06
1.00E+07	4.28E+06	3.40E+06	3.02E+06	2.71E+06
2.00E+07	5.10E+06	3.90E+06	3.30E+06	2.84E+06
5.00E+07	6.00E+06	4.35E+06	3.55E+06	2.96E+06

Table A5.24: Results of 400kV – Twin Conductor : Electric field at flame-tip

Air Gap Length	0.15m	0.3m	0.5m	1m
Conductivity (mho/m)	Electric field at flame Tip (V/m)	Electric field at flame Tip (V/m)	Electric field at flame Tip (V/m)	Electric field at flame Tip (V/m)
1.00E+05	3.00E+05	1.70E+05	1.10E+05	7.00E+04
2.00E+05	3.20E+05	2.00E+05	1.20E+05	8.60E+04
5.00E+05	3.60E+05	2.10E+05	1.50E+05	9.00E+04
1.00E+06	4.30E+05	2.50E+05	1.80E+05	1.00E+05
2.00E+06	5.30E+05	3.00E+05	2.00E+05	1.20E+05
5.00E+06	7.50E+05	4.00E+05	2.60E+05	1.50E+05
1.00E+07	9.40E+05	4.90E+05	3.00E+05	1.80E+05
2.00E+07	1.18E+06	5.70E+05	3.50E+05	1.90E+05
5.00E+07	1.40E+06	6.20E+05	4.00E+05	2.00E+05

Appendix 6

Results of Experiment 1: Rod-Plane

Table A6.1 Results for experiment 1: Rod-Plane

Air-gap Length [mm]	Breakdown Voltage [kV]	Standard Deviation [kV]	Corrected Breakdown Voltage [kV]
150	69.126	1.275	68.960
180	73.431	1.771	73.254

T= 18 °C; P=753mmHg;

Results of Experiment 2: Conductor Rod

Table A6.2 Results for experiment 2: Conductor Rod

Air-gap Length [mm]	Breakdown Voltage [kV]	Standard Deviation [kV]	Corrected Breakdown Voltage [kV]
100	45.879	0.336	45.148
200	75.030	0.869	73.834
300	103.566	0.336	101.916
400	133.947	0.912	131.813

T= 22°C; P= 753mmHg;

Results of Experiment 3: Parallel Lamina

Table A6.3 Results for experiment 3: Parallel Lamina

Air-gap Length [mm]	Breakdown Voltage [kV]	Standard Deviation [kV]	Corrected Breakdown Voltage [kV]
100	51.045	3.254	50.709
200	95.817	2.191	95.186

300	128.535	5.218	127.689

T= 20°C; P= 755mmHg;

Results of Experiment 4: Crossed Lamina

Table A6.4 Results for experiment 4: Crossed Lamina

Air-gap Length [mm]	Breakdown Voltage [kV]	Standard Deviation [kV]	Corrected Breakdown Voltage [kV]
100	75.030	3.532	74.663
150	109.716	5.007	109.180
300	150.552	6.140	149.817

T= 19.5°C; P= 755mmHg;

Results of Experiment 5: Particles

Table A6.5 Results for experiment 5: Particles

Air Gap Length	Particle Size	Particle Type	Breakdown Voltage [kV]	Standard Deviation [kV]	Corrected Breakdown Voltage [kV]
300	50	Brass	115.497	2.729	113.959
	100		99.384	5.301	98.060
	100	Pencil	90.405	2.750	89.201
	150		78.474	4.229	77.429
	200		48.708	2.357	48.059
400	100		126.813	4.811	125.124
500	150		136.284	3.928	134.469
	200		122.385	3.638	120.755
	250		106.149	4.834	104.735

T= 19.5°C; P= 755mmHg;

Results of Experiment 6: Fire Induced Flashover

Table A6.6 Results for experiment 6: Fire Induced Flashover

Air-gap Length [mm]	Breakdown Voltage [kV]	Corrected Breakdown Voltage [kV]
610	65.000	64.134
875	90.000	88.801
1360	130.000	128.269

T= 19.5°C; P= 755mmHg;

Appendix 7

Results of Three-Dimensional Simulations of 275kV and 400kV lines

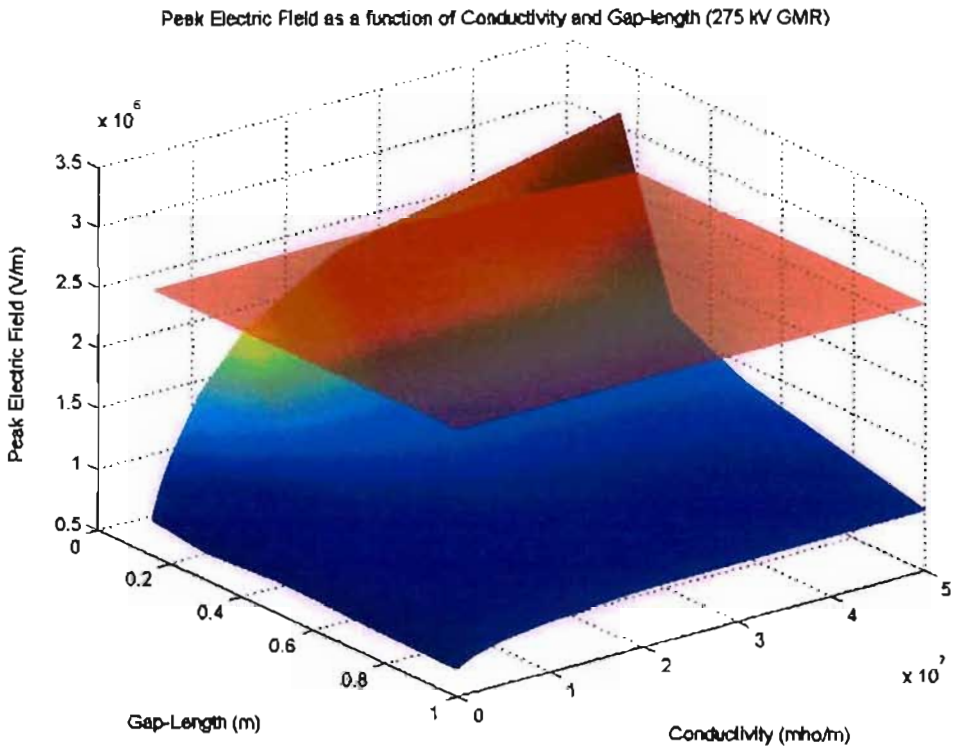

Figure A7.1: Peak Electric field strength at conductor surface as a function of conductivity: 275kV (GMR). The corona threshold field is shown as a red semi-transparent horizontal plane.

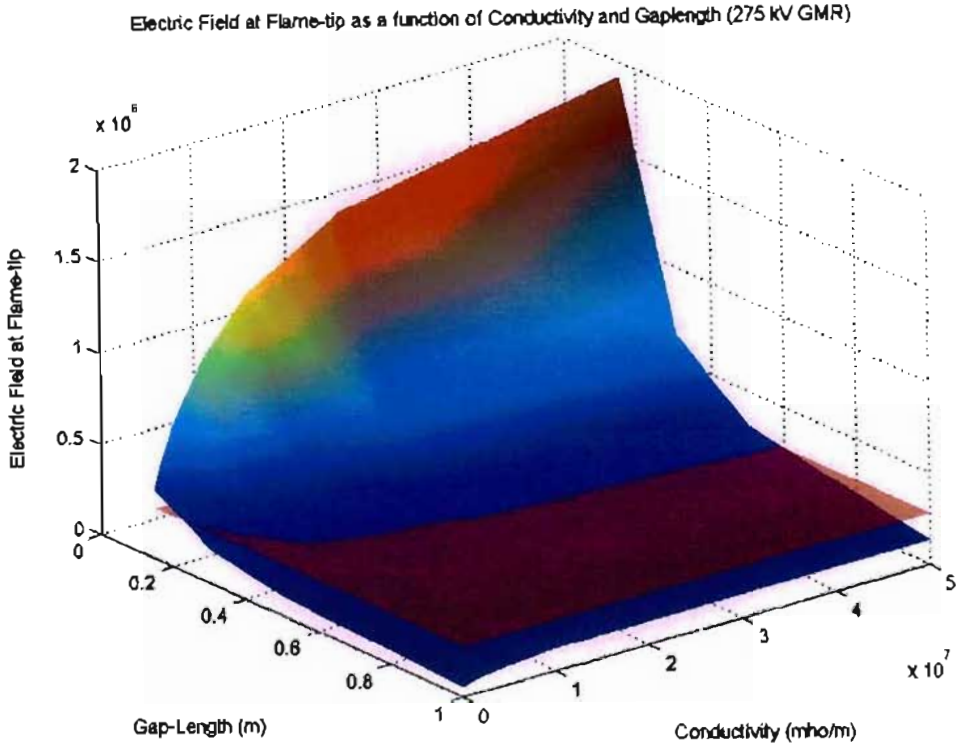

Figure A7.2: Electric field strength at flame tip as a function of conductivity: 275kV (GMR). The corona sustenance threshold is shown a red semi-transparent horizontal plane.

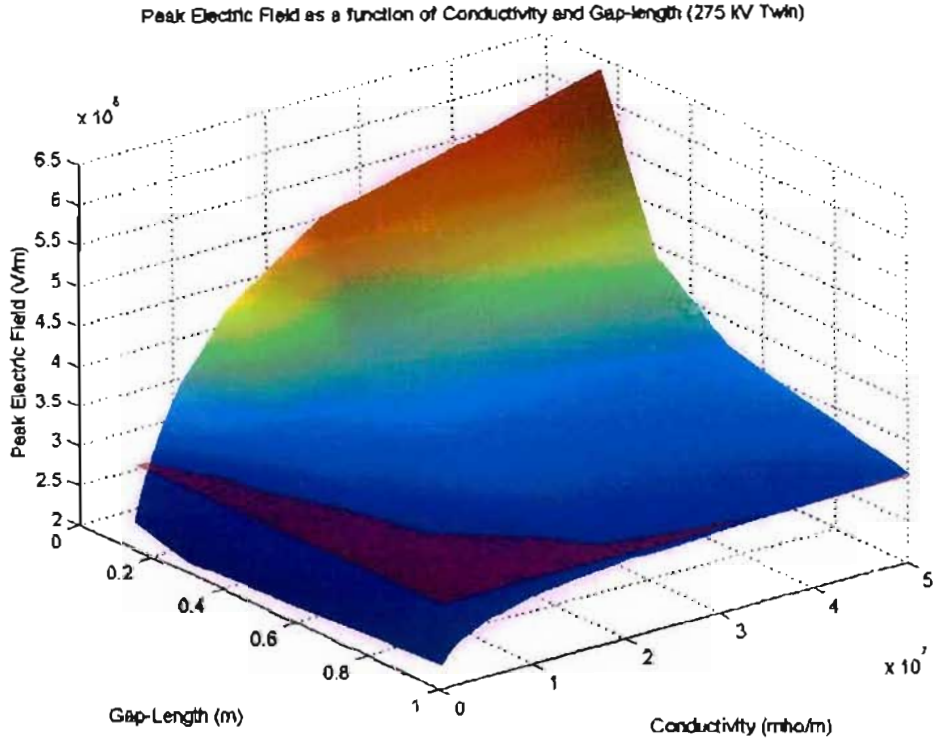

Figure A7.3: Peak Electric field strength at conductor surface as a function of conductivity: 275kV (Twin Bundle conductors). The corona threshold field is shown as a red semi-transparent horizontal plane.

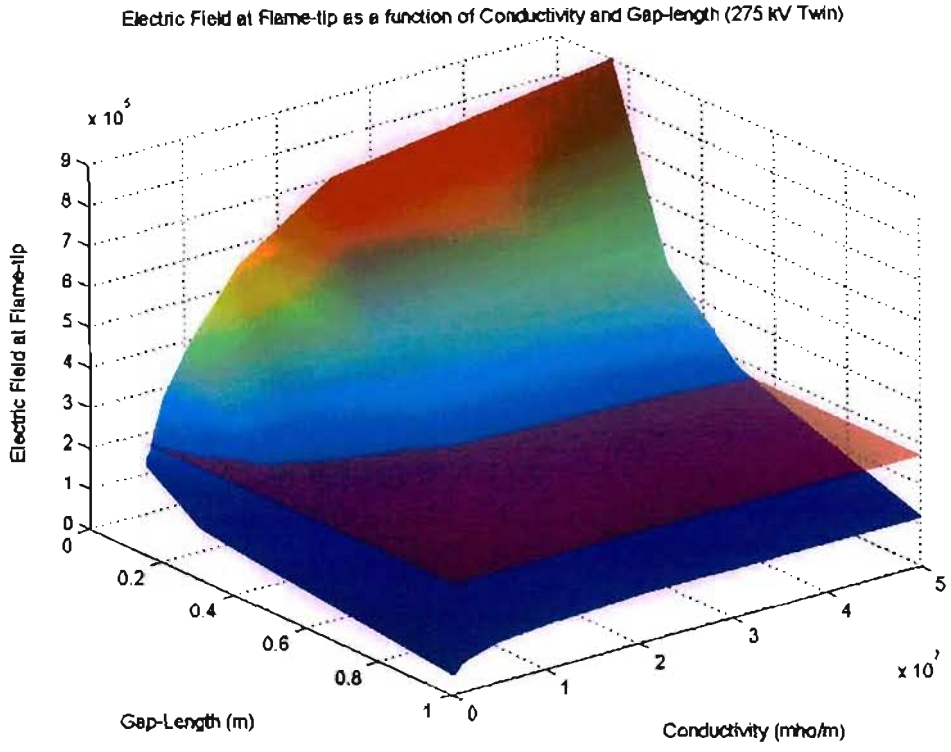

Figure A7.4: Electric field strength at flame tip as a function of conductivity: 275kV (Twin Bundle conductors). The corona sustenance threshold is shown a red semi-transparent horizontal plane.

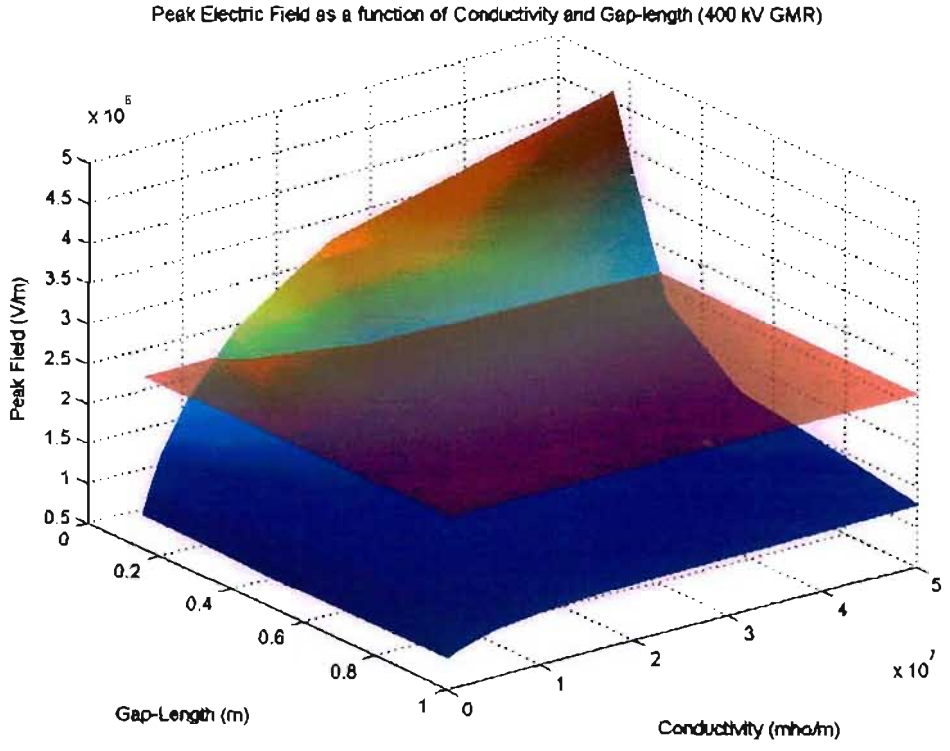

Figure A7.5: Peak Electric field strength at conductor surface as a function of conductivity: 400kV (GMR). The corona threshold field is shown as a red semi-transparent horizontal plane.

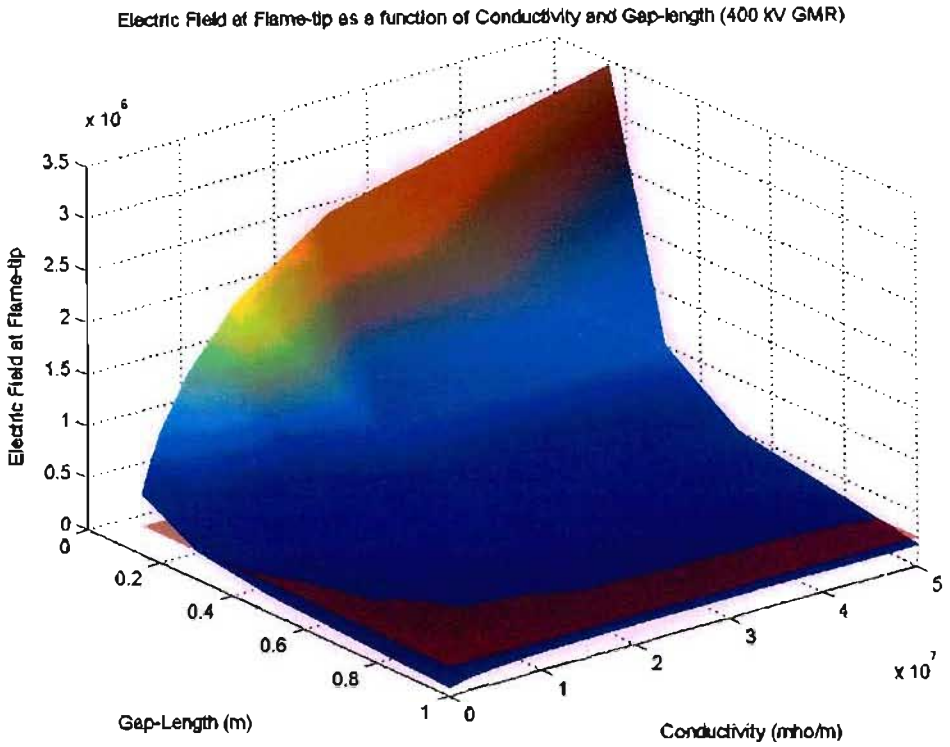

Figure A7.6: Electric field strength at flame tip as a function of conductivity: 400kV (GMR). The corona sustenance threshold is shown a red semi-transparent horizontal plane.

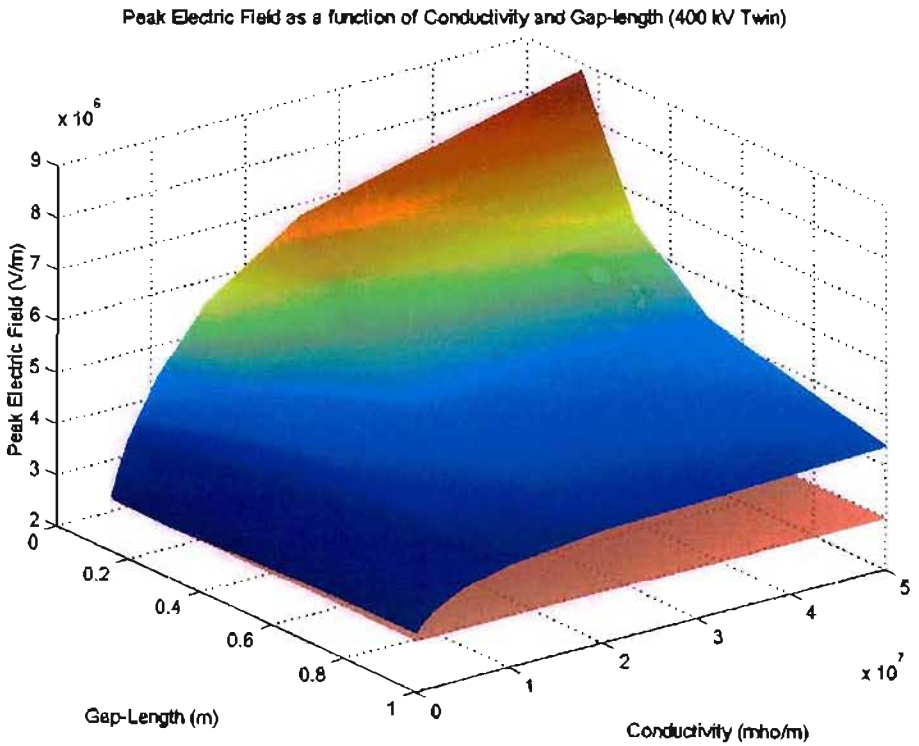

Figure A7.7: Peak Electric field strength at conductor surface as a function of conductivity: 400kV (Twin Bundle conductors). The corona threshold field is shown as a red semi-transparent horizontal plane.

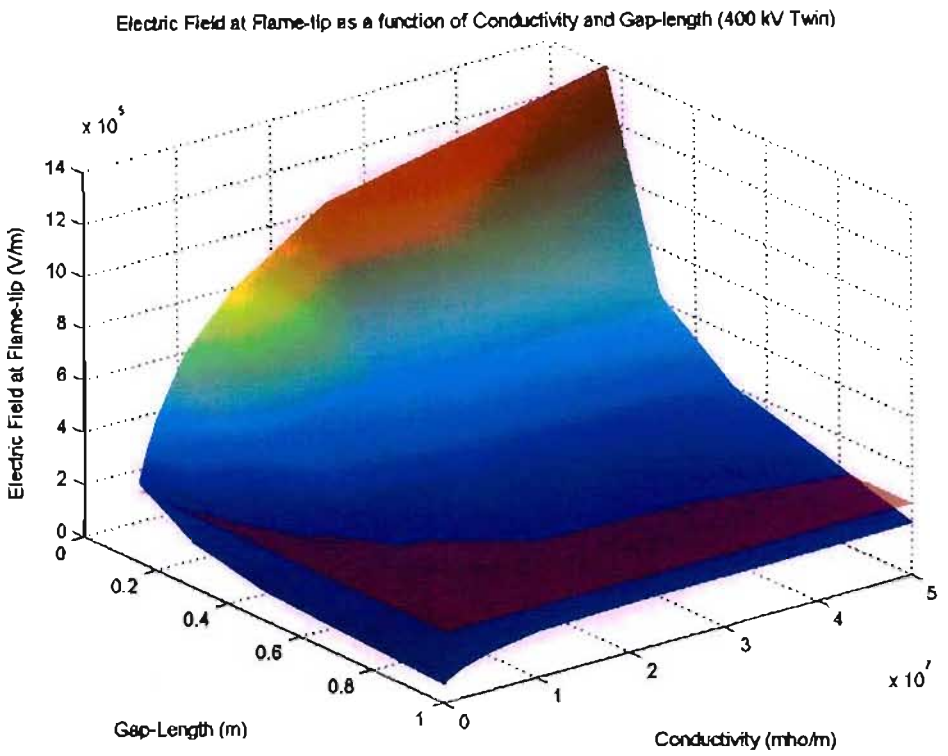

Figure A7.8: Electric field strength at flame tip as a function of conductivity: 400kV (Twin Bundle conductors). The corona sustenance threshold is shown a red semi-transparent horizontal plane.